ABSTRACT

TUHIN, MOHAMMAD OLIUDDIN. Experimental and Simulation Insights into Linear Multiblock Copolymer Systems: From Piezoresistive Sensors to Physical Organogels. (Under the direction of Drs. Richard J. Spontak and Melissa A. Pasquinelli).

Block copolymers have been investigated for last few decades because of their characteristic self-assembled nanodomain as well as molecular conformation (i.e. how the individual molecules take shape while forming the domains) driven applications. Driving force of the self-organization and thereby formation of these nanostructure functions in a similar fashion regardless of the number of copolymer forming blocks; whether it's 2 (diblock), 3(triblock), 5 (pentablock) or more. The molecular conformations, along their nanostructures, play a vital role defining the mesoscale properties of these materials, especially regarding the applications related to elasticity and extensibility. Triblock copolymer, because of their single midblock, is known to possess the simplest scenario of midblock conformation. Herein, using experimental and simulation methods, linear pentablock and heptablock copolymer-based systems (both neat and gel) along that of analogous triblock copolymers were studied where mineral oil (MO), having affinity of physically residing with midblock, was used as the solvent in the organogels.

In the first set of study of organogels, midblock selective solvents were simulated along triblock copolymers having different ranges of endblock fractions, and a detail phase diagram was constructed with the resultant nanostructures observed at equilibrium. One of the identified structures was 'Octahedral' morphology which is a unique addition to the family of block copolymer morphologies. The molecular conformations of the examined compositions depicted that the addition of the solvent changes the bridge fraction i.e. molecules connecting two nanodomains, at various degree upon the addition of the solvent and the spherical

morphologies were found to yield the highest bridge fraction both in neat and in the gel compositions.

The dissertation therefore, takes shift in examining the morphology and molecular conformations as a function of the structural influence of the triblock, pentablock and heptablock copolymers having endblock fraction of 0.2 leading to spherical or spheroidal morphologies. The morphologies from both experimental and simulation studies were found to be coherent in case of both neat and gel compositions of the copolymers. The new molecular conformations generated by the higher number of midblock were tabulated in detail along a newly proposed indexing method. The following section encompasses the influence of these structural complexities on the mesoscopic properties i.e. elastic and tensile characteristics. It was found that higher number of midblock provided increased elasticity and lower extensibility of the materials. However, such behavior can be a synergistic contribution of both having shorter midblock and higher number of midblock. As the chain length was kept constant in these series of studies mentioned in chapters 5 & 6, having higher number of midblock inevitably reduced the size of the midblock. Hence, it is still to be deconvoluted at which degree each of these factors contributed towards the mesoscale properties observed here.

In addition to the organogels, this study consists of exploring the effect of incorporation of electrically conductive carbonaceous nanoparticle i.e. carbon nanofiber (CNF) into both neat triblock copolymer and triblock copolymer/MO gels. The interplay of the networks formed by block copolymers and the networks of nanoparticle were detail studied for mesoscopic electro-mechanical responses of the CNF incorporated bulk material. It was found that, modulus-tunable thermoplastic elastomeric (TPE) gels imbibed with the midblock-selective oil exhibit well-behaved properties with increasing CNF content, but generally display nonlinear negative

piezoresistance at different strain amplitudes and stretch rates due to nanofiber mobility upon CPN strain-cycling. In contrast, a neat TPE possessing low hard-block content yields a distinctive strain-reversible piezoresistive response, as well as low electrical hysteresis, upon cyclic deformation.

Experimental and Simulation Insights into Linear Multiblock Copolymer Systems: From Piezoresistive Sensors to Physical Organogels

By
Mohammad Oliuddin Tuhin

A dissertation submitted to the Graduate Faculty of
North Carolina State University
in partial fulfillment of the
requirements for the degree of
Doctor of Philosophy

Chemical Engineering

Raleigh, North Carolina

2018

APPROVED BY:

_____	_____
Richard J. Spontak Co-Chair of Advisory Committee	Melissa A. Pasquinelli Co-Chair of Advisory Committee
_____	_____
Saad A. Khan	Erik Santiso

_____

Maurice Balik

DEDICATION

There are so many worthy candidates: persons, the deepest struggles, and very unorthodox dreams! I still could not decide on any specific one!!

That makes it all of them, doesn't it?

BIOGRAPHY

Tuhin was born in a coastal village of Noakhali, a southern district of Bangladesh, where the mighty river Meghna embraces the Bay of Bengal with its all windy rawness, grace, and beauty. Being raised in entirely nonurban serene surroundings, along with the yearly periodic visit of catastrophic cyclones of Indian Ocean, made these villagers both nonchalant towards the great risks and appreciative towards living a happy life with the bare minimum. Being one of them, he was not an exception.

His institutional education started with the then Char Akram Uddin Red Crescent Primary School which, by age, is four years younger than himself, and his father, as the head master, was chief navigator of the school starting from its hatchery age. However, despite being a formal student of the primary school, he was mostly 'home schooled' by his uncle who found a great pleasure in molding his tinder state with learning materials from beyond the designated classes. Later, he went to the Char Bata Khasher Hat High School and Dhaka City College leading to the subsequent landing in premise of the University of Dhaka. It was all about a journey for better education. Crossing the Atlantic Ocean to get into the graduate study at NC State University was the latest part of that course of mobility. This long ride starting from the age of 10 greatly helped him develop a knack of finding many homes beyond his original one along the way. Such a sweet and sour personal voyage is not showing any promise of endpoint yet, not even at horizon of the landscape!

During his childhood, water was almost everywhere in that coastal region, and, being raised under such circumstances, he developed an empathetic and intuitive sense about the underwater world. In addition to that, although motor cars were rarely seen within such a rurality, flying rockets were pretty regular in the clear sky during most afternoons. And, he got

hooked up with those shiny flying objects with long fanning out white tale of distant smoke. He is wondering if he can still do something with these long-lasting fascinations!

ACKNOWLEDGMENTS

["A Big book is a big nuisance" __ Callimachus. Although I solemnly agree with this Greek scholarly wisdom, I often prefer to make an exception when it comes in the context of being grateful, which is this section all about.]

In science, it's normal to challenge an established fact of thousands of years old. Scientific community eventually accepts that even when it opposes the mass people's sentiment as it happened in case of Gallileo and Copernicus. This is the beauty of scientific integrity- a never ending quest to accept the truth no matter where it comes from. That's why, the mentors in scientific community become leaders instead of bosses, unlike many other disciplines. Here, 'boss may NOT be always right' and the creative ventures of individual students vastly lies upon the successful practice of that notion. It was a privilege to have mentors with such kind of practice, as I found my advisors to be of the kind. They guided me when I felt lost, however, did not dictate me. I am very thankful to them for allowing me that liberty throughout my time here.

I still find it surprising how respectful Dr. Spontak is towards the opinion of the students. The way how he always weighs and provides importance to every single opinion, no matter how novice it is, has always been the treasure on the way of my development. Being in a position on top of the ladder with such a wide experience, expertise and recognition of the field and still behaving with such a respectful manner, almost like equal towards the pupil, is something that still fascinates me about him. I won't call him an epitome of such a nice and respectful personality as I am afraid that he might end up reading what I am writing here. I don't want him to cultivate even the slightest boastfulness out of such a humility- not even in his subconscious mind. We human beings are so vulnerable towards even very innocent

compliments and can end up collecting the poison from the honey flowing nectar. I am grateful that I found him with this quality and I hope he will continue nurturing this virtue. Because, it's such a great one!

I have a great fascination for the 'instinct' as parameter for making decisions. It might be a consequence of bias created by 'The Alchemist' (Paulo Coelho) followed by the bolstering effect of the 'Blink' (Malcolm Gladwell). Dr. Spontak used to warn me about my such kind of inclination in research. In my early days as a graduate student, I ended up saying something like- I feel like it's not right…& he corrected me saying something like, Tuhin, you don't decide in scientific research based on feelings! Now, as I gained some experience, I properly understand that he is so right! Then, again, at the very first stage, choosing himself as my potential supervisor was also based on my instinct! I could talk to him only once before the final decision, and, I even did not know that I should have consulted with the current group members. So, my instinct was a strong guiding beacon in driving me towards him as my supervisor. Now, I know that my instinct did not betray me! Then, what about his advice not to go with this tool in scientific research? I am not sure yet. Perhaps, I should consider it with a grain of salt. May be, I can work to train my instinct to hone its decision-making dial in scientific field as well. One nice day in future, I wish to discuss with him about my improvement on that sector as well. For now, I dearly thank him for being such a good example of how instinct can help making wise choices.

Procrastination can be a real nuisance in graduate school, especially when we are supposed to meet a whole lot of deadline of works. It's a luxury to tolerate being a last-minute procrastinating person. However, irrespective of all my sincere efforts, I was consistently inconsistent person to flow with the deadlines. Dr. Pasquinelli aka Dr. P, as she prefers to be

called, had to tolerate all those throughout these years. I can only imagine how much trouble I created by being such a sloth graduate student! I am grateful that she tolerated that kind of me for such a long time. I cherish the way how she secretly cared about me. Other than being worried about how I am doing under the pressure, it was beyond treasure how she secretly requested my colleagues to stay beside me, in case if I needed some extra support (sorry, Radhika, I could not resist the temptation of this leakage!). I dearly appreciate that! It was because of her I could get access to the entire facilities of the college of textile (CoT) whenever I needed. This access included the help and acquaintances of so many resourceful student researchers, faculty members, and administrative personnel. I dearly thank her for providing me such enormous privilege of opportunities!

There is another aspect of my PhD journey that, I think, is worth mentioning here. When I was giving my last presentation of the research project of the Nonwoven Institute (NWI), sitting in the audience, Dr. Spontak was sketching the potential chapters of my dissertation. By the end of the day, I came to know that we are letting the things of last three and half years go. It was the time to set new course for the entire dissertation according to the new sketches planned while I was presenting my last findings of the project. I was not sure if I should be terrified of the loss of all those works or be amazed with the hope of new prospects or be bewildered with the gravity of new research that I needed to propel through within such a short time. It's now, after surviving the battles, I can see that how brave, wise, and timely decision it was! For me, it was a practical lesson to know when to let it go, to withstand the pain of loss, and to still have enough breath to start over. It's my advisor's active guidance what kept me afloat till I reach at the harbor. I dearly thank them for bestowing me with the required guidance, support,

and the opportunity of learning to deal with such a massive setback. I can only see the importance of this last one after I could get a break to look back!

For me, entering graduate school was like bouncing onto merciless hard rock. It was a long struggle of survival for me, especially with the course works. Most of the time, I was hanging from edge of the bridge. Almost every year, I found solid walls touching my face ahead at some point. Every time Dr. Saad Khan aka Saad sir, as I call him, managed to get me some breathing room from nowhere. Such a helping hand not only helped me survive, rather enabled me to achieve more to cherish. I am aware that a whole lot of students across the campus were similarly, if not more than that, taken care of by him when they needed it the most. His such helping hand made a difference in the life of all those students. I believe such generous behavior of him, including that of many others, made this blooming campus as it is now and as it will be in future. I would like to thank him on behalf of all of friends who got in touch with his helping hand and all who will need that in future. I hope he will continue being such kind of person-always!

I would like to thank Dr. Behnam Pourdeyhimi for his invaluable support through personal suggestion as well as through the Nonwovens Institute (NWI). I specially acknowledge how he always prefers observing the research questions from the perspective of bigger picture. Such kind of intuition and instinct is a precious learning for me, a graduate student, who is still being cultured not to be lost into too much nitty-gritty while solving the problems. In addition to being supported with longest/maximum financial support, getting to know a whole diversified branch of research and the brains behind those through the NWI student body interactions was a window that I know not so many can get access to. Neither do many students get the invaluable opportunities of interactions with such a huge accumulation of smart experts who

are making changes from their pertinent leading seats of industrial research & development (R&D) sections. While working on my research project, I needed to take help starting from Dr. Pourdeyhimi to Jimei, William, that super nice guy Tri-Vu and many others. They provided me often far beyond than what they were supposed to do as part of their duty. I really appreciate all their time, attention, and effort that I was given. Above all, I value the friendships that could made while working as part of student researcher. All those connections that I am already bestowed upon, those that are going to happen in future made me indebted to this platform of NWI.

I admire Dr. Santiso for the reason how he addresses the problems using first principle method. At least that's the essence I got when I was learning from his transport phenomenon class, and from several times when I approached him with some conceptual questions. One day, I wish to develop the learning style using this skill which I believe is the smartest way of understanding any concept. I would like to mention another aspect of him what made me awe respectful about him. One day, it was close to midnight when I was stuck, along another friend, with a homework of his course. We emailed him for help. And, he ended up coming to the atrium of EB1 to help us with the homework- at that night. That's the type of person I found him- easy to approach, helpful and very insightful on what he knows. I did not need more reason to approach him to be part of my PhD endeavor. I hope he will continue being what he is. I also wish if I could learn more while I was still around NC State.

Along the same note, I would like to thank Dr. Balik for his kind consent to be part of the thesis committee. I have found him all along as the gentle man, another recognized figure in the field of polymer science.

Now, it's not easy to put even a minimum representative thing here about how treasure of pleasure and joy it was being in my groups, both M3G and Research group. I still remember that I was consulting with Dr. Saad Khan and was concerned about how much I will be able to learn hands-on research in the group. He confidently assured me and said that it's okay- Kenny will be there. I am glad that he was always there for more than what I could expect from a group member and continued to be so. I am grateful to him for being such a nice friend in so many ways. It will fall too short of description how the companionship of my labmates enriched me. Daniel, Heba, Justin, Joe, Iman, Sal, Yavuz, Wade, Melanie, Radhika, Ciera, Cody, Ya-Ting, Jing, Jacob, Syamal ad Erol- all names became associated with memorable times, here. Especially, I think, the 'coffee table' that Sooah, STP and Jiaqi made is an epitome of our friendly connectedness of in group. End of the day, it's those idiosyncrasy, tiny out of the box gestures, caring to each other when it was least expected and most needed makes life spicy and I had a treasure of that here. All those little, simple, and ordinary things. The ordinary things that ended up being the source of extraordinary pleasure. Throughout many other day-to-day interactions during all those nice sunny noon, gloomy cloudy days, some sleepy early mornings, exhausted late afternoons, lonely evenings or even at deep midnight ahead of any deadline. I am glad that I found such a vibrant company here and could have connections that I believe are meant to be life-long lasting. I believe that a team needs to survive through good days, bad days and angry days, and then it becomes a team. We surely did so here. My all colleagues from *both* groups- the co-swimmers in this intellectual stream of PhD, so many short time visiting scholars, long distant collaborators like Sebastian whom I even never met in person greatly enriched me in numerous ways. There are so many of them from present, from past and even from long past. Throughout many simple interactions, either academic or

very personal tiny ones, how those names with a face ended up being so many vibrant characters of my life chapters - still fascinates me. Having that kind of enormous treasure, I can write a neatly knitted long pleasant fabric of storyline of my graduate life here. I am very thankful to all these awesome people who provided me the privilege of enjoying their so precious company and let me befriend them!!!

It's worth mentioning how being a graduate student of the dept. of chemical and biomolecular engineering (CBE) itself makes a whole lot of difference. Such an easy access, comradeship, and the sense of oneness among the research labs is still unprecedented to me. Only this kind of homelike friendliness, environment and working strategy itself made a tremendous contribution towards me both as a student researcher and as a person. Such a sense of being 'Us' as a whole instead of being 'Us & Them' among the labs was a keystone in developing so many friendships in all 'Our' other labs. I dearly cherish those connections and would like to thank the department, including all associated persons, for providing me and my friends, such a research home. When I say 'all associated persons', I literally mean the whole ladder starting from the head of department, Dr. Fedkiw, dependable and caring smiley face of Sandra Bailey to the late-night sweepers who kept my surroundings neat, clean and healthy by creating sweet buzzing sounds of their vacuum cleaners. I am glad that I could have late night conversations with several janitors who worked here and was able to develop some sorts of friendships. Otherwise, I would never know how civility, understanding and culture I could learn from these people. All of these were possible because the CBE department provided me with such a space, access, and a group of friendly people. I hope, the department will continue being such an extraordinary embodiment, if not more than that, forever! Especially, I hope that, one day, department will make its ongoing interlab cooperation policy more official, and

thus more practicing, to enhance the borderless cooperative research capability. It was such a nice place to be, and I wish that it will be even far nicer place to be- for all in and around here!

Now, whatever I wrote in above sections might not have happened unless Dr. Ruhul Khan of the 'Institute of Nuclear Science and Technology' (Bangladesh) would so confidently recommend for me on the way to get into the graduate school of NC State. I still wonder what made him so strongly believe in me or how could he be so daring in believing in such an unlikely possibility for that time. One day, I hope that I will get a chance to ask him and will possibly get to know the secret reason. Now, I just would like to frankly acknowledge that his such an 'out of ordinary' step is the reason why I am writing this dissertation. It will be incomplete if finish the section without couple more names. I and Shah Md. Toufiqur Rahman started the graduate school journey together here, at NC State. I frankly admit that it was him from whom I learnt a good part of the course contents and those were instrumental to remain floated while swimming through this graduate school. It was Anwar Hossain aka Anwar vai as I call him, another current graduate student who was always there when I needed a little open window. Someone can potentially track the heartbeat of my entire graduate school life just by checking our chat history. The good days, the bad days, the confusing days, the colored days, the faded days-all sorts of days that that I went through. All different days have their own type of heartbeats, and any attentive one can hear/feel those. He was always there with some extra patience, attention, and time whenever I needed that listening stethoscope. I am grateful to both of them and wish them good luck for so soon to happen their own PhD defenses.

It's so profound source of confidence to have a supporting community like the one we have here- the student community of fellow Bangladeshi students. Knowing that there is such a net of support where I can fall back and that I can also have it to bounce back to the new heights

is great umbrella of home. Playing with little kiddo ‘Shuddho’ was such a necessary stress buster in so many occasions. Learning Matlab coding in simple way made me indebted to Mahmud, and he may never know how much important role that ended up playing in doing my overall doctoral research. While going through the research works of ‘Artificial Neural Network’, the research works of Sumon vai (Sumon dey), new visions of my potential future might have opened. There are so many small, brief, and significant such pearls that I could gather from so many of them. The butterfly effects of all those were instrumental in reaching at the stage where I am now and will be so in determining where I might end up in distant future.

I prefer not to write about the contribution of my family and the dearest ones of back home in Bangladesh. I might fall short in my description on how they kept me away from all the chores and normal ups and downs so that I can consistently focus on my tasks in hand, here. I will better mostly leave that on the shoulder of oriental shyness. In my part of the world, we don’t say much about the dearest ones. We just feel and be felt. We consider words to be too limited to express our deepest connections, contributions, and understandings. That’s the other side of the planet. A whole different kind of society and upbringings that helped embed my roots and supplied invaluable nutrients to develop my persona as what I am today. It’s tremendously fascinating how those people love me ignoring all the titles, degrees, or whatever accolade I earned or might end up earning. It’s just me as a person what matters there; such a sacred and pure the connections are! That’s what made me not to look up for any accolade unless it automatically flows down because of what I continue doing anyways. Because of being how I feel comfortable being, not how the society expects me to be. Building such a mostly indifferent of the surrounding expectation and having a non-recognition seeking psyche is

preciously peaceful. I am indebted to them for this kind of inbuilt treasure of peace. It's a never-ending episode of description that I can continue about them. So, for the sake of next sections, I will better leave it here sealing the envelop with the sign of eternal thankfulness!!!

TABLE OF CONTENTS

** These chapters were published in entirety

* These chapters have been submitted for publication.

LIST OF TABLES

CHAPTER 1

CHAPTER 7

LIST OF FIGURES

CHAPTER 1

CHAPTER 2

CHAPTER 4

CHAPTER 5

CHAPTER 7

CHAPTER 1

INTRODUCTION

1.1. Polymer, Block Copolymer and Development: Sketching the Route of Sequence

The development in human civilization is often marked with different milestone of inventions like bronze, steel, wheel, steam engine, transistor, airplane etc. Among those achievements so far, the era of bronze was initiated when people found that the intimate mixing of copper and tin produces an alloy which is much stronger metal than the copper itself. It took years when another alloy, much stronger than the bronze, steel was invented by heating the iron in the presence of charcoal. This way, thousands of years long practice and different degree of scientific understanding yielded super ductile and super resistant alloys. Later, the invention of the steam engine enabled mass production of steel in a controlled manner. This way, invention of these materials paved the way in building human civilization from one step towards the further ahead.

Polymer is another such trailblazer, not necessarily competing with the prior mentioned predecessors, in the field of scientific development, which had been going through revolutionary developments since the last century. The tracking back via knowledge of the initiation of human civilization indicates that polymer, as a structural material, is known to be existent and utilized since the prehistoric period. [1] The swiss lake dwellers were known to cultivate flax and wove linen 10 000 years ago. [2] The technology associated with weaving linen and different other plant fibers like cotton, coir hemp, sisal etc. are known to be used since 5000 B. C. Babylon was a well-known production and trading center of garments made up of wool and different animal hair since 4000 B.C. Another porteinaceous fiber, silk, can be mentioned as a notable early fiber originated in China in 3000 B. C. However, all of these were natural polymers as the chemistry of these materials

were unknown till the knowledge of synthetic chemistry started to grow in 18th century. By the end of 1930s there started a bloom of polymer related industry as can be observed from figure 1.1.[3] Since then, polymer became one of the fastest growing industry that are shaping the ongoing development of human civilization. Intuitively, because of the access into current sophisticated technologies, the overall development and understanding has a much higher pace than the predecessors mentioned in earlier paragraph! Such advancement includes both natural and synthetic kind of these materials.

Polymers, flexible and long chain macromolecules, consists of many repeating smaller molecules called monomer. Synthetic polymers are prepared by having specified monomers react in controlled way under designated conditions suitable for the intended production. Block copolymers are constructed as a long chain macromolecule where two or more chemically dissimilar blocks of these polymers are linked together with covalent bond. These types of polymers i.e. block copolymers, represent a broad-range of macromolecules constructed by connecting discrete linear chains comprised of dozens to hundreds of repeat units that are chemically identical, and spontaneously assemble into finely ordered soft materials. [4] This field is comprised of extensively wide spectrum of macromolecular physics and chemistry, ranging from the versatile synthetic routes and molecular architecture to application of advanced theoretical and computational methods.[5] Precise synthetic strategies of these macromolecules, with their self-assembling capability, provides extraordinary control over the resultant morphology, length scale of the self-assembled domains ranging from few nanometers to several micrometers, and thus enables diverse and expanding spectra of myriad applications, for example, nanoelectronics materials[6], drug delivery [6], advanced plastics[7], piezoresistive sensors[8,9], pressure-sensitive adhesives[10] etc. Having compositional and structural versatility along the numerous fields of

applications can be evidently traced by observing the trend of scientific research associated with block copolymers as is depicted [11] in figure 1.2.

There can be many variations in the architecture, chemistry, and thermodynamics associated with these polymers, which can be illustrated with couple of examples before being followed by more detail insights in the subsequent sections. As an example, two commodity polymers polystyrene (PS) and polybutadiene (PB) can be used to make block copolymers by connecting the PS & PB blocks using small amount of permanent linkage called cross-linkers. PS is a rigid transparent solid at room temperature and can be turned into viscous liquid above 100C whereas PB is already a viscous liquid at room temperature. So, connecting smaller domains of PS using long chains of PB enables to yield solid soft materials. Polyethylene (PE), another semicrystalline polymer can also be used in the place of PB where the PE chains are stacked periodically and forms physical cross-linked rubbery networks between glassy amorphous regions made up of PS. Both PS and PE belongs to the small list of commodity polymer that make up over 80% of total consumed global plastic production. [12]Thus having these as the blocks enables to get the properties of the kind of monomers belonged to a large proportion of total consumption. In addition to that, having bridges of soft polymers connecting rigid minority domains can be a profoundly useful design for the intended applicaitons. Using rubbery block as the bridging fraction connecting the rigid minority domains yield elasticity and are commercially used as thermoplastic elastomers, adhesive and bitumen formulations. [13] Thermoplastic elastomers are the materials that can be processed like plastics while the resultant products can be obtained with rubber elastic nature. On the other hand, having rigid bridges connecting soft minority domains enhances ductility and toughness. [14,15] Therefore, because of the choosing options from varieties of block forming polymers with diverse

properties like elasticity, permeability, ionic conductivity, toughness, creep resistance and optical clarity, block copolymers have found a wide range of applications.

1.2. Fundamentals of multiblock copolymers

In general, polymer molecules are keen to resist the mixing. Even polymers tend to phase separate in cases where their respective monomers mix homogenously. Such case arises from the very low entropy of mixing two polymer chains of *N* monomers each, which is approximately *1/N* smaller than the entropy associated with the constituent monomers. [12]Hence, when block copolymers are left for interaction in bulk or in a solution, the polymers tend to phase separate into their constituent domains of the blocks. They form microphase separated nanodomains of the minor components of constituent blocks, with some exceptions like the formation of lamellar morphologies, while forming different molecular conformations of the midblock as depicted in the figure 1.3.[16] As the term 'midblock' implies, such conformations require having at least one midblock e.g. as in triblock copolymer, to provide these physical networks.

Polymer chains, either in bulk or in high concentration, tend to form transient knots by entangling with each other. These knots may arise from either chemical bonds, or physical entanglements where the molecular weight equals to or higher than their corresponding entanglement molecular weight, or as an effect of the combination of both physical and chemical bonds. However, throughout this current study of dissertation, only physical bonds will be considered as no chemical bonds are expected to form in any case of consideration, unless specifically noted otherwise. Similar molecular arrangement is also expected in case of block copolymer-based systems. In these cases, because of microdomain formation, the polymer chains are characterized by their capability of connecting these domains. Especial point of interest arises from the molecular bridges connecting distinctive nanodomains. These midblock fractions determine the mechanical

properties of solid or semi-solid polymers and the flow properties in either molten state or in solution beyond minimum concentration of polymers needed to form micelle. This later minimum quantity required to form micelle is called critical micelle concentration for any constituent system.

Usually, block copolymer designs are constructed and developed intending to specific applications. That's why, a very small subset of the entire feasible chemical architecture of the BCP are explored and, even far smaller portion of those were developed and incorporated into commercially available products. So far, AB diblock and ABA triblock copolymers are the well-studied classes of BCPs in numerous experimental tools as well as computational studies leading to their comprehensive experimental and theoretical understanding of their bulk- and solution-phase behavior. [4] Having the combination of additional chemically distinct blocks and block types constituted of various functionality can open the new windows of innovative design opportunities for nanostructured materials with desired properties, often even without adding any significant commercial cost associated with the change of the design. As the boon of modern synthetic methods, now it's possible getting access into a broad portfolio of multiblock architecture as illustrated [17] in figure 1.4.

These multiblock copolymers can open up the window of unlimited potential for designing soft materials having been bound by meeting two conditions of synthetic accessibility of the structurers, and the availability of appropriate theoretical tools to guide the strategies required to follow in order to obtain the desired molecular design of the macromolecules along the processing conditions. Out of many, constructing macromolecules constituted of additional blocks can significantly benefit in the context of physical properties. For example, in addition to the well-studied AB di-BCP, the extension of linear chains as ABA, ABABA etc. can greatly influence the physical properties such as enhanced elasticity and fracture toughness [18] leaving the phase behavior

mostly unchanged. Adding different types of block copolymers such as ABC itself can produce pronounced types of more additional nanostructure [19] in comparison with the case of AB and ABA triblock copolymer where, these later ones typically adopt four major types of microphase self-assembled structures called spheres, cylindrical, double gyroid, and lamellae. As is explained in the review [17], additional numbers of blocks (n) along the chemically distinct block types (k) can profoundly extend the number of unique sequences producing the host of nanostructures. Having cyclic and different degrees of branching can offer further windows of possibilities [20] of phase complexity. Both of these possibilities are further illustrated in figure 1.4 and table 1.1.

In 1960, Schlick and Levy used sequential polymerization of styrene and isoprene to prepare tri-, penta-, hepta- and nonablock copolymers of $(AB)_nA$ and $(BA)_nB$ with n = 1,2,3, and 4.[21] Then a series of ABC and ABCBA block copolymer based materials were reported in next decade of early 1970s.[22-24] The next decades followed with the reporting of first ABC star ("miktoarm")[25]; ABCD linear[26,27] , miktoarms[28], and ring-shaped or cyclic block copolymers.[29] Block copolymer based systems comprising of $(AB)_n$ multiblock copolymers[30], ABABA type pentablock copolymer,[18] and ABABABA type heptablock copolymers were studied.

Although, the field of block copolymer has expanded towards a wide variety of material property, investigation, and applications, it's the spherical micelles that have still been at the focus of current state of art. The size of these spheres is bounded by the molecular weight of the constituent molecular weights, while such limitation of size can be lifted by producing other neighboring micelles like worm-like micelles, disks, or vesicles. It's still a challenging task to control the size of these disks and vesicles for the particular purposes. In the cases where ABC block copolymer is used, core-shell-corona or "onion" can also be constructed which has been explored as delivery vehicle [31,32]. Here, a specific molecule can be confiscated in the core with a surrounding thickness

of B shell, or if needed can be designed in a way to control the release rate. Having a cross-linked one microdomain of ABC triblock copolymer, and then, dispersing the resultant aggregates can generate additional interesting features. It was also reported that a class of block copolymer where B domain formed spheres at the A/C interface was observed to form "Janus" micelles. [20,33,34] So, the filed thus offers opportunity of having plenty of already established materials properties and numerous potential opportunities to be explored.

1.2.1. Block copolymer phase behavior

Block copolymers have long been used as an interesting field of materials due to their tunable capability of the formation of self-assembled nanostructure. These phase behaviors can be expressed in a simplistic method as the phase diagram mentioned in figure 1.5.[35] These phase behavior of the block copolymers are defined by molecular variables, molecular topology and specific block sequences as elaborated in the following sections-

So, the primary contributors to the phase behaviors are the degree of polymerization of each block (N_i), and the segmental pairwise interaction parameter, χ_{ij} associated with the corresponding blocks. In addition to these, there are some other secondary contributors like molar mass distribution, block flexibility, sub-block structure e.g. alternating, tapered or random, composition heterogeneity etc.[17] Hence, even a slight increase in the numbers of blocks (n) along the chemically distinct block types (k), along the wide spectrum options of choosing chemistries offers limitless potential chemical structures and functionalities.

The start of the above-mentioned possibilities can be attributed to some early works from the mid-20th century. It was 1960s, when the self-assembled properties observed in ABA type elastomeric materials were attributed to "microphase separation". [13] Later, the application of small angle x ray

scattering (SAXS) and transmission electron microscopy (TEM) facilitates the beginning of identification of nanoscale domains of the components and the ordered lattice symmetries. At the beginning of 1970s, the microphases from spheres to cylinders to lamellae to inverted cylinders and inverted spheres. [36] Later, in the 1980s, the location as well as the characterization of order-disorder transition (ODT) as a function of temperature came into light followed by the detection of order-order transition (OOT) between the constituting phases. By the end of this decade, the microphase separated domains within ODT became more established and also, additional phase like gyroid, and the rheological characteristics of different phases were highly studied and explored. [37-39]. Something here is noteworthy to mention that analogous, at least qualitatively, microphase separated morphologies are also evident in much larger scale cosmic events like at the core of the neutron stars, and researchers named those 'neutron pasta'. [40] It's really fascinating to observe how the material properties can be similar throughout the nanoscale to cosmic scale!

1.2.2. What are the strategies to choose which design of BCP to manufacture?

Because of boundless possibilities of creating block copolymers, it's indeed a daunting task to choose which one to aim for as preparing those are associated with heavy costs, needless to mention about the necessity of precise control over the strategy of chemistry involved. As it's not a practical approach to prepare any specific type of block copolymer for the sake of purely aesthetic reason, the block copolymer molecular designs are prepared with the aim of specific applications.

For example, in order to obtain a thermally stable and mechanically robust membranes having a dense set of specially designed nanopores require the use of a glassy, ductile, and chemically etchable blocks. [41] To get more specified goals in the intended products like the characteristics of biocompatibility, specific solubility constraints these arrays of choices will be further expanded. As an illustration, some possible combinations of a linear ABC terpolymer containing three types

of blocks, glassy polystyrene (PS), rubbery polyisoprene (PI), and polylactide (PLA) which is both etchable and bio renewable are presented in the scheme in figure 1.6. In the similar manner, polyethylene oxide (PEO), a water-soluble and biocompatible polymer, can be another potential choice to prepare block copolymers with additional functionality.

However, it's a growing challenge to decide which block copolymer to synthesize, using which monomers, and by choosing which kind of or which combination of synthetic methods to choose from the available synthesis tool-kits to obtain the specific type of block copolymer. Computer simulation can be very needed and useful tool in these cases to sort out the viable routes of synthesis and to narrow down the most optimized choice of product out of many potential possibilities.

1.2.3. Role of synthetic chemistry

As it's intuitive from the previous sections, synthetic chemistry plays an important role in deciding the feasible structure of the block copolymers that are deemed possible. The living anionic polymerization is the most used method of the BCP production of now-a-days. After the first reporting of living anionic polymerization in mid 1950s in production of styrene and styrene/isoprene block copolymers [42], the method was successful in producing polymers with very narrow distribution of chain lengths. Synthesis of *SIS* and *SBS* triblock copolymer found a great success in the field using this method. [43] Further modification of the blocks like hydrogenation or fluorination enables further increase in the choice of properties obtainable from the BCPs. For example, catalytic hydrogenation of the diene blocks, midblock of SIS and SBS, yields polypropylene and polyethylene, respectively. Hydrogenation can also be applied into PS to produce polycyclohexylethylene which is a very rigid and temperature resistant transparent plastic.

Such hydrogenation of PS blocks was also successfully employed in *SBSBS* pentablock copolymer and, was found to yield new type of tough, transparent plastic with optical properties. [7,15]

To elucidate the target-oriented strategy of preparing the block copolymers/soft material within affordable range of associated cost require an in depth understanding of the structure as well as the properties influenced by that. The continuous advances in the computational/theoretical tools can be used as a predictive guiding route for the synthesis.

1.2.4. Major usability of the block copolymers at a glimpse

According to the review of Ref. [5], the major benefits of block copolymers can be listed as following-

A) Obtaining precise morphology

B) Control over length scale

C) Theoretical tools to predict equilibrium properties

As a general usefulness, block copolymers can suppress the macrophase separation retaining the properties of their constituent homopolymers. Thus, they can take advantage of their homopolymers only without using the nanostructure forming characteristic of them. Such limited useful ness is sometime referred to as 'scalar' benefit of the block copolymers. For an instance, poly[styrene-*b*-isoprene-*b*-styrene] is a very useful class block copolymer. For this kind of polymers, it's the microphase separation of the styrene and isoprene blocks that leads to robust application of their elastomeric behavior, not any structure. [44] Now, along the properties of components, particular type of nanodomain, spatial orientation, short or long-range ordering of the nanostructure, connectivity, and orientation of the nanodomains bring all new interesting features into play regarding the current and future potential applications. Block copolymers having such

kind of versatile usefulness is sometimes termed as the ones with 'vector' properties. While the ones with 'scalar' properties are primarily used in commodity products and these later ones can also be particularly in high-value-added, in specialty markets.

1.3. Understanding the solvent selectivity and gelation in BCP-gels

One advantage of using bock copolymer is that the morphologies can be tuned just by adding block selective solvent/s. In these contexts, selectivity indicates the thermodynamic preference of the diluent molecules towards a specific block of the copolymer. In case of strongly selective systems, the diluent molecules almost entirely reside onto one microdomain, and behave as addition of the respective block. Such selectivity of the solvent towards specific blocks are strongly temperature-dependent, and as the temperature is increased the selectivity was found to be decreased gradually. Studies [45,46] on the influence of different solvents having varied selectivity towards specific blocks of poly[styrene-*b*-isoprene] (*SI)* block copolymers illustrated that such increase in temperature is analogous to the addition of neutral good solvent to the BCP.

It was already demonstrated by Hanley and Lodge [47] that all nanostructures in a pure block copolymer can also be produced in a block copolymer/solvent system if the solvent is neutral. The self-assembly in these block copolymers are dominated by two driving forces: short-range attractive forces (A-B attractive forces) and long-range repulsive forces (A-B repulsions). [48]As a result of these two forces, the balancing act between the interfacial tension and the chain stretching entropy defines the formation of the self-assembled structures. As indicated before, these self-assembled nanostructures can be various types like spherical, cylindrical, gyroid, and lamellar, [49] where the spherical and cylindrical ones are usually termed as micelles. Several morphological and molecular architecture tends to change in the presence of a single solvent selective to one block. [50,51] In these the morphological ordering of the block copolymers are similar to that of the

bulk block copolymer except the fact that the ordering is governed by the solvent-polymer interaction as the dominant force. Additional studies also reported the change in morphological spectra in ternary systems consisting of one block copolymer and two selective solvents [52], and one selective solvent and one selective homopolymer.[53]

Based on the strength of interaction between the block copolymer and the solvent, the aggregate forming micelles or aggregates can be solvated at some degree. However, if these micelles will form short-range or the long-range ordering is determined by the respective processing conditions and represents a competition between the micelle ordering and the physical network formation.[54,55]Higher polymer concentration favors the long-range ordering[55,56], where the aggregate forming endblocks can exchange, as an example, in the case of annealing of the gels at higher temperature, were it was found to favor the long-range ordering.[57,58] In another way, it can be expressed that if the volume fraction of the micelle forming micro-domains are increased, at some point these micelles start depicting more intermicellar correlations and, at a very strong such correlations they start to show the crystalline-type morphological characteristics on the mesoscopic length scale. Such structures are dominantly known as cubic structures of spherical micelles, hexagonally packed structures of cylinders or rodlike micelles or lamellar structures of extended discs. [59] At such a higher quantity of block copolymer concentration, the overall inter-micellar connection can be extended to the entire 3- dimensional volume of the sample, and thus can provide a macroscopically isotrophic physical gel. Since each of such microdomains are connected to the extended three-dimensional network, peeling off any micelle will require to extract the polymer molecules from all surrounding microdomains. Such phenomenon provides the structural stability of the structure by restricting the chain mobility. The presence and characterization of the microdomains either in neat block copolymer or in block copolymer gel can be identified using

small angle scattering patterns. The signature of the gel can also be corroborated using rheological experiments where even at low shear frequencies ω, a finite elastic response where the storage modulus, G' (ω, T) provides greater value than that of the loss modulus G'' (ω, T). The microstructure driven response is directly related to the elastic response within macroscopic scale,[60] and such elastomeric behavior is synonymous to the nature of classical elastomers (rubbers) where vulcanization introduces the permanent cross-links.

However, long -range ordering was not found to impact the micelle size of the respective micelles. [57] Like the neat block copolymers, in the block copolymers in BCP/gel, the BCP midblocks, emanating from the micellar core, form networks of bridges or loops based on if the respective polymer chain is located as part of the same or different micelles.

On the other hand, AB or ABA type block copolymers can also be dissolved into endblock (A-block) selective solvents which is incompatible with the B-block. In such cases, the microdomains will be formed of the dense core of B-blocks and the corona of flexible A-block chains will emerge and create either spherical, rod, thread or disk like shape. [61]

To understand how the mesoscopic properties are influenced in the BCP/midblock-selective solvent, it's important to examine how the bridges connecting the microdomains are influenced in those systems. Using midblock selective solvent, tetradecane at different polymer concentration, a detail study on the SIS triblock copolymer were carried out using elegant dielectric technique. [62,63] as an attempt to examine the midblock fractions is those systems. It was found that the bridge fraction decreases as the triblock copolymer was diluted. Another research group examined the gel modulus along the change in gel microdomain structure as a function of various degrees of dilution of BCPs using midblock selective solvent. [57,64-66] They observed strong power-law dependence of the modulus of the triblock in the corresponding gel. Here, one pertinent question arises from the

uncertainty on the fact that if the changes in the modulus is the contribution of bridge or that of the entanglement. Or, if it's the result of both, then what's the degree of influence of either one and how that might be changed in different conditions?

Because, in addition to the loop/bridge ratio, the dilution of block copolymers changes the micellar structure like aggregation number and the intermicelle spacing. [64,65] The entanglement density also decreases as the polymer content is decreased while the solvent content is increased. Therefore, it's still an ongoing challenge to find out exactly how and at which degree the loop/bridge ratio and the entanglement contributes towards the rheological response of any corresponding block copolymer gel.

For *SIS/cyclohexane* based systems, in a reported study [56], it was speculated that the overlap concentration [c*] was reached even below 1 wt% of triblock concentration, considering the solution lied in semi dilute regime. Such scenario indicates that the chains coming out of the neighboring micelles exhibit much overlapping and, thus can heavily entangle even below 1 wt% of block copolymer concentration.

Such kind of gels made up of unentangled end-linked polymers are expected to depict the plateau modulus [67,68] G_0^{Rouse}:

$$G_0^{Rouse} = RT\,[c/M] \qquad (1)$$

Here, M = molecular weight between the junction points. For triblock copolymer-based systems, this indicates the midblock molecular weight of the copolymer. T is absolute temperature and *c* is the polymer concentration. The numerical value of G_0 is the value of G' in plateau region at the frequency where G'' exhibits a minimum. The observation of similar scaling was also reported in another analogous gel where the solvent was chosen to be heptane. [67] So, for nonassociating

polymer solutions, this plateau modulus is scaled differently as it requires the concentration[69] of polymer several times c* to exhibit the entangled behavior.

When the midblocks are interlocked, it works effectively as a bridge between micelles. Such entangled loops contribute to the elasticity of the networks. [70-72] Thus, the plateau modulus of the network, according to the theory of associating entangled polymers,[70] can be expressed with the following relationship:

$$G_0^{ent} \sim (1/N_e)\, c^{3v/(3v-1)} \qquad (2)$$

Where, v = Flory exponent = 0.588, and N_e = number of blobs per entanglement, and this Ne is independent of concentration in the semidilute regime. This modulus for entangled nonassociating homopolymers in the semidilute regime was found experimentally [73] to scale with the concentration of power-law exponent in the range of 2-2.5, and with the theoretical scaling exponents of 7/3 in θ solvents[74] and 9/4 in good solvents.[73]

Some other factors contributing to the networks in BCP-gels are number density of micelle, intermicelle distance. Decrease in number density of micelle will increase the inter-micelle separation, which will make the bridging among micelles, and entanglement between loops from neighboring micelles, more difficult.

As is enumerated so far, the ratio of loop/bridge in the multiblock copolymer-based systems dictate how either the bulk or the polymer in solution will behave. If the loop/bridge becomes very high, and the loops produced from the micelles don't create any interlocking entanglement, the micelles will create a flowerlike conformation like of the figure 1.7. There will not be attraction between these flower-like micelles even though these are made up of multiblock copolymers.

When this ratio of loop/bridge is relatively small, the bridging chains can produce an association, which, then can yield the phase-separated solution at low polymer contents,[75,76] and physical networks in case of high polymer contents.[62-67,70,77,78]

1.3.1. Rheological property analysis in BCP/solvent gel

Unlike the case of diblock copolymers where the non-similar chains repel each other due to thermodynamic incompatibility, having multiblock copolymers like ABA, ABABA or ABABABA multiblock copolymers, the bridging of the chains creates an entropic attraction between the corresponding micelles.[67,70,75,77] In addition to that, the multiblocks, unlike the diblock copolymers, can form different midblock driven conformations. These physical cross-linked networks contribute to the physical properties of the gels. The bridges and the interlocking loops can transmit stress between the corresponding micelles and thus can contribute to the shear modulus of the gel. However, the unentangled micelles don't contribute into such stress of the material. Using the rubber elasticity theory, for a gel, the shear modulus, G' for an Neohookean material isotrophically swollen by solvent can be expressed[79]as following:

$$G = \upsilon k_B T \frac{d^2}{{R_0}^2} = f\left(\frac{\varphi_p \rho RT}{M}\right)\frac{d^2}{{R_0}^2} \qquad (3)$$

Here,

υ = number density of the elastically active chains

M = molecular weight of the corresponding polymer

f = fraction of the elastically active polymer molecules

${R_0}^2$ = mean-squared end-to-end distance of the corresponding equilibrium solution of molecules with a molecular weight (MW) equal to the average MW between cross-links.

Among the remaining parameters, ρ and φ_p represent the volume fraction and the density of the polymer, respectively.

As is expected, for triblock copolymer gels, the increase in bridge/loop ratio is synonymous to the increase in the number of elastically active chains, and thus the modulus is also increased. Previous studies of triblock copolymers in midblock selective solvents using Monte Carlo simulation [60,80,81] and experimental dielectric studies [62] reported that the number of bridges is increased with increase in the concentration of polymer. Semenov's theoretical studies on triblock copolymer gel indicated that the triblock micelles strongly attract each other and that the bridge fraction scales with the micelle aggregation number and the concentration of micelles in solution. [70]

Micellization of diblock and triblock copolymers were detail studied using theoretical tools, especially the critical micelle concentration (CMC) of diblock copolymers in homopolymer solvents [82]; diblock[83] and triblock[84] in a selective solvents were reported to be well-studied. In those studies, the researchers used free energy approach in determining the critical micelle concentration in these cases. Their studies identified the scaling relationships between block length, core and corona radius, and aggregation number. Additional experimental studies [76] and theoretical studies[85,86] for styrene-based systems focused for triblocks in selective solvents were also conducted to scale the aggregation number with concentrations of triblocks. It was concluded out of the findings from those examinations that the increase in the triblock concentration is accommodated by creating more micelles, not by increasing the aggregation number.

For the sake of comparison, it's notable to mention that the analogous systems of dilute solutions of surfactants or copolymers [75] and the Pluoronic systems in water[87] depicts opposite behaviors regarding the scaling of aggregation number and the increase in the concentration of the block copolymers.

The concept of aggregation number (g), the number of endblocks per micelle core, can further be illustrated as a relationship considering that the triblock copolymer gels can be modelled as a random distribution of hard spheres in a liquid: [54,58,60,88,89]

$$g = \left(\frac{2\rho\varphi_p N_{av}}{M}\right)\left(\frac{4\pi R^3}{3\eta}\right) \quad (4)$$

where N_{av} represents the Avogadro number. Comprising the same parameters, it is also possible to evaluate the average distance between micelle cores, D, as following-

$$D = \left(\frac{4\pi R^3}{3\eta}\right)^{1/3} \quad (5)$$

Theses equations again can bolster the idea that if new polymer chains are put into a system, they need to be accommodated using some mechanisms. The two such possible mechanisms are: either the average spacing between micelles will decrease, or the aggregation number will be increased. The increase in the average micelle spacing favors the formation of loops as accommodating more inter-micelle space requires the midblock fractions (bridges) to be more stretched.

Detail studies on ABA/solvent forming physical gel[57,65,67] also depicted that these materials show characteristics dynamic elastic modulus (G') as independent of frequency and as greater than the dynamic viscous modulus (G'') in the linear viscoelastic regime.[90] These triblock copolymer/midblock selective solvent gels can retain the properties of both liquid phase along the robust nature of elastic solid.

Block copolymer microstructures are also reported to be susceptible to the alignment by flow, and in thin films, electric fields can also generate the alignment of the nanostructures. [91,92] Koppi et. al proved that different flow conditions can orient the lamellae either parallel or perpendicular to the shear planes. [93] Both diblocks and ABA triblocks are mostly proved to show similar response

towards the shear flow and it was concluded that chain architecture does not play deterministic role in such behavior of the materials towards the shear flow. However, the other studies [94,95] regarding ABABA pentablocks refute the notion of that assumption. It was observed that the multiblock architectures can provide processing advantage, because of their near absence of parallel orientation, in addition to the generation of "forbidden" transverse orientation. Among different diblock morphologies like S^{bcc}, C, G, L, the response toward the flow orientation, even in the linear viscoelastic limit, the response is very different.[96] Hence, while doing the rheological characterization of the BCP based materials, it's the low frequency dynamic moduli that was found to be the most accessible route to characterizing thermally induced order-order-transition (OOTs) and the order-disorder-transition (ODTs).[97]

1.3.2. Addition of AB diblock into ABA/MO gel to further increase the bridge fraction

A previous study [66] carried out to examine the impact of systematically adding AB diblock copolymers into ABA/MO gel at constant copolymer composition was observed to enhance the solid like behavior of the gel, as is indicated by the increase in magnitude of dynamic elastic modulus. It was also reported that addition of AB diblock to a non-gelled ABA/solvent can induce the gelation in the system. [6161]

It was found that the presence of AB diblock created the phenomenon of 'tail-induced volume exclusion' within the micellar coronas and thus the population of bridged B midblocks are increased, which in turn also contributed in increasing the dynamic elastic modulus (G'). In another study of ABA lamellar triblock copolymer using self-consistent field theory [98] also revealed such increase in the bridged B midblocks upon addition of the AB diblock copolymer. It was found that, as the interfacial volume exclusion was increased due to the addition of AB, the midblock fractions of ABA/AB exceeds the midblock fraction in the pure ABA copolymer (figure

1.8). This is an important phenomenon that can further be explored in multiblock copolymer/midblock selective solvents, where multiblock copolymer will be comprised of block copolymers having more than one midblock.

1.3.3. Insight into some common applications of ABA/solvent gel

Among many other types of applications, the styrene based ABA triblock copolymer have been used in various applications as thermoplastic elastomers,[99]as substrate for microfluidic systems,[100] and as pressure sensitive adhesives.[101-103] Triblock in liquid crystal solvents were also studied and found to benefit out of homogeneity of self-assembled elastic solids with rapid switching times and excellent optical properties. [104] Block copolymers comprised of hydrophilic midblocks and short hydrogenated or fluorinated hydrophobic end blocks found extensive use in thickening agents in surface coatings and cosmetics, oil recovery, and waste water treatment.[50,52] Hydrogels made up of triblocks with poly(lactide) endblocks attracted much interest in the field of tissue engineering as their elastic modulus is similar to that of the soft tissue.[105]

Thermoreversible gels [106,107] are another important type block copolymer-based gels found use in different fields. The interaction between micelle forming minor component, e.g endblcks and the solvent, χ_{AS} is dependent on temperature, and as result of such kind of dependency their micelle forming characteristics can be tuned according to the change in temperature (figure 1.9).[108]

In the absence of long range ordering, two transition temperatures predominantly play important role in dictating the thermoreversibility of block copolymer gels. The first one is the critical micelle temperature (CMT), at which the micelle forming parts, e.g. minor blocks of polymer molecules start to aggregate, and micelles are formed. Decreasing in temperature worsens the solvent quality of the corresponding micelle forming blocks and the solvents are expelled from the aggregates. [108]

The glass transition temperature (Tg) is the second one below which still slightly swollen micelle forming domains form elastic solid. Here, one thing worth mentioning is that the systems depends on endblock crystallization for network formation, the gelation kinetics is much slower than that in the system governed by glass transition temperature.[108] Both of these transitions were also found to be dependent of block length and gel concentration as was evident from the study of PMMA-PnBA-PMMA triblocks and alcohol based systems.[109] as the CMT of this system is below 100C and the glass transition temperature is slightly above the room temperature, the system is particularly useful for different sytems, especially as it's easier to remove the volatile alcohol for processing applications where casting must be dried before sintering.

Acrylic or styrene-based gel systems usually have long relaxation times [110], while the aqueous systems lack such long relaxation time and tend to gel on heating. [81]Styrene based commercially available SEBS triblock/MO based gels can also form thermoreversible gels. However, such system has broader transition between liquid and solid behavior. [57]

It's also worth mentioning that both too short and too long relaxation times can be problematic depending on the type of processing application, especially for molding. In case of too short relaxation time at low temperature, the gel characteristics of the material, necessary for molding, will be lost. On the other hand, having very high relaxation time will make the viscosity too high and thus it will be difficult for the material to pour into mold.

1.4. Interplay of the molecular bridge and elasticity in multiblock copolymer-based systems

While the nanostructures have important applications, sometimes, block copolymer-based systems are designed to obtain sets of physical properties e.g. modulus, thermal conductivity, birefringence, and dielectric constant etc. Among these intended properties, correlating the linear and non-linear *practical toughness* for linear bicomponent diblock, tribock and pentablock copolymer were detail studied using a series of hydrogenated series of these class, and it was concluded that this mesoscopic property can be roughly correlated to the bridge fractions connecting the domains. Using a real-space implementation of SCFT[111], there was another theoretical attempt of such correlation in case of ABABA pentablock copolymer.[112] The correlation is intuitive considering the fact that to propagate the crack throughout the samples made up of these material, the bridging blocks must either be cleaved or one of dangling ends corresponding to the block copolymer chains must be pulled out of the mesophase, that will eventually lead into the dissipation of great amount of energy. However, it's worth mentioning that such properties are not solely dependent of the molecular bridge fractions. Some other related determining factors in the context are expected to be grain size, processing and thermal history of the mesophase morphology, orientation of the nanostructure within the material, molecular weight.

One good way to capture the mesoscopic properties like elasticity is to consider how individual chains behave while dealing with the interplay of energy and entropy contributions towards the chain conformations. Previous study [113] reported the results of such single chain stretching of multiblock copolymers in selective solvent. In selective solvents, the multiblock copolymers, because of the self-assembly nature, form secondary and tertiary structures, which results different hierarchical elastic responses. In the understanding of rubber elasticity, it's the classical practice to study the single chain elasticity before getting into the exploration of elastic properties of the

mesoscopic network. [73,114,115]These chains can either follow Gaussian chain model or non-Gaussian model. The elastic nature of the chains depends on the model the chains are following. For Gaussian model, purely entropic nature of the elastic force exists and the number of chain conformations of a chain having fixed ends at constant distance R defines it. The number of conformations obtained in this case can be expressed as, $P(\mathrm{R}) \propto \exp(-3R^2/(2Nb^2))$. Here, Nb^2 is the mean-square end-to-end distance of the chain, $\langle R^2 \rangle$. Thus, the resulting force can be expressed with the Hooke's law based on entirely entropic contribution:

$$\varphi = \frac{3k_BT}{b}\left(\frac{R}{Nb}\right) \tag{6}$$

While considering this force, the energetic contribution is not neglected, and this linear regime of the force can be detected by experiments. However, for the larger extensions, R/b > $\sqrt{N}$, of the chains, the chain conformations decrease in number. Because of that, the force rises strongly at large deformations of the chains, and hence, the finite chain length needs to be considered.

Now, in a good solvent, the chains follow the self-avoiding walks (SAW), which is non-Gaussian in nature. The chains depict non-linear response of force and is expressed as following:

$$\varphi \cong \frac{k_BT}{b}\left(\frac{R}{Nb}\right)^{3/2} \tag{7}$$

It's the asymptotic free energy, $F \propto k_BT\,(R/(N^{3/5}b))^{5/2}$ is the reason why such non-linear response is observed.

1.4.1. Multiblock copolymers in a good solvent

As it was discussed in earlier sections, linear $(AB)_n$ multiblock copolymers can be a seen as a polymer chain consisting of numbers of diblock copolymers bonded head to tail. Under different circumstances, these multiblock copolymers can form different types of micelles starting from

"hairy" micelles to micelles where multiple micelles are joined together by the extended polymer chain.

In "hairy" micelles, the cores are made up of A monomers and the coronas consists of B monomers. Usually, such a morphology is formed when the block copolymer molecules tend to aggregate predominantly governed by loops. The optimal size of these micelles are determined as a result of interplay of several factors like the interfacial energy, the free energy associated with the deformation of core and corona, and the excluded volume effect generated repulsion inside the coronas.

In the light of the detail derivation of these factors in interacting micelle and non-interacting micelles, as is reported in a previous study [113], the preferred micelles sizes can also be suggested. In non-interacting micelles, multiblock copolymer micelles consist of optimal number of blocks, p^*, and are expected to take self-avoiding walk (SAW) if there is no attractive interaction between the micelles. That indicates that there is no exchange of bridges among the neighboring micelles. As a result of that the coronas repel each other, and yield SAW pattern of mobility. The size of these "hairy micelles" will thus be $R_m = R_A + R_B$. As a whole, the radius of the noninteracting micelle can be obtained from the following relationship:

$$R_{multi} \approx R_m \left(\frac{n_a}{p^*}\right)^{3/5} \quad (8)$$

Where, n_a denotes the number of A blocks in the micelle forming multiblock copolymer.

On the other hand, if the A-B blocks possess attractive interaction between them, adsorption of loops and bridges will yield secondary structures in the system. Combination of more than two such micelles, where their coronas overlap with each other, form a self-assembled globule in a

large scale. This analogous to the formation of two-dimensional semidilute solution. In the figure 1.10, a dense super globule consisting of such secondary structure forming block copolymer forming micelles are depicted. As is evident that the cores stays in the same neighborhood as a result of having adsorbed coronas on the surface of the spherical surface of A type block copolymers. The size of such a globule can be obtained as

$$R_{multi} \approx (\frac{n_a}{p^*})^{1/3} R_m \quad (9)$$

Regarding the mechanical properties, such formation of secondary structure produces distinctive elastic responses in multiblock copolymer based systems. In the same manner, interconnection of the corona blocks forming the cores can also form secondary structures by exchanging molecular bridges. It's analogous to the formation of physical microgels, and this secondary structure also induce elastic behavior in the corresponding block copolymer-based systems.

1.5. Elastic response of multiblock copolymers under uniaxial stretching

Since the block copolymers form both primary (micelle core) and versatile secondary structures, the result of the application of any external force evolves around the sequential unfolding of these structures. The deformation starts with the change of the self-assembly structure from sphere to elongated ellipsoid, the applied force and the extension follows the linear relationship in this region. As the sequential step, the micelles aligned with the direction of external pulling gets dissociated leading to the unfolding of the primary structure, micelle core, as the next step. As is reported in a previous study, there exists a regime which corresponds to the co-existence of the elongated globular structure and the aligned micelle structure. [113] As a result of that, a van der Waals loop type force-extension curve appears for these systems upon the application of external force. Such case, thus, yields a tadpole like structure as route of the dissociation of the individual

micelles from their host globular structure (figure 1.11). During this unfolding of the secondary structure, the force remains constant from the onset of unfolding as long as the secondary structure is formed by the bridges of adsorption category. This uncoiling of this secondary structure corresponds to the energetic scenario where the elastic energy exceeds the gain in energy as a result of adsorption between micelles. For obtaining the wholistic view of the response, it's required to consider the next step as well, which is the unfolding of the micelle cores. Several case of the structural response upon application of external force is noted in the following sections in the light of another reported study [113].

1.5.1. Case-1: Adsorption of coronas between cores generated secondary structure breaking

Considering that the number of B blocks per unit core are is constant, and that, at equilibrium, the core surfaces hold position at approximately D distance from each other, kinematic and energetic picture can be drown for the breaking of secondary structure. If the fraction of the surface of core covered by adsorbed polymer is σ_{eff}, the [116]Derjaguin approximation[116,117] can be used to evaluate the spring constant for the bridging contacts as following-

$$k_{mD} = k_B T \sigma_{eff} R_m / D^3 \quad (10)$$

This, the free energy associated with the debridging can be expressed as

$$F^* = -k_B T R_m / D \quad (11)$$

However, the influence of such bridging attraction becomes negligible on the scales larger than individual micelles. The dense superglobule micelles formed because of micelle self-assembly attached by adsorbing B blocks yields an effective surface tension of the super globule as –

$$\gamma_{eff} = \frac{F^*}{{R_m}^2} \quad (12)$$

Therefore, according to Halperin and Zhulina[118] , the critical force for unravelling the superglobule can be expressed as $\varphi_c = k_B T \sigma_{eff}/D$. As a following step of this unraveling, the extension of the strings of micelles occurs followed by the relaxation of the adsorbed bridges at the critical force $\varphi_c = \sim F^*/D$. Testing the mechanical response upon application of external force is expected to depict such linear constant force regime, $\varphi_c = k_B T/D$, under imposed elongation.

It was thus concluded that the overall extension of the secondary structure can be characterized by two subsequent steps following the initial ellipsoidal deformation. As the first of two, the deformation of the corona can be attributed to the constant force plateau in force extension curve. Thereafter, additional stretching of the strings is resulted from the increase in force, and the output is obtained as a linear response.

1.5.2. Case-2: Topological bridges generated secondary structure breaking

Now, secondary structure can also be the output of connected coronas of the block copolymers where one multiblock visits the micelle more than once (figure 1.13). This way, the neighboring micelles are connected by the B blocks, the required force differs to deform these microgels than what was needed uncoil simply corona adsorbed joined micelles. According to the studies of Happerin and Zhulina[118], this force is much larger than the former case. The corresponding critical force is expressed as

$$\varphi_{cr,m} = k_B T/d_{fl} \qquad (13)$$

This critical force is much smaller than both the analogous force associated with the extraction of an A block and the force required to rupture micelle-micelle contact. However, the debridging force is much higher as it associates with the extraction of the A blocks involved in all bridges.

1.5.3. Case-3: Dissolution of primary structure

The study of the same researcher also illuminated the dissociation of the primary structure, the individual micelles. While doing so, the elastic response of the individual chains of multiblock copolymers were considered as a response to the applied external force. At the magnitude of force when the cores start breaking down, all structures are dissolved into a series of *Pincus blobs.* It's also intuitive that while going through the extension under force, the optimal sizes of the core and corona gets shifter towards smaller sizes. As a sequential process of the breaking of each micelle, the release of each core forming block is followed by bringing the corona blocks aligned in the direction of the applied force. As the unfolding happens, the release of the first block from micelle core is expected to drop the value of force to smaller extent as a result of abrupt release of the attached corona. The discreteness of such occurrence as an output of the repetition of such process yields *sawtooth pattern* in the force-extension curve. Additional force eventually will stretch the system at an extent so that the remaining micelle will become unstable and lead to abrupt release of the open chain configurations. This is expected to provide steeper decrease in the *sawtooth pattern* of the force extension curve. However, in the systems having many micelles, while one individual micelle breaks down, there might still be enough strength of the remaining micelles that can provide enough resisting force to mitigate the abruptness in decrease of the force due to the individual release of core blocks. At the finale of the process, all core forming micelles can uncoil resulting the Halperin and Zhulina's tadpole picture. [118]

In addition to the contributing factors illustrated in previous sections, it's notable to mention that, A-B-A type thermoplastic elastomers based on styrene-butadiene & styrene-isoprene was also studied to explore the impact of molecular architecture on their stress-strain properties.[119] Their study aimed to find out several pertinent answers on how *block lengths, compositions,* and the

molecular composition of the corresponding blocks can impact the physical properties of the block copolymers. The polystyrene content was the 'reinforcing filler' while the polybutadiene functioned as the cross-linking segment in their system in bulk block copolymeric system. The investigation, as the results are reported in figure 1.13, proved that both of the tensile stress and the ultimate tensile strength depends only on the composition of polystyrene, not on the block lengths.

1.6. Computational approach as an understanding and guiding tool

Theoretical and simulation studies has enumerated significant role in understanding the experimental observations by means of identifying and explaining different types of metastable structures observed in experiments.[120] The polymer self-consistent field theory (SCFT) by Matsen and Schick[121,122] was one of the pioneering implementation that enabled the thermodynamics and structural analysis of the polymeric spatially periodic distinctive mesophases characterized by arbitrarily complex symmetry such as the gyroid phase of block copolymers. Having in depth understanding of the self-assembly principles along the development of enhanced synthetic routes enable the experimentalists obtain variety of useful block copolymer nanostructures. Such exploration associated with increased number of chemically distinct blocks and architectural complexity require continuously increased investigation into finding out additional number of binary interactions such as interfacial tension or Flory "χ" parameters. It's noteworthy to mention that such richness in the dissimilarity of the blocks provides numerous consistent complex morphologies. In addition to the novelty of connected copolymer blocks, having rigid or sterically constrained blocks such as liquid crystalline, conjugated blocks or dendrimers can also produce different self-assembly behavior.

While having those rich mesophases are extensively useful in various fields, there are too many parametric matrixes that the experimentalists need to deal with to pin point the desired product. Some of those particular designing factors are block compositions, architecture, molecular weight and temperature, and optimizing such a big array of contributing factors are very laborious to explore. Further difficulty arises as, even well-developed morphologies can be so many in number that the massive scale of required characterization become a difficult task to deal with. Because of these challenges, theoretical studies and understandings became very useful as both the guiding and understanding tool for the experimentalists as more complex block copolymer systems kept evolving with versatile focus of applications.

1.6.1. Choice of simulation method: dissipative particle dynamics (DPD)

Advanced computational efficiency coupled with the high-performance computation capability enhanced the study of complex fluid applications at different level of interest ranging from electronic level to macroscale. It's crucial to determine which simulation approach will be suitable for any intended field of study. Several atomic scale investigations of the different interactions between polymer and discrete nanofillers have been reported by different methods like analytical continuum mechanics,[123,124] reactive potentials,[125,126] and classical force fields.[127-129] In such atomistic methods, the number of particles used in the simulations is equal to the real system which is mimicked to explore the real time properties; hence, as the scale of the system under considerations is increased significantly, the complexity of the whole simulated system becomes computationally more challenging. This fact leaves the atomistic simulations as a non-suitable choice for exploring the overall morphology at length-scales most relevant to the nanocomposites, i.e. tens of nanometers (nm) to microns. Other than the challenge regarding size scale, the biggest challenge lies in simulating over the equilibration times that are *orders of magnitude* longer than

a nanosecond, a typical limit of atomic scale simulations, the most common being the molecular dynamics (MD).

On the other hand, coarse-grained methods offer an attractive solution and allow computationally efficient mesoscale simulations. Such mesoscale simulation techniques can be used to overcome the length and time-scale restrictions, and a large number of particles can be simulated for much longer time to study equilibrium morphology and structural properties effectively. [130] The coarse-grain simulation systems like dissipative particle dynamics (DPD) is such a modelling attempt in that direction.

DPD simulation is a point particle- based method where a dissipative particle commonly called a 'bead' represents the center of mass of a mesoscopic portion of fluid. Each bead represents a collection of N_{eg} - (MD) atoms or monomers, where N_{eg} is called the coarse-graining number and their atomic level details are ignored.

From physical point of view, each of these dissipative particle or bead is considered as a collection of molecules that can move in a coherent fashion. The positions and momenta of the spherical "beads" are propagated and updated in a continuous phase space at discrete time steps. But, unlike the Lennard-Jones forces of interaction in MD simulation, here, the "beads" feel a short range soft pair-wise conservative potential which is the fundamental characteristic of the system. To elaborate it further in details, if the interparticle distance tends to become zero, the force between the corresponding particles become infinity as can be observed from the following Lennard-Jones equation, widely used in MD simulation-

$$u(r) = 4\epsilon \left[\frac{\sigma_{LJ}}{r}^{12} - \frac{\sigma_{LJ}}{r}^{6} \right] \quad (14)$$

Such hard-core characteristic of the force employed in MD simulations makes the method impractical for larger systems as it limits the maximum timesteps that can be employed to numerically integrate the equations of motion. On the other hand, in DPD simulations, a collection of particles is grouped (coarse-grained) together as is depicted in figures 1.14 and 1.15.[131,132]

Now if these DPD clusters become larger in size and time employed for integration of the equation of motion is long enough, the effective potential between these interacting groups become softer. In plain narrative, this 'soft potential' means that the force between the interacting particles is no longer infinite at zero separation. Such behavior can reasonably mimic the fluids as there, the centers of the packets of corresponding fluids can overlap while they pass through each other. Thus, the choice of such soft potential enables both to simulate larger fluid system and to have an effective time-step of several picoseconds, 3-4 orders of magnitude larger than typical time-steps employed in a MD simulation. [133]

The total force, F_{ij}, interacting between two DPD beads, $i\ and\ j$ can be expressed as the following-

$$F_{ij} = {F_{ij}}^{C} + {F_{ij}}^{D} + {F_{ij}}^{R} \qquad (15)$$

Here, ${F_{ij}}^{C}$ is the purely repulsive conservative force. ${F_{ij}}^{D}$ represents the damping or dissipative (frictional) force characterizing the viscosity that slows down the particle motion with respect to each other. The remaining term in the equation, ${F_{ij}}^{R}$,is the representation of random (stochastic) force that characterizes the thermal or vibrational energy of the system. It's to be noted that for added characterization of the systems of consideration, additional force/s need to be considered. For example, to mimic the polymer chains made up of DPD beads, spring force acting between the beads need to be considered, further detail of that will be illustrated in the subsequent sections containing DPD simulation of polymer chains. Other than using the conservative potential, the

way how the DPD beads act to maintain the thermostat using dissipative (frictional) and random (noisy) force, the beads can also be considered as a collection of self-repelling frictional and noisy balls. As three types of forces associated here satisfy the Newton's Third Law, the classical DPD model conserve the mass and momentum balance, and such conservation is the essential key to dictate the hydrodynamic behavior of a fluid at a large scale.[134,135]It's pertinent to mention that in another analogous method, Brownian Dynamics, only mass diffusion can be studied as the total momentum of the particles is not conserved. It's also noteworthy to distinguish DPD from MD simulation in the context of potential used in both methods. The potential, chosen in MD, is based on theoretical-molecular model of the physical system to be simulated, whereas, in principle, DPD associates with the potentials of forms that are not dependent on the physical systems. However, DPD potentials involve parameters that require to be chosen properly to obtain accurate approximation of the corresponding systems. For the application of DPD simulations in polymer solutions and to investigate the thermodynamics of mixing of different polymeric materials, Groot and Warren[136] developed correlation between interaction potentials and Flory-Huggins theory which is well known in its application to the equilibrium thermodynamics of polymer solutions.[137,138]

In general, Dissipative particle dynamics (DPD)[139] simulation has been extensively used as a popular mesoscale technique in various fields of study like polymer-CNT composites,[140-142] morphology of block copolymers,[143] micelle formation,[144-146] polymer viscosity, self-assembly of nanoparticles in polymers.[147] Usually, polymer molecules are mimicked in DPD by using linkage of several beads with springs, either Hookean or FENE[148]. The quality or the selectivity of the solvents can be simulated by careful selection of the solvent-solvent and solvent-monomer conservative interactions. One important characteristic of the polymer-based systems is

entanglement formed by the polymer macromolecules. As the soft interactions between DPD beads allow polymer crossing[149], this simulation model, with current design, is unable to mimic the entanglement of macromolecules. However, as the dynamic properties of the corresponding block copolymers were not the focus of study, this incapability of mimicking the entanglement is expected not to play any differentiating role regarding the outputs of study reported throughout the next chapters.

1.7. References

1. Seymour, R. B. Polymer science before and after 1899: notable developments during the lifetime of Maurits Dekker. *Journal of Macromolecular Science—Chemistry* 1989, *26*, 1023-1032.
2. Seymour, R. B. *History of polymer science and technology;* New York: Dekker: 1982.
3. Utracki, L. History of commercial polymer alloys and blends (from a perspective of the patent literature). *Polymer Engineering & Science* 1995, *35*, 2-17.
4. Bates, F.; Fredrickson, G. PHYS TODAY. *Phys Today* 1999, *52*, 32.
5. Lodge, T. P. Block copolymers: past successes and future challenges. *Macromolecular chemistry and physics* 2003, *204*, 265-273.
6. Ruiz, R.; Kang, H.; Detcheverry, F. A.; Dobisz, E.; Kercher, D. S.; Albrecht, T. R.; de Pablo, J. J.; Nealey, P. F. Density multiplication and improved lithography by directed block copolymer assembly. *Science* 2008, *321*, 936-939.
7. Bates, F. S.; Fredrickson, G. H.; Hucul, D.; Hahn, S. F. PCHE-based pentablock copolymers: Evolution of a new plastic. *AIChE J.* 2001, *47*, 762-765.
8. Cochrane, C.; Koncar, V.; Lewandowski, M.; Dufour, C. Design and development of a flexible strain sensor for textile structures based on a conductive polymer composite. *Sensors* 2007, *7(4)*, 473-492.
9. Mattmann, C.; Clemens, F.; Tröster, G. Sensor for measuring strain in textile. *Sensors* 2008, *8(6)*, 3719-3732.
10. Creton, C.; Hu, G.; Deplace, F.; Morgret, L.; Shull, K. R. Large-strain mechanical behavior of model block copolymer adhesives. *Macromolecules* 2009, *42(20)*, 7605-7615.

11. Feng, H.; Lu, X.; Wang, W.; Kang, N.; Mays, J. W. Block copolymers: Synthesis, self-assembly, and applications. *Polymers* 2017, *9*, 494.
12. Ruzette, A.; Leibler, L. Block copolymers in tomorrow's plastics. *Nature materials* 2005, *4*, 19.
13. Holden, G.; Legge, N.; Quirk, R.; Schroeder, H. Thermoplastic Elastomers, 1996. *Hanser-Gardner Publications, Cincinnati* .
14. Knoll, K.; Nießner, N. In *In Styrolux and styroflex -from transparent high impact polystyrene to new thermoplastic elastomers: Syntheses, applications and blends with other styrene based polymers;* Macromolecular Symposia; Wiley Online Library: 1998; Vol. 132, pp 231-243.
15. Ryu, C. Y.; Ruokolainen, J.; Fredrickson, G. H.; Kramer, E. J.; Hahn, S. F. Chain architecture effects on deformation and fracture of block copolymers with unentangled matrices. *Macromolecules* 2002, *35*, 2157-2166.
16. Tallury, S. S.; Spontak, R. J.; Pasquinelli, M. A. Dissipative particle dynamics of triblock copolymer melts: A midblock conformational study at moderate segregation. *J. Chem. Phys.* 2014, *141*, 244911.
17. Bates, F. S.; Hillmyer, M. A.; Lodge, T. P.; Bates, C. M.; Delaney, K. T.; Fredrickson, G. H. Multiblock polymers: panacea or Pandora's box? *Science* 2012, *336*, 434-440.
18. Hermel, T.; Hahn, S.; Chaffin, K.; Gerberich, W.; Bates, F. Role of molecular architecture in mechanical failure of glassy/semicrystalline block copolymers: CEC vs CECEC lamellae. *Macromolecules* 2003, *36*, 2190-2193.
19. Matsushita, Y.; Mogi, Y.; Mukai, H.; Watanabe, J.; Noda, I. Preparation and morphology of multiblock copolymers of the (AB) n type. *Polymer* 1994, *35*, 246-249.

20. Christodoulou, S.; Driva, P.; Iatrou, H.; Hadjichristidis, N. Synthesis and micellization behavior of Janus H-shaped A2BC2 terpolymers. *Macromolecules* 2008, *41*, 2607-2615.
21. Schlick, S.; Levy, M. Block-polymers of styrene and isoprene with variable distribution of monomers along the polymeric chain. Synthesis and properties. *J. Phys. Chem.* 1960, *64*, 883-886.
22. Cooper, W.; Hale, P.; Walker, J. Elastomeric block polymers from ethylene sulphide. *Polymer* 1974, *15*, 175-186.
23. Price, C.; Lally, T.; Stubbersfield, R. Microphase separation in an ABC block terpolymer. *Polymer* 1974, *15*, 541-543.
24. Fielding-Russell, G.; Pillai, P. Phase structure of solution cast films of α-methylstyrene/butadiene/styrene block copolymers. *Polymer* 1974, *15*, 97-100.
25. Iatrou, H.; Hadjichristidis, N. Synthesis of a model 3-miktoarm star terpolymer. *Macromolecules* 1992, *25*, 4649-4651.
26. Pan, J.; Chen, M.; Warner, W.; He, M.; Dalton, L.; Hogen-Esch, T. E. Synthesis of block copolymers containing a main chain polymeric NLO segment. *Macromolecules* 2000, *33*, 4673-4681.
27. Watkins, D. M.; Fox, M. A. Synthesis and photophysical characterization of aryl-substituted polynorbornenediol acetal and ketal multiblock copolymers. *Macromolecules* 1995, *28*, 4939-4950.
28. Iatrou, H.; Hadjichristidis, N. Synthesis and characterization of model 4-miktoarm star co- and quaterpolymers. *Macromolecules* 1993, *26*, 2479-2484.

29. Yin, R.; Amis, E. J.; Hogen-Esch, T. E. In *In Synthesis of macrocyclic polystyrene-polydimethylsiloxane block copolymers;* Macromolecular Symposia; Wiley Online Library: 1994; Vol. 85, pp 217-238.
30. Mogi, Y.; Nomura, M.; Kotsuji, H.; Ohnishi, K.; Matsushita, Y.; Noda, I. Superlattice structures in morphologies of the ABC triblock copolymers. *Macromolecules* 1994, *27*, 6755-6760.
31. Talingting, M. R.; Munk, P.; Webber, S.; Tuzar, Z. Onion-Type Micelles from Polystyrene-block-poly (2-vinylpyridine) and Poly (2-vinylpyridine)-block-poly (ethylene oxide). *Macromolecules* 1999, *32*, 1593-1601.
32. Fendler, J. H. Membrane mimetic chemistry: characterizations and applications of micelles, microemulsions, monolayers, bilayers, vesicles, host-guest systems, and polyions; John Wiley & Sons Inc: 1982.
33. Erhardt, R.; Böker, A.; Zettl, H.; Kaya, H.; Pyckhout-Hintzen, W.; Krausch, G.; Abetz, V.; Müller, A. H. Janus micelles. *Macromolecules* 2001, *34*, 1069-1075.
34. Erhardt, R.; Zhang, M.; Böker, A.; Zettl, H.; Abetz, C.; Frederik, P.; Krausch, G.; Abetz, V.; Müller, A. H. Amphiphilic Janus micelles with polystyrene and poly (methacrylic acid) hemispheres. *J. Am. Chem. Soc.* 2003, *125*, 3260-3267.
35. Orilall, M. C.; Wiesner, U. Block copolymer based composition and morphology control in nanostructured hybrid materials for energy conversion and storage: solar cells, batteries, and fuel cells. *Chem. Soc. Rev.* 2011, *40*, 520-535.
36. Molau, G. E. Colloidal and morphological behavior of block and graft copolymers. In *Block Polymers*Springer: 1970; pp 79-106.

37. Bates, F. S.; Fredrickson, G. H. Block copolymer thermodynamics: theory and experiment. *Annu. Rev. Phys. Chem.* 1990, *41*, 525-557.
38. Schaertl, W.; Tsutsumi, K.; Kimishima, K.; Hashimoto, T. FRS study of diffusional processes in block copolymer/homopolymer blends containing glassy spherical micelles. *Macromolecules* 1996, *29*, 5297-5305.
39. Fredrickson, G. H.; Bates, F. S. Dynamics of block copolymers: theory and experiment. *Annual Review of Materials Science* 1996, *26*, 501-550.
40. Caplan, M.; Horowitz, C. Colloquium: Astromaterial science and nuclear pasta. *Reviews of Modern Physics* 2017, *89*, 041002.
41. Jackson, E. A.; Hillmyer, M. A. Nanoporous membranes derived from block copolymers: from drug delivery to water filtration. *ACS nano* 2010, *4*, 3548-3553.
42. Szwarc, M. Living polymers. Their discovery, characterization, and properties. *Journal of Polymer Science Part A: Polymer Chemistry* 1998, *36*.
43. Geoffrey, H.; Ralph, M. *Block polymers of monovinyl aromatic hydrocarbons and conjugated dienes* 1966.
44. Gergen, W.; Lutz, R.; Davison, S.; Holden, G.; Legge, N.; Schroeder, H. Thermoplastic Elastomers. *Hanser Publisher, Munich* 1996, 297.
45. Lodge, T. P.; Pudil, B.; Hanley, K. J. The full phase behavior for block copolymers in solvents of varying selectivity. *Macromolecules* 2002, *35*, 4707-4717.
46. Hanley, K. J.; Lodge, T. P.; Huang, C. Phase behavior of a block copolymer in solvents of varying selectivity. *Macromolecules* 2000, *33*, 5918-5931.
47. Hanley, K. J.; Lodge, T. P. Effect of dilution on a block copolymer in the complex phase window. *Journal of Polymer Science Part B: Polymer Physics* 1998, *36*, 3101-3113.

48. Förster, S.; Plantenberg, T. From self-organizing polymers to nanohybrid and biomaterials . *Angewandte Chemie International Edition* 2002, *41(5)*, 688-714.
49. Matsen, M.; Thompson, R. Equilibrium behavior of symmetric ABA triblock copolymer melts. *J. Chem. Phys.* 1999, *111*, 7139-7146.
50. Berret, J.; Calvet, D.; Collet, A.; Viguier, M. Fluorocarbon associative polymers. *Current Opinion in Colloid & Interface Science* 2003, *8*, 296-306.
51. Agrawal, S. K.; Sanabria-DeLong, N.; Tew, G. N.; Bhatia, S. R. Rheological characterization of biocompatible associative polymer hydrogels with crystalline and amorphous endblocks. *Journal of materials research* 2006, *21(8)*, 2118-2125.
52. Annable, T.; Buscall, R.; Ettelaie, R. Network formation and its consequences for the physical behaviour of associating polymers in solution. *Colloids and Surfaces A: Physicochemical and Engineering Aspects* 1996, *112*, 97-116.
53. Krishnan, A. S.; Smith, S. D.; Spontak, R. J. Ternary Phase Behavior of a Triblock Copolymer in the Presence of an Endblock-Selective Homopolymer and a Midblock-Selective Oil. *Macromolecules* 2012, *45*, 6056-6067.
54. Nie, H.; Bansil, R.; Ludwig, K.; Steinhart, M.; Koňák, Č.; Bang, J. Time-Resolved Small-Angle X-ray Scattering Study of the Kinetics of Disorder− Order Transition in a Triblock Copolymer in a Selective Solvent for the Middle Block. *Macromolecules* 2003, *36(21)*, 8097-8106.
55. Kleppinger, R.; Mischenko, N.; Reynaers, H. L.; Koch, M. H. J. Long-range order in physical networks of gel-forming triblock copolymer solutions. *Journal of Polymer Science Part B: Polymer Physics* 1999, *37(15)*, 1833-1840.

56. Vega, D. A.; Sebastian, J. M.; Loo, Y.; Register, R. A. Phase behavior and viscoelastic properties of entangled block copolymer gels. *Journal of Polymer Science Part B: Polymer Physics* 2001, *39*, 2183-2197.
57. Laurer, J. H.; Mulling, J. F.; Khan, S. A.; Spontak, R. J.; Bukovnik, R. Thermoplastic elastomer gels. I. Effects of composition and processing on morphology and gel behavior. *Journal of Polymer Science Part B: Polymer Physics* 1998, *36*, 2379-2391.
58. Reynders, K. A. R. E. N.; Mischenko, N.; Kleppinger, R.; Reynaers, H.; Koch, M. H. J.; Mortensen, K. Ordering phenomena in ABA triblock copolymer gels. *Journal of Applied Crystallography* 1997*, 30(5-2)*, 684-689.
59. Mortensen, K. Structural studies of aqueous solutions of PEO-PPO-PEO triblock copolymers, their micellar aggregates and mesophases; a small-angle neutron scattering study. *Journal of Physics: Condensed Matter* 1996, *8(25A)*, A103.
60. Mischenko, N.; Reynders, K.; Koch, M. H. J.; Mortensen, K.; Pedersen, J. S.; Fontaine, F.; Graulus, R.; Reynaers, H. Small-angle x-ray and neutron scattering from bulk and oriented triblock copolymer gels. *Macromolecules* 1995, *28(6)*, 2054-2062.
61. Mortensen, K.; Brown, W.; Nordén, B. Inverse melting transition and evidence of three-dimensional cubatic structure in a block-copolymer micellar system . *Physical review letters* 1992, *68(15)*, 2340.
62. Watanabe, H.; Sato, T.; Osaki, K. Concentration Dependence of Loop Fraction in Styrene− Isoprene− Styrene Triblock Copolymer Solutions and Corresponding Changes in Equilibrium Elasticity. *Macromolecules* 2000, *33*, 2545-2550.
63. Watanabe, H.; Sato, T.; Osaki, K.; Yao, M.; Yamagishi, A. Rheological and dielectric behavior of a styrene− isoprene− styrene triblock copolymer in selective solvents. 2.

contribution of loop-type middle blocks to elasticity and plasticity. *Macromolecules* 1997, *30*, 5877-5892.

64. Laurer, J.; Mulling, J.; Khan, S.; Spontak, R.; Lin, J.; Bukovnik, R. Thermoplastic elastomer gels. II. Effects of composition and temperature on morphology and gel rheology. *Journal of Polymer Science Part B: Polymer Physics* 1998, *36*, 2513-2523.
65. Laurer, J.; Khan, S.; Spontak, R.; Satkowski, M.; Grothaus, J.; Smith, S.; Lin, J. Morphology and rheology of SIS and SEPS triblock copolymers in the presence of a midblock-selective solvent. *Langmuir* 1999, *15*, 7947-7955.
66. Spontak, R. J.; Wilder, E. A.; Smith, S. D. Improved network development in bidisperse AB/ABA block copolymer gels. *Langmuir* 2001, *17*, 2294-2297.
67. Raspaud, E.; Lairez, D.; Adam, M.; Carton, J. Triblock copolymers in a selective solvent. 2. Semidilute solutions. *Macromolecules* 1996, *29*, 1269-1277.
68. De Gennes, P. *Scaling concepts in polymer physics;* Cornell university press: 1979; .
69. Graessley, W. W. Polymer chain dimensions and the dependence of viscoelastic properties on concentration, molecular weight and solvent power. *Polymer* 1980, *21*, 258-262.
70. Semenov, A.; Joanny, J.; Khokhlov, A. Associating polymers: equilibrium and linear viscoelasticity. *Macromolecules* 1995, *28*, 1066-1075.
71. Rubinstein, M.; Leibler, L.; Colby, R. H. Dynamics of Reversible Networks. *Abstracts of Papers of the American Chemical Society* 1991, *202*, 172-POLY.
72. Tanaka, F.; Edwards, S. F. Viscoelastic Properties of Physically Cross-Linked Networks - Transient Network Theory. *Macromolecules* 1992, *25*, 1516-1523.
73. Edwards, S. F. The theory of polymer dynamics. 1986.

74. Colby, R. H.; Rubinstein, M. Two-parameter scaling for polymers in θ solvents. *Macromolecules* 1990, *23(10)*, 2753-2757.
75. Lairez, D.; Adam, M.; Carton, J.; Raspaud, E. Aggregation of telechelic triblock copolymers: From animals to flowers. *Macromolecules* 1997, *30*, 6798-6809.
76. Raspaud, E.; Lairez, D.; Adam, M.; Carton, J. Triblock copolymers in a selective solvent. 1. Aggregation process in dilute solution. *Macromolecules* 1994, *27*, 2956-2964.
77. Borisov, O.; Halperin, A. Micelles of polysoaps: the role of bridging interactions. *Macromolecules* 1996, *29*, 2612-2617.
78. Laurer, J. H.; Mulling, J. F.; Khan, S. A.; Spontak, R. J.; Bukovnik, R. Thermoplastic elastomer gels. I. Effects of composition and processing on morphology and gel behavior. *Journal of Polymer Science Part B: Polymer Physics* 1998, *36*, 2379-2391.
79. Ferry, J. D. Viscoelastic properties of polymers. 1980.
80. Kim, S. H.; Jo, W. H. A Monte Carlo simulation for the micellization of ABA-and BAB-type triblock copolymers in a selective solvent. *Macromolecules* 2001, *34(20)*, 7210-7218.
81. Annable, T.; Buscall, R.; Ettelaie, R.; Whittlestone, D. The rheology of solutions of associating polymers: Comparison of experimental behavior with transient network theory. *Journal of Rheology* 1993, *37(4)*, 695-726.
82. Leibler, L.; Orland, H.; Wheeler, J. C. Theory of critical micelle concentration for solutions of block copolymers. *The Journal of chemical physics* 1983, *79(7)*, 3550-3557.
83. Nagarajan, R.; Ganesh, K. Block copolymer self-assembly in selective solvents: Spherical micelles with segregated cores. *The Journal of Chemical Physics* 1989, *90(10)*, 5843-5856.
84. Procházka, O.; Tuzar, Z.; Kratochvíl, P. Association of a three-block copolymer BAB in selective solvents for blocks B: spherical micelles. *Polymer* 1991, *32(16)*, 3038-3044.

85. Wijmans, C. M.; Eiser, E.; Frenkel, D. Simulation study of intra-and intermicellar ordering in triblock-copolymer systems. *The Journal of chemical physics* 2004, *120(12)*, 5839-5848.

86. Nguyen-Misra, M.; Mattice, W. L. Micellization and gelation of symmetric triblock copolymers with insoluble end blocks. *Macromolecules* 1995, *28(5)*, 1444-1457.

87. Alexandridis, P.; Alan Hatton, T. Poly(ethylene oxide)□poly(propylene oxide)□poly(ethylene oxide) block copolymer surfactants in aqueous solutions and at interfaces: thermodynamics, structure, dynamics, and modeling. *Colloids and Surfaces A: Physicochemical and Engineering Aspects* 1995, *96*, 1-46.

88. Flanigan, C. M.; Crosby, A. J.; Shull, K. R. Structural development and adhesion of acrylic ABA triblock copolymer gels. *Macromolecules* 1999, *32(21)*, 7251-7262.

89. Bansil, R.; Nie, H.; Li, Y.; Liao, G.; Ludwig, K.; Steinhart, M.; ... Lal, J. Structure and ordering kinetics of micelles in triblock copolymer solutions in selective solvents. *Macromolecular Symposia* 2002, November, *90(1)*, 161-172.

90. Kavanagh, G. M.; Ross-Murphy, S. B. Rheological characterisation of polymer gels. *Progress in Polymer Science* 1998, *23(3)*, 533-562.

91. Keller, A.; Pedemonte, E.; Willmouth, F. Kolloid ZZ Polym. 238, 385 (1970). *Nature (London)* 1970, *225*, 538.

92. Hadziioannou, G.; Mathis, A.; Skoulios, A. Synthesis of 3-block styrene-isoprene-styrene copolymer single-crystals via plane shear-flow. *Colloid Polym. Sci.* 1979, *257*, 136-139.

93. Koppi, K. A.; Tirrell, M.; Bates, F. S.; Almdal, K.; Colby, R. H. Lamellae orientation in dynamically sheared diblock copolymer melts. *Journal de Physique II* 1992, *2*, 1941-1959.

94. Vigild, M.; Chu, C.; Sugiyama, M.; Chaffin, K.; Bates, F. Influence of shear on the alignment of a lamellae-forming pentablock copolymer. *Macromolecules* 2001, *34*, 951-964.
95. Hermel, T. J.; Wu, L.; Hahn, S. F.; Lodge, T. P.; Bates, F. S. Shear-induced lamellae alignment in matched triblock and pentablock copolymers. *Macromolecules* 2002, *35*, 4685-4689.
96. Zhao, J.; Majumdar, B.; Schulz, M. F.; Bates, F. S.; Almdal, K.; Mortensen, K.; Hajduk, D. A.; Gruner, S. M. Phase behavior of pure diblocks and binary diblock blends of poly (ethylene)− poly (ethylethylene). *Macromolecules* 1996, *29*, 1204-1215.
97. Fredrickson, G. H.; Bates, F. S. Dynamics of block copolymers: theory and experiment. *Annual Review of Materials Science* 1996, *26*, 501-550.
98. Kane, L.; Norman, D. A.; White, S. A.; Matsen, M. W.; Satkowski, M. M.; Smith, S. D.; Spontak, R. J. Molecular, nanostructural and mechanical characteristics of lamellar triblock copolymer blends: effects of molecular weight and constraint. *Macromolecular rapid communications* 2001, *22*, 281-296.
99. Hotta, A.; Clarke, S. M.; Terentjev, E. M. Stress relaxation in transient networks of symmetric triblock styrene− isoprene− styrene copolymer. *Macromolecules* 2002, *35(1)*, 271-277.
100. Sudarsan, A. P.; Wang, J.; Ugaz, V. M. Thermoplastic elastomer gels: an advanced substrate for microfluidic chemical analysis systems. *Analytical chemistry* 2005, *77(16)*, 5167-5173.
101. Creton, C. Pressure-sensitive adhesives: an introductory course. In 2003; Vol. 28(6), pp 434-439.

102. Drzal, P. L.; Shull, K. R. Adhesive failure of model acrylic pressure sensitive adhesives. *The Journal of Adhesion* 2005, *81(3-4)*, 397-415.

103. Flanigan, C. M.; Crosby, A. J.; Shull, K. R. Structural development and adhesion of acrylic ABA triblock copolymer gels. *Macromolecules* 1999, *32(21)*, 7251-7262.

104. Kempe, M. D., Scruggs, N. R., Verduzco, R., Lal, J., & Kornfield, J. A. Self-assembled liquid crystalline gels designed from the bottom up. *Nature Materials* 2004, *3(3)*, 177-182.

105. Agrawal, S. K.; Sanabria-DeLong, N.; Tew, G. N.; Bhatia, S. R. Rheological characterization of biocompatible associative polymer hydrogels with crystalline and amorphous endblocks. *Journal of materials research*. *Journal of materials research* 2006, *21(8)*, 2118-2125.

106. He, Y., & Lodge, T. P. Thermoreversible Ion Gels with Tunable Melting Temperatures from Triblock and Pentablock Copolymers. *Macromolecules* 2008, *41(1)*, 167-174.

107. Sato, T.; Watanabe, H.; Osaki, K. Thermoreversible physical gelation of block copolymers in a selective solvent. *Macromolecules* 2000, *33*, 1686-1691.

108. Drzal, P. L., & Shull, K. R. Origins of Mechanical Strength and Elasticity in Thermally Reversible, Acrylic Triblock Copolymer Gels. *Macromolecules* 2003, *36(6)*, 2000-2008.

109. Seitz, M. E.; Burghardt, W. R.; Faber, K. T.; Shull, K. R. Self-Assembly and Stress Relaxation in Acrylic Triblock Copolymer Gels. *Macromolecules* 2007, *40(4)*, 1218-1226.

110. Le Meins, J. F.; Tassin, J. F. Elastic modulus and relaxation times in telechelic associating polymers. *Colloid and Polymer Science* 2003, *281(3)*, 283-287.

111. Drolet, F.; Fredrickson, G. H. Combinatorial screening of complex block copolymer assembly with self-consistent field theory. *Physical Review Letters* 1999, *83(21)*, 4317.

112. Drolet, F.; Fredrickson, G. H. Optimizing chain bridging in complex block copolymers. *Macromolecules* 2001, *34(15)*, 5317-5324.

113. Lee, N. K.; Johner, A.; Vilgis, T. A. Single chain stretching of block copolymers under different solvent conditions. *Macromolecules* 2002, *35(15)*, 6043-6054.

114. Treloar, L. R. G. *The physics of rubber elasticity;* Oxford University Press: 1975; .

115. Edwards, S. F.; Vilgis, T. A. The tube model theory of rubber elasticity. *Reports on Progress in Physics* 1988, *51(2)*, 243.

116. Rentsch, S.; Pericet-Camara, R.; Papastavrou, G.; Borkovec, M. Probing the validity of the Derjaguin approximation for heterogeneous colloidal particles. *Physical Chemistry Chemical Physics* 2006, *8(21)*, 2531-2538.

117. Fleer, G.; Stuart, M. C.; Scheutjens, J. M.; Cosgrove, T.; Vincent, B. *Polymers at interfaces*. *Springer Science & Business Media* 1993.

118. Halperin, A.; Zhulina, E. B. On the deformation behaviour of collapsed polymers. *Europhysics Letters* 1991, *15(4)*, 417.

119. Morton, M.; McGrath, J. E.; Juliano, P. C. In *In Structure-property relationships for styrene-diene thermoplastic elastomers;* Journal of Polymer Science: Polymer Symposia; Wiley Online Library: 1969; Vol. 26, pp 99-115.

120. Matsen, M. W.; Bates, F. S. Unifying weak-and strong-segregation block copolymer theories. *Macromolecules* 1996, *29(4)*, 1091-1098.

121. Matsen, M. W.; Schick, M. Stable and unstable phases of a diblock copolymer melt. *Phys. Rev. Lett.* 1994, *72*, 2660.

122. Matsen, M. W.; Schick, M. Self-assembly of block copolymers. *Current Opinion in Colloid & Interface Science* 1996, *1(3)*, 329-336.

123. Wagner, H. D. Nanotube–polymer adhesion: a mechanics approach. *Chemical Physics Letters* 2002, *361*, 57-61.

124. Lau, K. Interfacial bonding characteristics of nanotube/polymer composites. *Chemical Physics Letters* 2003, *370*, 399-405.

125. Frankland, S.; Harik, V. Analysis of carbon nanotube pull-out from a polymer matrix. *Surf. Sci.* 2003, *525*, L103-L108.

126. Frankland, S.; Harik, V.; Odegard, G.; Brenner, D.; Gates, T. The stress–strain behavior of polymer–nanotube composites from molecular dynamics simulation. *Composites Sci. Technol.* 2003, *63*, 1655-1661.

127. Lordi, V.; Yao, N. Molecular mechanics of binding in carbon-nanotube–polymer composites. *J. Mater. Res.* 2000, *15*, 2770-2779.

128. Liao, K.; Li, S. Interfacial characteristics of a carbon nanotube–polystyrene composite system. *Appl. Phys. Lett.* 2001, *79*, 4225-4227.

129. Xu, X.; Thwe, M. M.; Shearwood, C.; Liao, K. Mechanical properties and interfacial characteristics of carbon-nanotube-reinforced epoxy thin films. *Appl. Phys. Lett.* 2002, *81*, 2833-2835.

130. Müller-Plathe, F. Coarse-Graining in Polymer Simulation: From the Atomistic to the Mesoscopic Scale and Back. *ChemPhysChem* 2002, *3*, 754-769.

131. Moreno, N.; Nunes, S. P.; Calo, V. M. Geometrically-Consistent Model Reduction of Polymer Chains in Solution. Application to Dissipative Particle Dynamics: Model Description. *arXiv preprint arXiv:1405.2763* 2014.

132. Pivkin, I. V.; Caswell, B.; Karniadakis, G.; Lipkowitz, K. Dissipative particle dynamics. *Reviews in computational chemistry* 2011, *27*, 85-110.

133. Maiti, A.; Wescott, J.; Kung, P. Nanotube–polymer composites: insights from Flory–Huggins theory and mesoscale simulations. *Molecular Simulation* 2005, *31*, 143-149.

134. Espanol, P. Hydrodynamics from dissipative particle dynamics. *Phys. Rev. E* 1995, *52*, 1734-1742.

135. Marsh, C. A.; Backx, G.; Ernst, M. H. Static and dynamic properties of dissipative particle dynamics. *Physical Review E* 1997, *56(2)*, 1676.

136. Groot, R. D.; Warren, P. B. Dissipative particle dynamics: bridging the gap between atomistic and mesoscopic simulation. *J. Chem. Phys.* 1997, *107*, 4423.

137. Flory, P. J. *Principles of polymer chemistry;* Cornell University Press: 1953; .

138. Sperling, L. H. *Introduction to physical polymer science;* John Wiley & Sons: 2005; .

139. Liba, O.; Kauzlarić, D.; Abrams, Z. R.; Hanein, Y.; Greiner, A.; Korvink, J. G. A dissipative particle dynamics model of carbon nanotubes. *Molecular Simulation* 2008, *34*, 737-748.

140. Maiti, A.; Wescott, J.; Goldbeck-Wood, G. Mesoscale modelling: recent developments and applications to nanocomposites, drug delivery and precipitation membranes. *International journal of nanotechnology* 2005, *2*, 198-214.

141. Wang, Y.; Ju, S.; Cheng, H.; Lu, J.; Wang, H. Modeling of Polyethylene and Functionalized CNT Composites: A Dissipative Particle Dynamics Study. *The Journal of Physical Chemistry C* 2010, *114*, 3376-3384.

142. Wang, Y.; Ju, S.; Huang, T. J.; Wang, H. Modeling of polyethylene, poly (l-lactide), and CNT composites: a dissipative particle dynamics study. *Nanoscale research letters* 2011, *6*, 1-8.

143. Roy, S.; Markova, D.; Kumar, A.; Klapper, M.; Müller-Plathe, F. Morphology of phosphonic acid-functionalized block copolymers studied by dissipative particle dynamics. *Macromolecules* 2009, *42*, 841-848.

144. Cui, Y.; Zhong, C.; Xia, J. Multicompartment micellar solutions in shear: A dissipative particle dynamics study. *Macromolecular rapid communications* 2006, *27*, 1437-1441.

145. Fraser, B.; Denniston, C.; Müser, M. H. On the orientation of lamellar block copolymer phases under shear. *J. Chem. Phys.* 2006, *124*, 104902.

146. Li, X.; Deng, M.; Liu, Y.; Liang, H. Dissipative particle dynamics simulations of toroidal structure formations of amphiphilic triblock copolymers. *The Journal of Physical Chemistry B* 2008, *112*, 14762-14765.

147. Liu, D.; Zhong, C. Cooperative Self-Assembly of Nanoparticle Mixtures in Lamellar Diblock Copolymers: A Dissipative Particle Dynamics Study. *Macromolecular rapid communications* 2006, *27*, 458-462.

148. Schlijper, A. G.; Hoogerbrugge, P. J.; Manke, C. W. Computer simulation of dilute polymer solutions with the dissipative particle dynamics method. *Journal of Rheology* 1995, *39(3)*, 567-579.

149. Spenley, N. Scaling laws for polymers in dissipative particle dynamics. *EPL (Europhysics Letters)* 2000, *49*, 534.

1.8. Figures and Tables

Table 1.1: The table includes the molecular variables influencing the self-assembly of block copolymers. The content of the table was taken from Ref 17

Primary
Topology; linear, branched, etc.
Number of blocks, n
Number of block types, k
Block degree of polymerization, N_i
Interaction parameters, χ_{ij}
Secondary
Block flexibility, b_i
Molar mass distribution, $Đ_i$
Sub-block structure (e.g., tapered)
Composition heterogeneity

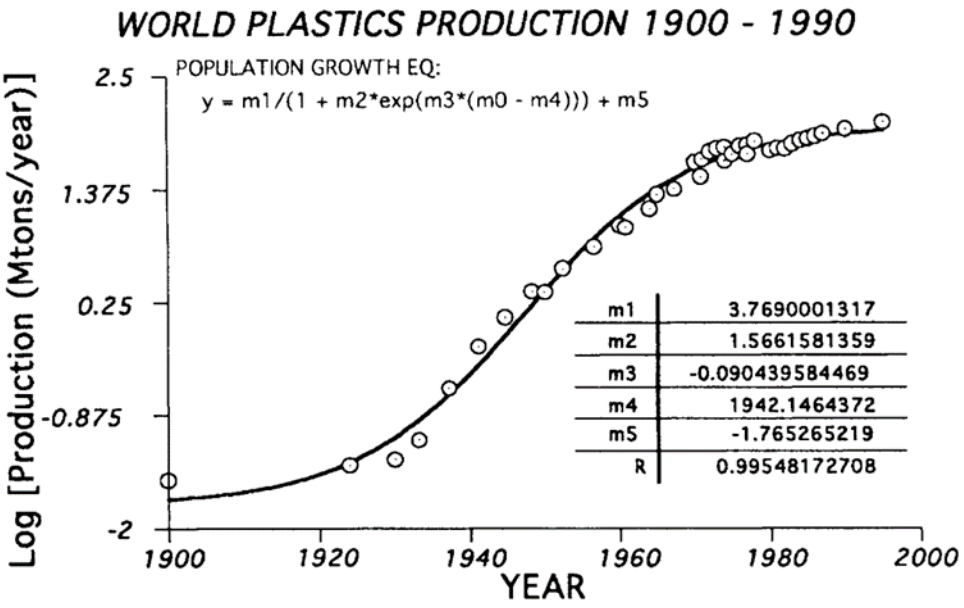

Figure 1.1: The production of plastic in world during the years 1900 to 1990 in million metric tons per years. The image was taken from Ref. 3

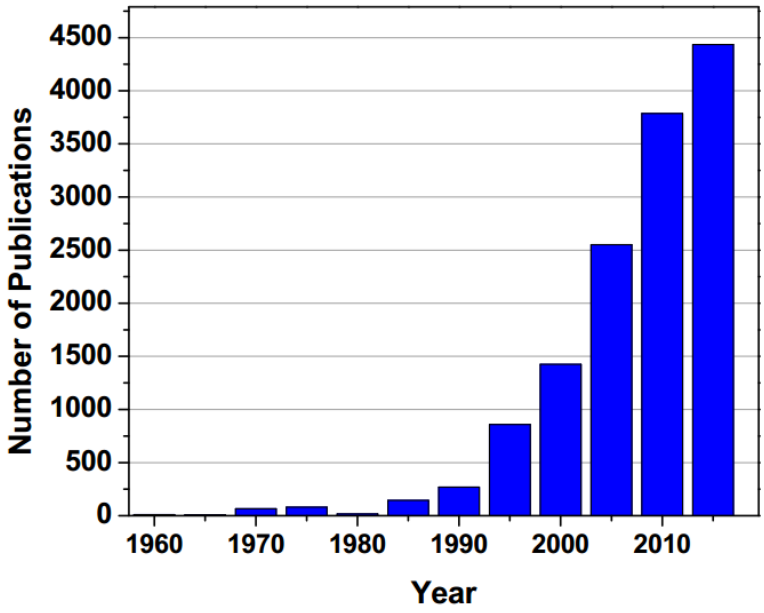

Figure 1.2: Total number of publications with block copolymer as topic against year. The data were collected based on the resources of Web of Science (2017 Clarivate Analytics). The image was taken from Ref. 11

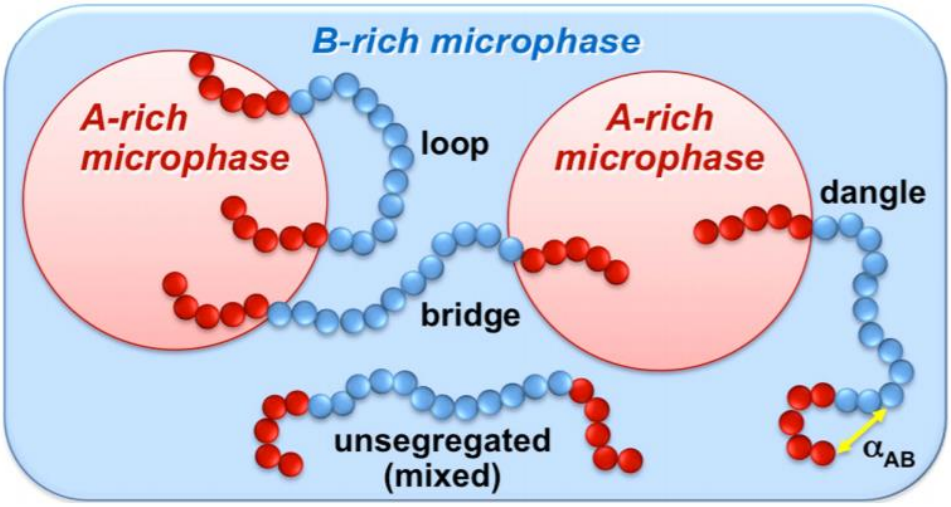

Figure 1.3: A schematic depicting the formation of midblock conformations in a microphase separated ABA triblock copolymer. Here, the circular A-rich phase represents the micelle formed by the minority volume fraction blocks of the copolymer whereas the remaining part belongs to the major portion block of the copolymer. I the image, α_{AB} indicates the repulsion parameter between the dissimilar blocks of A and B. The image was taken from Ref. 16

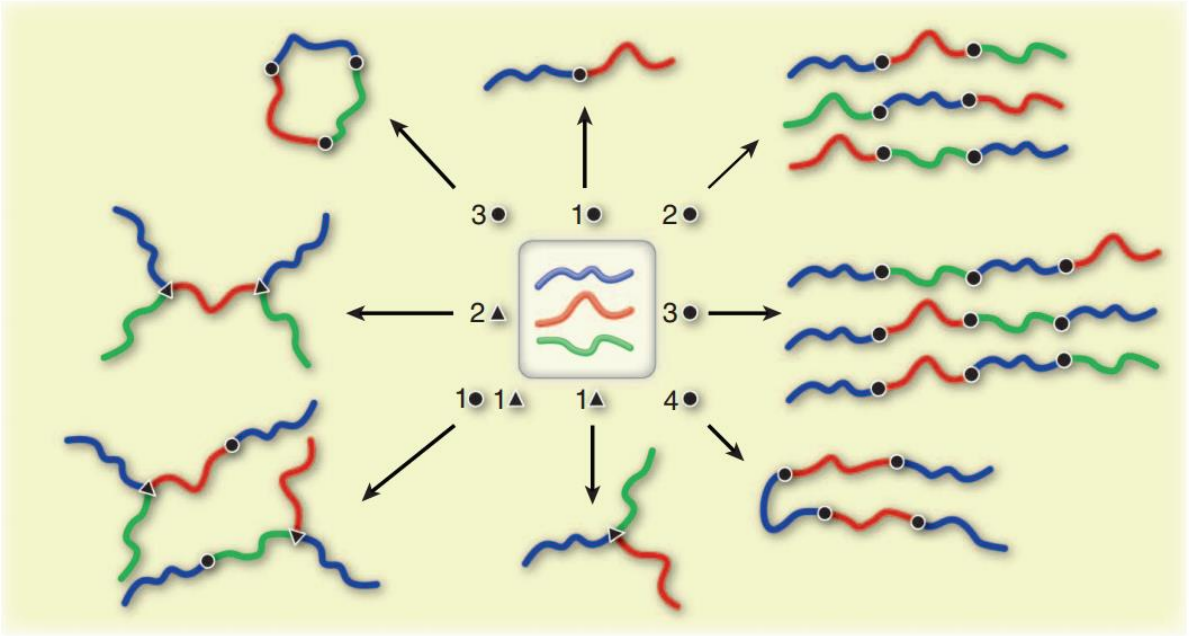

Figure 1.4: Schematic representation of a subset of a vast array of structural complexity of block copolymers with variation in block types (k = 2, 3) along the variation in number of blocks (n) and the functionality of the connector at each block-block juncture i.e. difunctional, trifunctional, triangles and circles. The black dots and triangular markers depict the number and type of connectors used in each structure. The image was taken from Ref 17

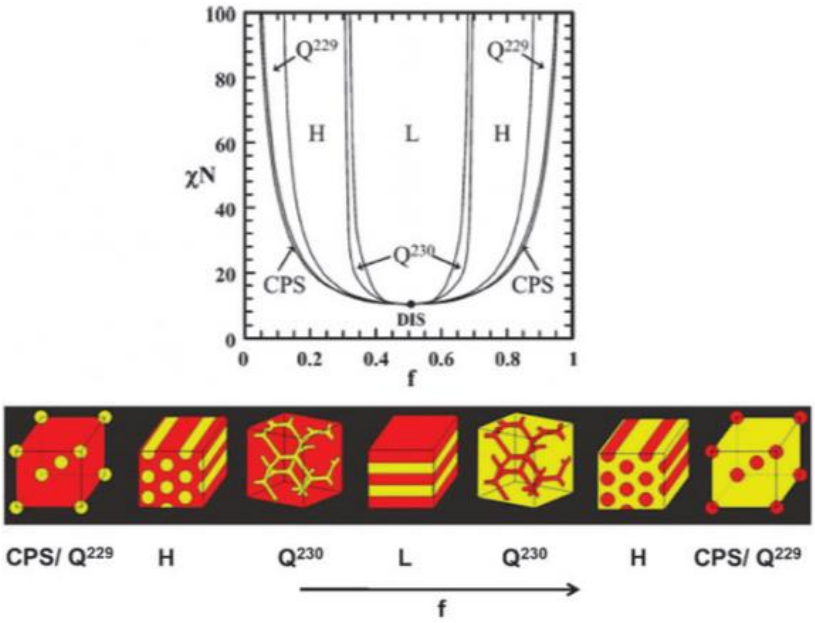

Figure 1.5: Depiction of the theoretical phase diagram of diblock copolymer (top) along the corresponding nanostructure morphologies belongs to the diagram (bottom) with increase in the volume fraction (f) of one block with respect to the remaining one. The morphologies include spheres (CPS or Q^{229}), hexagonally packed cylinders (H), cubic bicontinuous gyroid (Q^{230}), and the lamellae (L). The image was taken from Ref. 35

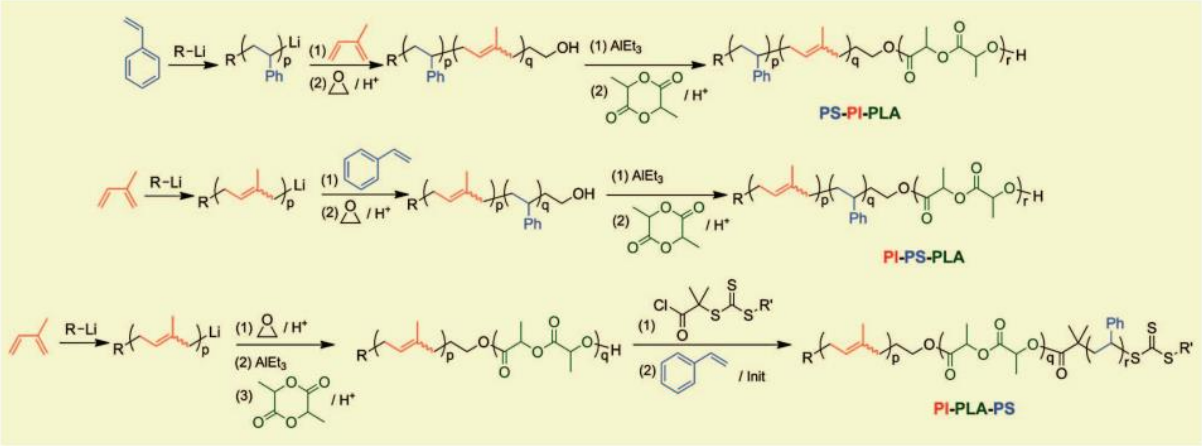

Figure 1.6: An example of the combinatorial synthetic routes of producing three distinct triblock linear terpolymer structures of polystyrene (PS), polyisoprene (PI) and polylactic acid (PLA) blocks using living anionic, metal-catalyzed ring-opening, and reversible addition-addition-fragmentation chain transfer-controlled radical polymerization. Design route includes alkyl groups (R and R′), phenyl groups (Ph), ethyl group (Et), and the degrees of polymerization (p, q, and r). The image containing reaction schemes was taken from Ref. 17

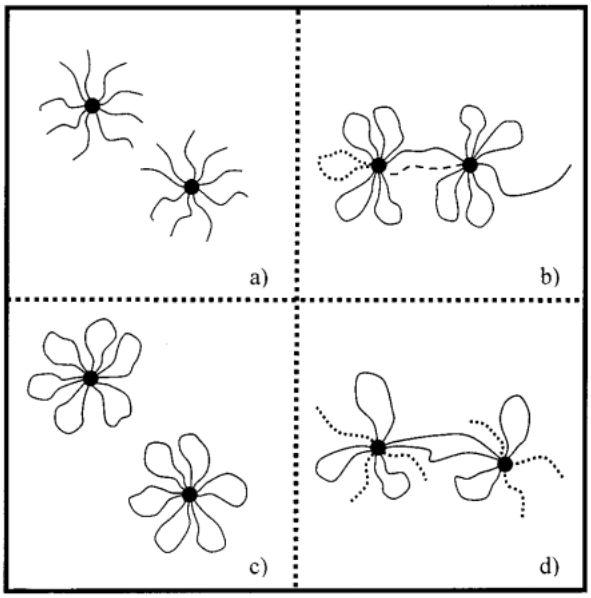

Figure 1.7: In the first row, (a) micelles are formed by diblock copolymer in selective solvent and (b) depicted is the illustration of triblock copolymer formed micelles in midblock-selective solvent where the dotted line represents the loop conformation and the dashed line represents bridge conformation. In the next row schematics depicts the (c) flowerlike conformations formed by triblock copolymer as a result of very high loop/bridge ratio, and (d)combination of micelles formed by deblocks (dotted line) and by triblocks (solid line). The image was taken from Ref. 56

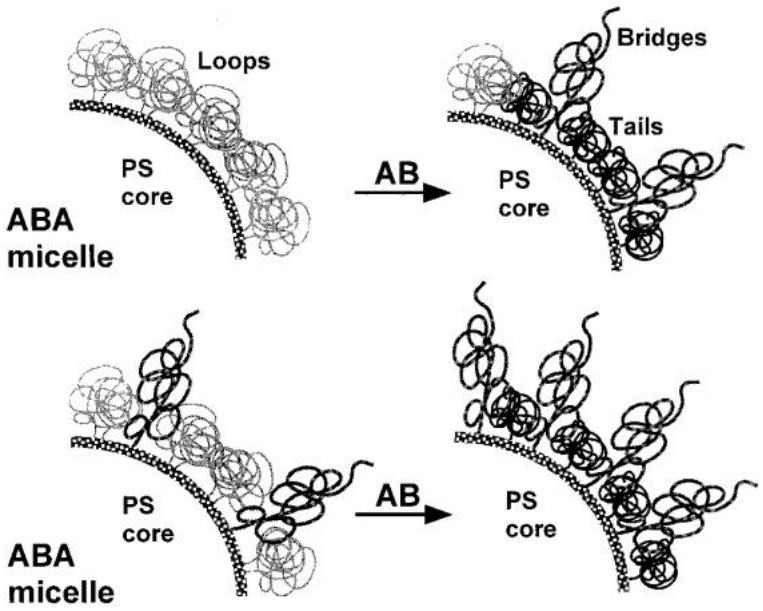

Figure 1.8: Illustration of how addition of AB diblock copolymer can enhance the increase of bridge fraction in ABA/B-block selective gel. (Top) the grey lines represent the loop formation as the primary conformation at low concentration of ABA. Addition of smaller quantity of AB diblock facilitates volume exclusion effect and as a result some B-midblocks are forced to come out of the corona to form bridge. The size of the blocks used in this study are: molecular weight of A-block, $M_A{}^{(AB)} \approx M_A{}^{(ABA)}$ and that of B-block, $M_B{}^{(AB)} < M_B{}^{(ABA)}/2$. At the bottom picture, at higher concentration of ABA, where bridged midblocks already exist in the system, addition of AB diblock further increases the bridge fraction due to increased number of tail. The increase of such bridge population favors the physical-gelation if the quantity of the bridge fraction is more than the minimum required amount to form gel network. The image was taken from Ref. 66

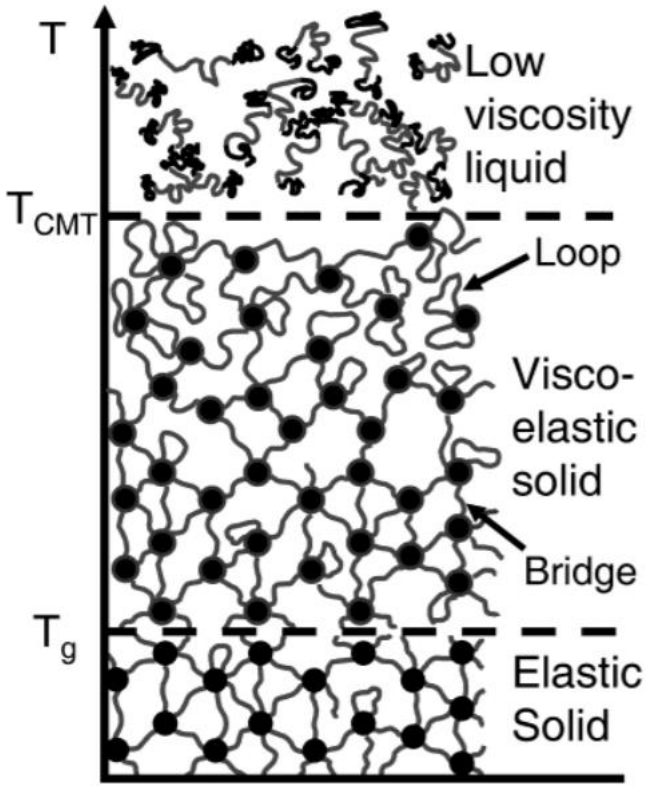

Figure 1.9: Depiction of acrylic triblock copolymer gels in alcohol as an illustration of the temperature-dependent structure. The image was taken from Ref. 108

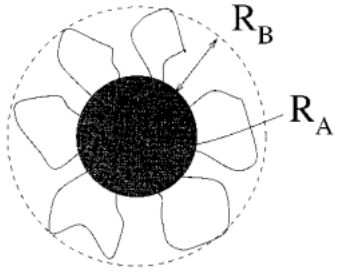

Figure 1.10: hairy micelle formation of a multiblock copolymer in a midblock selective solvent as a result of micro-phase separation. The radius of the core (R_A) and the radius of the corona (R_B) are also mentioned in order to compare the size of both. The image was taken from Ref. 113

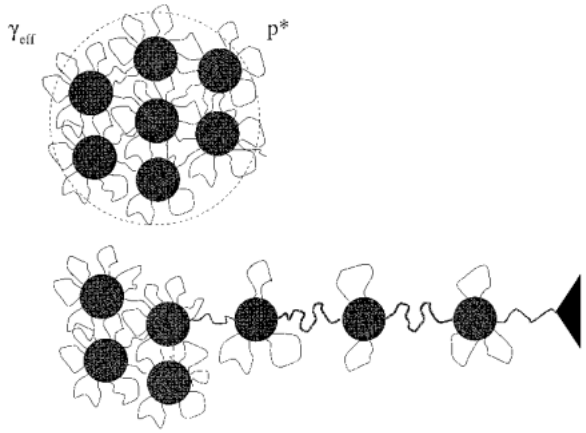

Figure 1.11: Schematic illustration of the dense superglobule micelle formation(top), and the "pearl necklace structure" formation of block multiblock copolymers as a result uniaxially applied force (bottom). The image was taken from Ref. 113

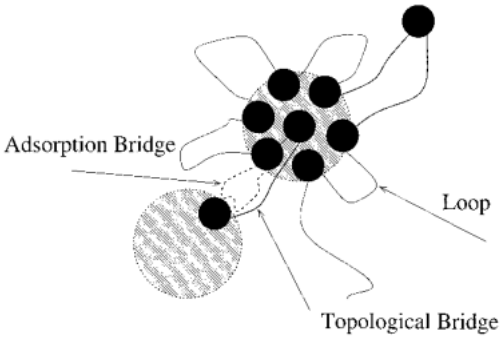

Figure 1.12: The micelle assembly can be formed because of two types of bridging attractions: adsorption of the corona bridges into neighboring corona and the topological exchange of coronas between bridges. The image was taken from Ref. 113

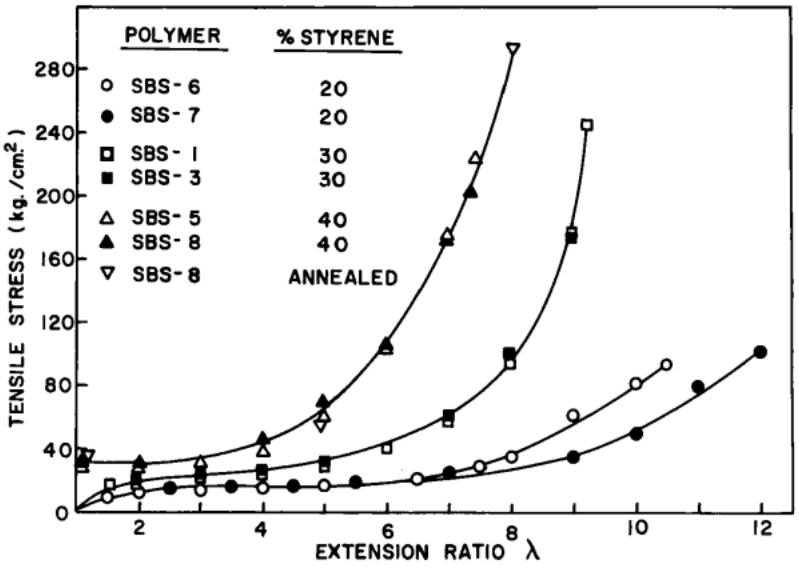

Figure 1.13: The figure represents the tensile properties of SBS triblock copolymers as a function of block size and the composition. The image was taken from Ref. 119

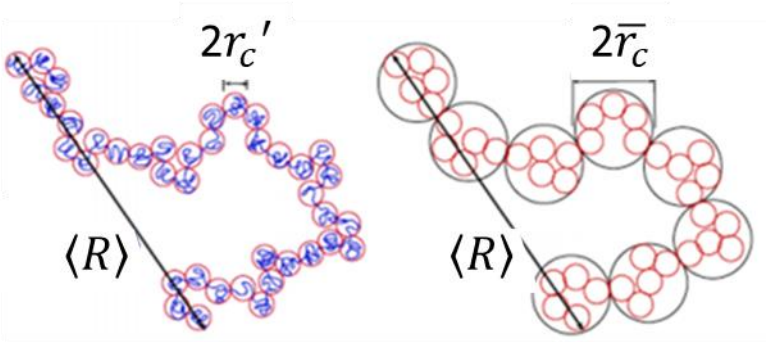

Figure 1.14: Schematic representation of the process of coarse graining of a polymer chain. The image taken from Ref. 131

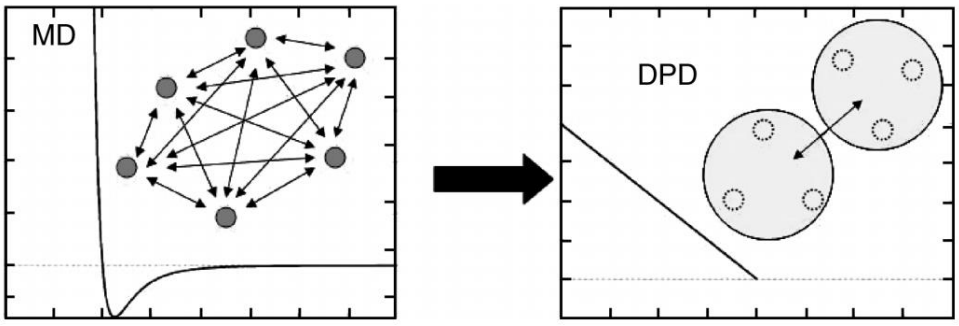

Figure 1.15: (Left) a depiction of Lennard-Jones hard interaction potential interplaying with the atomistic units of consideration. (Right) the soft interaction potential acting between the center of mass of a cluster of fluid molecules considered as a coarse-grained unit for the corresponding system. The image was taken from Ref. 132

CHAPTER 2

CLASSICAL CONCEPT OF PERCOLATION THEORY

2.1. Introduction

Conductive polymer composites are, as a rule, strongly disordered systems[1, 2] , whereas the conductivity in these materials are driven by the connectivity of the conductive fillers. The concept of percolation theory has been widely used to describe the properties of these composites and to establish a quantitative relationship between composite structure and its conductivity[1]. The first studies on the percolation theory was reported to be established by Flory in 1941[3-5] and Stockmayer in 1943[6] while they were investigating the gelation process in branched polymers. The mathematical formalism of the theory was first reported in a study of 1957.[7] However, including a wide range of applications in versatile fields,[8] not being exclusively confined into describing the electrical phenomenon, percolation theory has seen significant advances describing the electrophysical properties of the world of material science, which began to be extensively applied at the beginning of the early 1970s.[9,10] In the context of electrophysical properties, this theory is applied only to systems having conductive sites (or bonds) in a nonconductive medium. The percolation theory is closely related to the theory of critical phenomenon[11], which indicates that both relations contain universal character.

2.2. Fundamental concept of percolation

In general, the percolation threshold is identified with the asymptotic variation of any material property $\mathcal{P}$ (electrical conductivity, thermal conductivity, mechanical properties etc.) near a characteristic concentration ϕ^*,

$$\mathcal{P} \sim |\phi^* - \phi|^{-\delta} \quad (1)$$

Where ϕ the volume fraction of the suspended particles and the critical exponent is δ denotes the exponential variation of the value of $\mathcal{P}$ near the threshold concentration ϕ^*.

This equation (1) have been successfully used to describe the electrical and thermal conductivity[12-15], dielectric constant[16], and shear modulus[17] of composites, the permeability of porous media[18], and transport properties, such as the viscosity of fluid suspensions of rigid particles[19-21]. The illustration of the exact percolation network can better be explained with the lighting up of a bulb as depicted in the figure 1.

Now, let's consider some new parameters as $\mathcal{P} = \sigma$, $\phi = \varphi$ and $\phi^* = \varphi_C$ to illustrate the case of percolation threshold in the context of electrical conductivity for polymer composites.

When a dispersed filler component having conductivity σ_f is gradually incorporated into a polymer matrix having a conductivity σ_p, the composite prepared gains a conductivity value σ. When the volume filler fraction φ reaches a critical value φ_C (called percolation threshold), an infinite conductive cluster (IC) of the filler particles is formed, and consequently, the composite becomes electrically conductive. [22] Further increase in the concentration of the filler from φ_C to a limit F (figure 2), the value of σ rapidly increase and reaches at a maximum value of σ_m which is several orders of magnitude higher than the value of φ_C. Before reaching at the critical point of percolation threshold, the conductivity of the composite equals to that of the polymer or slightly higher.

In the context of the illustration depicted in figure 1, for real two phase systems, the sharp conductivity increase occurs within the concentration region $\varphi_{C1} < \varphi < \varphi_{C2}$ called the smearing region[23]. Such region is the result of the finite conductivity of phases and the finite size of clusters

and samples. However, since the value of φ_{C2} can only be estimated in real systems, the value of φ_{C1} is considered as φ_C and it is considered that the conductivity change is controlled by the same rule for both the smearing region and the highly filled region.[24] Such reaching of the value of φ_C at the point of $\varphi_{C1}$is considered as the signature of the beginning of IC formation.

Here, the value of σ_p can be affected by different parameters like shape, polydispersity, possible orientation of the dispersed particles arising from the effect of external fields,[25] spacial dimension of the dispersion medium e.g. thickness of the composite film.

2.3. Formation of IC and percolation threshold in polymer composites

Beginning with a very low value, as the concentration of the conducting particles are increased, small agglomerates of the particles are first formed in the system. These agglomerates, then, lead to the formation of conducting single clusters characterized by a mean cluster size denoted by the so-called correlation length ξ (as depicted in Figure 3).

Then, at some concentration of the conductive particles φ_C, referred to as the percolation threshold, conducting bridges are formed across the single clusters. These clusters may be formed by either single particles or by the agglomerates. After that an infinite conductive clusters (IC) is formed composed of the originally isolated clusters and the system is jumpwise transformed into a conducting state which is the signature of σ_p. Further increase in concentration of the conducting phase leads to larger IC by absorbing the small single clusters and thus arises a monotonic rise of the system conductivity.

The notion of percolation length ξ also stays valid and functional for the case $\sigma > \sigma_p$. Further increase in the concentration of the conducting particles leads the absorption of the isolated largest clusters resulting the increase in the density of IC. The critical behavior of the correlation length

can be expressed with a relationship as $\xi = |\tau|^{-\nu}$, where $\tau = \frac{(\sigma-\sigma_p)}{(1-\sigma_p)}$, which characterizes the closeness of a system to the percolation threshold and ν is the critical index of correlation length.

According to previous study[26], commonly accepted values of this critical index of correlation length are 4/3 for the two-dimensional case and 0.88 for three-dimensional case. For the films systems, the ν index can be related to the films thickness by the following expression[27]:

$$\frac{\sigma_p(h) - \sigma_p(\infty)}{\sigma_p(\infty)} \sim \frac{1}{h^q} \qquad (2)$$

Where $Pc(h)$ and $Pc(\infty)$ are the percolation thresholds for bulk sample and film with thickness h, and $q \approx \frac{1}{\nu}$. Using model calculations, different systems[27] resulted the values of q from 1 to 1.7 depending on the structural characteristics of percolation system.

2.4. Electrical network percolation in metal-filled polymer composites (influencing factors)

Metal-polymer composites became technologically significant material because of their unique nature of having electrical characteristics close to those of metal, whereas the mechanical properties and processing methods like typical plastics.[28] The electrical properties of the metal-polymer composites are dependent on various factors like the nature of conducting filler, the spatial distribution of conducting filler, the contact interaction between particles and the interaction between polymer and filler.[24]

2.4.1. Nature of conducting filler and the spatial distribution of conducting filler

Several studies[28-33] were carried out to investigate the influence of the shape and spatial distribution (random or ordered) of the dispersed filler particles on percolation threshold. It was observed that the more the shape of particles deviates from the spherical one, the lower becomes the percolation threshold. This effect is particularly noticeable in the case of conducting short

fibers with high aspect ratio length/diameter (l/d). [31,34] Such influence can be expressed in normalized form as[30]

$$\frac{\sigma - \sigma_c}{\sigma_m - \sigma_c} = \left(\frac{\sigma - \sigma_p}{F - \sigma_p}\right)^t \quad (3)$$

By defining the normalized conductivity (s) and normalized filler volume content (ψ) as

S = $\frac{\sigma-\sigma_c}{\sigma_m-\sigma_c}$ and ψ = ($\frac{\sigma-\sigma_c}{F-\sigma_c}$) gives a simplified expression as S =ψ^t.

Where, σ_m denotes the maximum conductivity and F (packing factor) corresponds to the specific system parameters. Here, the value of F depends on the particle shape and on the possibility of skeleton or chain structure formation.[35]This parameter F can be expressed as:

$F = \frac{V_f}{(V_f + V_P)}$, where V_f the volume is occupied by the filler particles at the highest possible filler fraction and V_P is the volume occupied by the polymer (space among filler particles). Thus this packing factor takes into account for the particle shape, fractional size and the spatial distribution of the particles.

For randomly packed monodispersed spherical particles of any size, the packing factor is equal to 0.64.[36,37]The deviation of particle shape from spherical type or volume filler skeleton structure formation[24] leads the decrease in the value of F. Hence, as a rule, real fillers have F values smaller than 0.64.[35,38]As, expected, the polydispersity in filler particles results higher value of F.[39,40]

To calculate the packing factor in the framework of lattice model, Scher and Zallen[41] established a relationship correlating the percolation threshold for the systems where polymer-conductive phase interaction does not exist:

$$\varphi_C = X_C F \quad (4)$$

where, X_C is a critical parameter which has the meaning of a site percolation probability. For any lattice type, the values of X_C and F varies in such a way that $\varphi_C \approx 0.16$. This equation was also found to be valid in case of randomly distributed conductive sites.[42] However, counting the polymer-conductive phase interactions along filler phase geometry requires additional parameters to reflect the interaction between polymer and filler phase using relatively more complex equation.[24,43]

2.4.2. Polymer-filler interaction

Previous studies[24,44,45] depicted that the stronger the polymer-filler interaction is, the better the polymer wets the fillers and thus σ_p becomes higher. Hence, if the filler-filler interparticle interaction energy is lower than the filler-matrix interaction energy, each conducting particle is expected to be covered with isolating polymer layer due to strong bond formation. This phenomenon will lower the conductivity and thus will give rise to the value of the percolation threshold. On the other hand, if the filler-polymer interaction energy is lower than the interparticle filler interaction energy an ordered chain structure of the conducting phase will be favored.

2.4.3. Matrix viscosity, particle size and formation of 'double percolation'

The viscosity of polymer melt and the means of obtaining the polymer composites are another two factors that were found to provide difference in spatial filler distribution.[24,28,31,45-47] Considering a single polymer matrix, decrease in polymer matrix viscosity promotes the chain structure formation and thus lowers the value of percolation threshold[1]. Similar effect was also reported for the deterioration of particle-polymer compatibility and particle size. Both of the deterioration[1] of the compatibility and having smaller particle size promotes the probability of chain structure formation, which lowers the percolation threshold.[48]

Incorporating filler particles into the blend of two polymers owing large difference in their respective melt viscosities may dictate two simultaneous incidents: filler can mostly be located in the polymer phase having higher melt viscosity and thus can initially create filler-filled island structure into the one having lower melt viscosity. Above the percolation threshold, $\sigma > \sigma_p$ these islands become connected forming an interpenetrating branched continuous structure having ordered dispersed filler as depicted in figure 4.

Sumita et al.[49] used the term 'double percolation' to describe such composites with two phase polymer matrix. Formation of such structure can lower the value of σ_c as was observed while iron (Fe) particles were incorporated into the blend of two polymers, polyethylene, PE (melt flow index 1.6 g/10 min) and polyoxymethylene, POM (melt flow index 10.9 g/10 min). Due to double percolation network formation, PE/POM-Fe was observed to depict much lower value of percolation threshold than that of PE-Fe and PMO-Fe composites.[50] However, disconnection of any of these two percolation networks will make the composite non-conductive.

2.4.4. Processing methods and shell structure

Regarding the processing methods, some methods can provide ordered filler distribution with or without filler topology and thus can lower the value of Pc.[28,31,45-47]

Dispersed filler segregated structure in polymer matrix can be achieved by different technological methods like, pressing the mixture of thermoplastic polymer powder having particle size D and of conductive filler having particle size d (D>>d)[28,47,53,54]; extrusion or casting of a mixture of incompatible polymers provided that only one polymer contains conductive filler[44,49,55]; filling the conductive and non-conductive fillers simultaneously, having particle size d and d_1 respectively, with d_1>d.[56]

It can be noted that for the appearance of conductivity in these systems, it's not required that each polymer particles will be covered with a monolayer of conductive particles in contact with each other. As is depicted in figure 5(b) adopted from[52], minimal polymer particle covering with metallic particles may provide conductive cluster appearance at $\varphi = \varphi_C$. Additional increase in the filler content will increase the number of layers n of metallic particles on the kernel surface and in the decrease of the size L of the unfilled region, L = D-nd (figure 5(c)).

2.5. Thermal network percolation in composites

In many previous studies[47,57-59], the percolation behavior (λ) of thermal conductivity in polymer composites having dispersed filler concentration was found to be absent. Hence, later, several attempts[60,61] were found to be carried out to include additional thermal conductivity related parameters in order to connect those to IC appearance. It was predicted that the percolation threshold (λ) will appear only if the ratio of filler conductivity, λ_f to polymer conductivity, λ_p is larger than 10^5.[61] The absence of the thermal percolation in previous case was also explained.[62] The reason of the absence was explained as due to the fact that the ratio of thermal conductivities of the dispersed fillers, λ_f and the thermal conductivities of the polymer matrix, λ_p were not more than 10^3, whereas the filler electrical conductivity, σ_f, was 10^{10}-10^{20} times larger than the polymer conductivity, σ_P.

$$\lambda_{\parallel} = \lambda_p(1-\varphi) + \lambda_f\varphi \quad (5)$$

$$\lambda_{\perp} = 1/[(1-\varphi)/\lambda_p + \varphi/\lambda_f \quad (6)$$

Here, φ is the content of plates with thermal conductivityλ_f.

Later, it was reported[63,64] that Lichtenecker's equation, in modified form, is convenient in describing the concentration dependence of thermal conductivity in two-phase systems with dispersed second phase. The modified equation was proposed[64] as following-

$$log\lambda = \log \lambda_p + \left(\log \lambda_F - \log \lambda_p\right)(\varphi/F)^N \qquad (7)$$

Here, λ_F is the maximum thermal conductivity of the composite at $\varphi = F$ and the exponent N is constant. The value of F =1 is considered for the case when the filler phase fills up all composite volume at $\varphi = F$ (limit content), which means the filler content changes from 0 to 1 volume fraction and it becomes $\lambda_F = \lambda_f$. Alloys and solutions are the example of such systems. For the dispersed fillers, F was reported not to exceed 0.5-0.6.[65]. The percolation index, N, is dependent on the filler size, filler shape, and filler distribution in the composites.

The direction of the filler phase also was found to influence the thermal property analysis of two-phase materials.[66] The largest and the smallest two phase-system thermal conductivity can be explained with the equations of (3) and (4), respectively. Here, the largest system may be represented as a set of parallel plates extending towards the direction of heat flow and the smallest one as the plates (phases) stacked in series with respect to the direction of heat flow (figure-6).[51]

2.6. Mechanical percolation in nanocomposites

As is evident from the previous chapters that both of the electrical and thermal percolations are mainly described by geometrical parameters such as percolation threshold and the percolating volume fraction. However, previous studies[67,68] illustrated that the mechanical percolating effects depend also on the nature of the joints between percolating particles. Previous simulation studies[69] revealed that only a network of beams displays a behavior of mechanical percolation as soon as the first infinite aggregate is formed because of the rigid joints. On the contrary, the network of

bars in any matrix having geometrical percolation acts just as randomly dispersed rods because of the momentless joints. One previous study[67] of the mechanical percolation in cellulose whisker nanocomposites described such phenomenon having similar role of the joints between percolating whiskers due to many hydrogen bonds, which made the whole network rigid.

In order to express the mechanical percolation behavior of the composites, several models were introduced in previous studies.[69-73] For example, one of those presented by Ouali *et al.*[73]uses The Series-Parallel model to describe the mechanical percolation model and Favier *et al.*[67] showed good agreement of this model with their experimental results obtained while studying cellulose whisker incorporated nanocomposites for mechanical measurement, the shear modulus (G_c), of the composites with the following equation:

$$G_c = \frac{(1-2\psi+\psi X_r)G_s G_r+(1-X_r)\psi {G_r}^2}{(1-X_r)G_r+(X_r-\psi)G_s} \quad (8)$$

Where X_r is the volume fraction of the rigid phase, and G_r and G_s are the shear moduli of rigid and soft phases, respectively. The percolating volume fraction ψ corresponds to the fraction of rigid whiskers active in the transfer of forces from one whisker to another and, according to the percolation theory[73] , can be estimated as following:

$$\psi = 0 \qquad X_r < X_c \quad (9)$$

$$\psi = X_r \left(\frac{X_r - X_c}{1 - X_c}\right)^b \qquad X_r \geq X_c \quad (10)$$

Here, the critical volume fraction,X_c represents the percolation threshold required to reach at the geometrical percolation of the whiskers and, the b is the percolation exponent, which equals to 0.4 for 3-D analysis.[74,75]

According to the previous studies[76-78], this percolation threshold depends on the aspect ratio of the object studied and on their orientation distribution. Another study[79] revealed also that the percolation threshold calculated for a non-uniform length distribution is lower than the one calculated for a uniform length distribution having the same average length.

2.7. References

1. Roldughin, V.; Vysotskii, V. Percolation properties of metal-filled polymer films, structure and mechanisms of conductivity. *Progress in Organic Coatings* 2000, *39*, 81-100.
2. Bierwagen, G.; Fishman, R.; Storsved, T.; Johnson, J. Recent studies of particle packing in organic coatings. *Progress in Organic coatings* 1999, *35*, 1-9.
3. Flory, P. J. Molecular size distribution in three dimensional polymers. i. gelation1. *J. Am. Chem. Soc.* 1941, *63*, 3083-3090.
4. Flory, P. J. Molecular size distribution in three dimensional polymers. III. Tetrafunctional branching units. *J. Am. Chem. Soc.* 1941, *63*, 3096-3100.
5. Flory, P. J. Molecular size distribution in three dimensional polymers. II. Trifunctional branching units. *J. Am. Chem. Soc.* 1941, *63*, 3091-3096.
6. Stockmayer, W. H. Theory of molecular size distribution and gel formation in branched-chain polymers. *J. Chem. Phys.* 1943, *11*, 45-55.
7. Broadbent, S. R.; Hammersley, J. M. In *In Percolation processes;* Mathematical Proceedings of the Cambridge Philosophical Society; Cambridge Univ Press: 1957; Vol. 53, pp 629-641.
8. Saberi, A. A. Recent advances in percolation theory and its applications. *Physics Reports* 2015, *578*, 1-32.
9. Shklovskiĭ, B.; Efros, A. Percolation theory and conductivity of strongly inhomogeneous media. *Soviet Physics Uspekhi* 1975, *18*, 845.
10. Kirkpatrick, S. Teoriya i svoistva neuporyadochennykh materialov (Theory and Properties of Disordered Materials). *Mir, Moscow* 1977.
11. Ma, S. *Modern theory of critical phenomena;* Da Capo Press: 2000; .

12. Wang, Y.; Rubner, M. Electrically conductive semiinterpenetrating polymer networks of poly (3-octylthiophene). *Macromolecules* 1992, *25*, 3284-3290.

13. Abeles, B.; Pinch, H.; Gittleman, J. Percolation conductivity in W-Al 2 O 3 granular metal films. *Phys. Rev. Lett.* 1975, *35*, 247.

14. Clarke, P.; Orton, J.; Guest, A. Electrical-conductivity and Hall-effect measurements in semiconducting powders. Study of percolation effects. *Physical Review B* 1978, *18*, 1813.

15. Hsu, W. Y.; Berzins, T. Percolation and effective-medium theories for perfluorinated ionomers and polymer composites. *Journal of Polymer Science: Polymer Physics Edition* 1985, *23*, 933-953.

16. Hsu, W. Y.; Holtje, W. G.; Barkley, J. R. Percolation phenomena in polymer/carbon composites. *J. Mater. Sci. Lett.* 1988, *7*, 459-462.

17. Hsu, W. Y.; Wu, S. Percolation behavior in morphology and modulus of polymer blends. *Polymer Engineering & Science* 1993, *33*, 293-302.

18. Maruyama, K.; Okumura, K.; Miyazima, S. Critical exponents of continuum percolation. *Physica A: Statistical Mechanics and its Applications* 1992, *191*, 313-315.

19. Metzner, A. Rheology of suspensions in polymeric liquids. *Journal of Rheology (1978-present)* 1985, *29*, 739-775.

20. Kitano, T.; Kataoka, T.; Shirota, T. An empirical equation of the relative viscosity of polymer melts filled with various inorganic fillers. *Rheologica Acta* 1981, *20*, 207-209.

21. Bouillot, J.; Camoin, C.; Belzons, M.; Blanc, R.; Guyon, E. Experiments on 2-D suspensions. *Adv. Colloid Interface Sci.* 1982, *17*, 299-305.

22. Stauffer, D. Scaling theory of percolation clusters. *Physics reports* 1979, *54*, 1-74.

23. Efros, A.; Shklovskii, B. Critical Behaviour of Conductivity and Dielectric Constant near the Metal-Non-Metal Transition Threshold. *Physica status solidi (b)* 1976, *76*, 475-485.

24. Mamunya, E.; Davidenko, V.; Lebedev, E. Compos Interf 1997, 4, 169. *CrossRef*| *CAS* .

25. Antonov, A.; Batenin, V.; Vinogradov, A.; Kalachev, A.; Kulakov, A.; Lagar'kov, A.; Matytsin, S.; Panina, L.; Rozanov, K.; Sarychev, A. Electrophysical Properties of Percolation Systems. *Institute for High Temperatures, Russian Academy of Science, USSR, Moscow* 1990.

26. Sokolov, I. Dimensions and Other Geometrical Critical Parameters in the Percolation Theory. *Usp.Fiz.Nauk* 1986, *150*, 233-237.

27. Barber, M.; Domb, C.; Lebowitz, J. Phase Transitions and Critical Phenomena, vol. 8Academic. *New York* 1983, 146.

28. Polymers—Properties, M. Applications, edited by SK Bhattacharya. 1986.

29. Chen, I.; Johnson, W. Alternating-current electrical properties of random metal-insulator composites. *J. Mater. Sci.* 1991, *26*, 1565-1576.

30. Mamunya, E.; Davidenko, V.; Lebedev, E. Percolation conductivity of polymer composites filled with dispersed conductive filler. *Polymer Composites* 1995, *16*, 319-324.

31. Bigg, D.; Stutz, D. Plastic composites for electromagnetic interference shielding applications. *Polymer composites* 1983, *4*, 40-46.

32. Sun, J.; Gokturk, H.; Kalyon, D. Volume and surface resistivity of low-density polyethylene filled with stainless steel fibres. *J. Mater. Sci.* 1993, *28*, 364-366.

33. Göktürk, H. S.; Fiske, T. J.; Kalyon, D. M. Effects of particle shape and size distributions on the electrical and magnetic properties of nickel/polyethylene composites. *J Appl Polym Sci* 1993, *50*, 1891-1901.

34. Bridge, B.; Folkes, M.; Jahankhani, H. Low voltage electrical properties of polypropylene filled with stainless steel fibres and a model of sample conductivity based on fibre geometry. *J. Mater. Sci.* 1989, *24*, 1479-1485.

35. Mamunya, E.; Davidenko, V.; Lebedev, E. Properties of functionally filled polymer system in function of properties and content of disperse fillers. *Composites Polym Mater* 1991, 37-47.

36. Katz, H. S.; Milewski, J. V. *Handbook of fillers and reinforcements for plastics;* Van Nostrand Reinhold Co.: 1978; .

37. McGeary, R. Mechanical packing of spherical particles. *J Am Ceram Soc* 1961, *44*, 513-522.

38. Katz, H. S.; Milewski, J. V. *Handbook of fillers and reinforcements for plastics;* Van Nostrand Reinhold Co.: 1978; .

39. Isichenko, M. B. Percolation, statistical topography, and transport in random media. *Reviews of modern physics* 1992, *64*, 961.

40. Sahimi, M. Flow phenomena in rocks: from continuum models to fractals, percolation, cellular automata, and simulated annealing. *Reviews of modern physics* 1993, *65*, 1393.

41. Scher, H.; Zallen, R. Critical density in percolation processes. *J. Chem. Phys.* 1970, *53*, 3759.

42. Lux, F. Models proposed to explain the electrical conductivity of mixtures made of conductive and insulating materials. *J. Mater. Sci.* 1993, *28*, 285-301.

43. Wessling, B. Dispersion hypothesis and non-equilibrium thermodynamics: key elements for a materials science of conductive polymers. A key to understanding polymer blends or other multiphase polymer systems. *Synth. Met.* 1991, *45*, 119-149.

44. Mamunya, Y. P. Morphology and percolation conductivity of polymer blends containing carbon black. *Journal of Macromolecular Science—Physics* 1999, *38*, 615-622.

45. Miyasaka, K.; Watanabe, K.; Jojima, E.; Aida, H.; Sumita, M.; Ishikawa, K. Electrical conductivity of carbon-polymer composites as a function of carbon content. *J. Mater. Sci.* 1982, *17*, 1610-1616.

46. Mamunya, Y. P. Morphology and percolation conductivity of polymer blends containing carbon black. *Journal of Macromolecular Science—Physics* 1999, *38*, 615-622.

47. Kusy, R. P.; Corneliussen, R. D. The thermal conductivity of nickel and copper dispersed in poly (vinyl chloride). *Polymer Engineering & Science* 1975, *15*, 107-112.

48. Sumita, M.; Sakata, K.; Asai, S.; Miyasaka, K.; Nakagawa, H. Dispersion of fillers and the electrical conductivity of polymer blends filled with carbon black. *Polymer bulletin* 1991, *25*, 265-271.

49. Sumita, M.; Sakata, K.; Hayakawa, Y.; Asai, S.; Miyasaka, K.; Tanemura, M. Double percolation effect on the electrical conductivity of conductive particles filled polymer blends. *Colloid Polym. Sci.* 1992, *270*, 134-139.

50. Mamunya, Y. P.; Muzychenko, Y. V.; Pissis, P.; Lebedev, E.; Shut, M. Percolation phenomena in polymers containing dispersed iron. *Polymer Engineering & Science* 2002, *42*, 90-100.

51. Mamunya, Y. P.; Davydenko, V.; Pissis, P.; Lebedev, E. Electrical and thermal conductivity of polymers filled with metal powders. *European polymer journal* 2002, *38*, 1887-1897.

52. Kusy, R. Influence of particle size ratio on the continuity of aggregates. *J. Appl. Phys.* 1977, *48*, 5301-5305.

53. Malliaris, A.; Turner, D. Influence of particle size on the electrical resistivity of compacted mixtures of polymeric and metallic powders. *J. Appl. Phys.* 1971, *42*, 614-618.

54. Mamunya, E.; Davidenko, V.; Lebedev, E. Influence of the Geometric Parameters of the Framework Formed by Dispersed Fillers on the Properties of Polymer Composites. *Kolloidn. Zh.* 1990, *52*, 145-150.

55. Tchoudakov, R.; Breuer, O.; Narkis, M.; Siegmann, A. Conductive polymer blends with low carbon black loading: polypropylene/polyamide. *Polymer Engineering & Science* 1996, *36*, 1336-1346.

56. Gul, V.; Shenfil, L. Elektroprovodyashchie polimernye kompozitsii. *Polymer Conducting Composites), Moscow: Khimiya* 1984.

57. Progelhof, R.; Throne, J.; Ruetsch, R. Methods for predicting the thermal conductivity of composite systems: a review. *Polymer Engineering & Science* 1976, *16*, 615-625.

58. Bigg, D. Thermal conductivity of heterophase polymer compositions. In *Thermal and electrical conductivity of polymer materials*Springer: 1995; pp 1-30.

59. Sundstrom, D. W.; Lee, Y. Thermal conductivity of polymers filled with particulate solids. *J Appl Polym Sci* 1972, *16*, 3159-3167.

60. Agari, Y.; Uno, T. Thermal conductivity of polymer filled with carbon materials: effect of conductive particle chains on thermal conductivity. *J Appl Polym Sci* 1985, *30*, 2225-2235.

61. Rymarenko, N. L.; Voitenko, A. I.; Novikov, V. V.; Privalko, V. P. *Ukrain Polym J* 1992, *1*, 259–266.

62. Mamunya, E. Electrical and thermal conductivity of metal-filled polymer composites. *Funct Mater* 1998, *5*, 410-412.

63. Progelhof, R.; Throne, J.; Ruetsch, R. Methods for predicting the thermal conductivity of composite systems: a review. *Polymer Engineering & Science* 1976, *16*, 615-625.

64. Mamunya, E. Electrical and thermal conductivity of metal-filled polymer composites. *Funct Mater* 1998, *5*, 410-412.

65. McGeary, R. Mechanical packing of spherical particles. *J Am Ceram Soc* 1961, *44*, 513-522.

66. Salazar, A.; Sanchez-Lavenga, A.; Terron, J. M. *J Appl Phys* 1998, *84*, 3031–3041.

67. Favier, V.; Cavaille, J.; Canova, G.; Shrivastava, S. Mechanical percolation in cellulose whisker nanocomposites. *Polymer Engineering & Science* 1997, *37*, 1732-1739.

68. Kuo, C.; Gupta, P. K. Rigidity and conductivity percolation thresholds in particulate composites. *Acta metallurgica et materialia* 1995, *43*, 397-403.

69. Favier, V.; Dendievel, R.; Canova, G.; Cavaille, J.; Gilormini, P. Simulation and modeling of three-dimensional percolating structures: case of a latex matrix reinforced by a network of cellulose fibers. *Acta Materialia* 1997, *45*, 1557-1565.

70. Favier, V.; Chanzy, H.; Cavaille, J. Polymer nanocomposites reinforced by cellulose whiskers. *Macromolecules* 1995, *28*, 6365-6367.

71. Favier, V.; Canova, G.; Cavaillé, J.; Chanzy, H.; Dufresne, A.; Gauthier, C. Nanocomposite materials from latex and cellulose whiskers. *Polym. Adv. Technol.* 1995, *6*, 351-355.

72. Takayanagi, M.; Uemura, S.; Minami, S. In *In Journal of Polymer Science Part C;* Polymer Symposia; 1964; Vol. 5, pp 113-122.

73. Ouali, N.; Cavaillé, J.; Perez, J. Elastic, viscoelastic and plastic behavior of multiphase polymer blends. *Plastics, Rubber and Composites Processing and Applications (UK)* 1991, *16*, 55-60.

74. Staufer, D.; Aharony, A. Introduction to percolation theory. *Tailor & Francis, London* 1985.

75. De Gennes, P. *Scaling concepts in polymer physics;* Cornell university press: 1979; .

76. Balberg, I.; Binenbaum, N.; Wagner, N. Percolation thresholds in the three-dimensional sticks system. *Phys. Rev. Lett.* 1984, *52*, 1465.

77. Ueda, N.; Taya, M. Prediction of the electrical conductivity of two-dimensionally misoriented short fiber composites by a percolation model. *J. Appl. Phys.* 1986, *60*, 459-461.

78. Yin, X.; Kobayashi, K.; Yoshino, K.; Yamamoto, H.; Watanuki, T.; Isa, I. Percolation conduction in polymer composites containing polypyrrole coated insulating polymer fiber and conducting polymer. *Synth. Met.* 1995, *69*, 367-368.

79. Balberg, I.; Binenbaum, N. Computer study of the percolation threshold in a two-dimensional anisotropic system of conducting sticks. *Physical Review B* 1983, *28*, 3799.

2.8. Figures

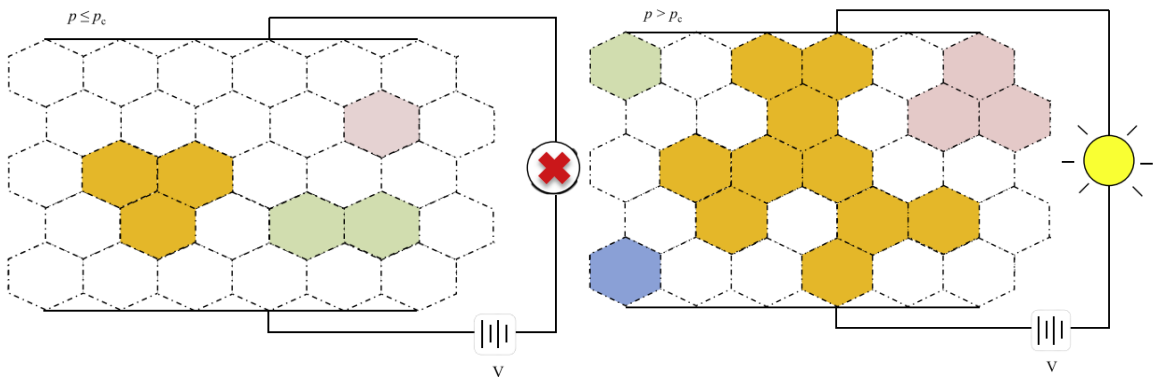

Figure 1: Schematic illustration of a simple circuit including a bulb and a voltage source connected to an insulator honeycomb lattice which can be furnished by a fraction of ϕ of metallic plaquettes. Once the value of ϕ eaches at the critical value of ϕ^*, a spanning metallic cluster emerges which connects the two sides of the lattice and the bulb suddenly lights up. Reaching at this exact point of connectivity is the signature of network percolation. Image taken from Ref. 8.

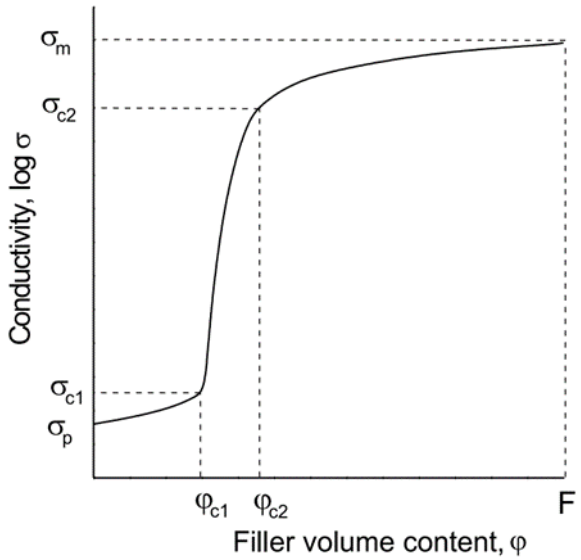

Figure 2: Typical dependence of electrical conductivity (logarithm) on conductive filler volume content. Image taken from Ref. 23.

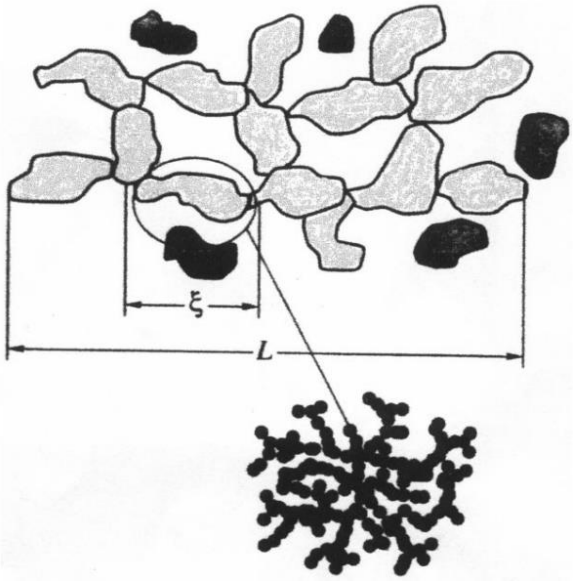

Figure 3: The structure of conducting composition at $\sigma > \sigma_p$ and the correlation length.

Image taken from Ref. 1.

(a) (b)

Figure 4: Structure model of the PE/POM-Fe composite at (a) $\varphi < \varphi_C$ and (b)$\varphi > \varphi_C$. Image taken from Ref. 51.

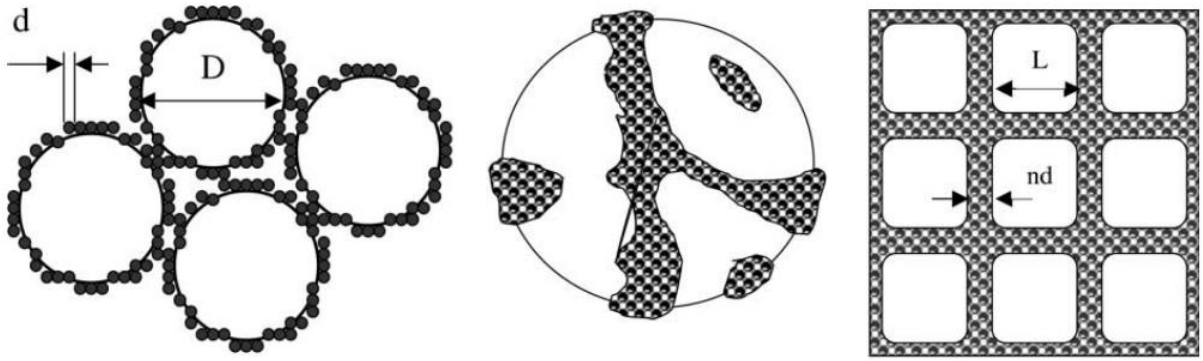

(a) (b) (c)

Figure 5: (a) Schematic representation of the assumed distribution of polymer and metal particles having D and d sizes, respectively.[51] (b) The minimal particle covering with metallic particles needed for conductivity arising in the system[52] and (c) schematic representation of the shell structure model having shell thickness equal to nd [51]. Image taken from Ref. 23.

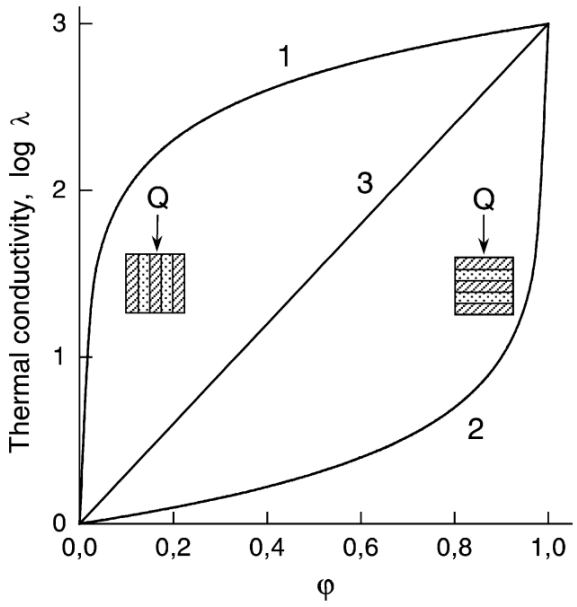

Figure 6: The two-phase thermal conductivity depending on the composition of the system: (1) The largest thermal conductivity calculated according to equation (3); (2) the smallest thermal conductivity according to equation (3); (3) thermal conductivity according to Lichtenecker's equation (5). The values of λ_p and λ_f were fixed at 1 and 10^3, respectively, for the sake of calculation. Q is the direction of heat flow. Image taken from Ref. 23.

CHAPTER 3

Thermoplastic Elastomer Systems Containing Carbon Nanofibers as Soft Piezoresistive Sensors**

ABSTRACT

Soft, wearable or printable strain sensors derived from conductive polymer nanocomposites (CPNs) are becoming increasingly ubiquitous in personal-care applications. Common elastomers employed in the fabrication of such piezoresistive CPNs frequently rely on chemically-crosslinked polydiene or polysiloxane chemistry, thereby generating relatively inexpensive and reliable sensors that become solid waste upon application termination. Moreover, the shape anisotropy of the incorporated conductive nanoparticles can produce interesting electrical effects due to strain-induced spatial rearrangement. In this study, we investigate the morphological, mechanical, electrical, and electromechanical properties of CPNs generated from thermoplastic elastomer (TPE) triblock copolymer systems containing vapor-grown carbon nanofiber. Modulus-tunable TPE gels imbibed with a midblock-selective aliphatic oil exhibit well-behaved properties with increasing CNF content, but generally display nonlinear negative piezoresistance at different strain amplitudes and stretch rates due to nanofiber mobility upon CPN strain-cycling. In contrast, a neat TPE possessing low hard-block content yields a distinctive strain-reversible piezoresistive response, as well as low electrical hysteresis, upon cyclic deformation. Unlike their chemically-crosslinked analogs, these physically-crosslinked and thus environmentally benign CPNs are fully reprocessable by thermal and/or solvent means.

** This chapter was published in its entirety:

Turgut, A., Tuhin, M. O., Toprakci, O., Pasquinelli, M. A., Spontak, R. J., & Toprakci, H. A. (2018). Thermoplastic Elastomer Systems Containing Carbon Nanofibers as Soft Piezoresistive Sensors. *ACS Omega*, *3*(10), 12648-12657.

3.1. Introduction

Concurrent development of portable electronic devices and soft responsive materials is responsible for generating a new class of functional devices for personal healthcare and electronic textiles.[1-5] Such devices augment flexible polymeric materials with electronic capabilities for a wide range of sensory applications, such as motion or pulse monitoring.[6,7] They can be freestanding as, for example, a wristband[8,9] or printed as a thin conductive coating on a substrate, including fabrics.[10] While inherently conductive polymers such as polypyrrole are often suitable for these purposes,[11-13] they are generally expensive to process and frequently unstable. Conductive polymer nanocomposites (CPNs), consisting of electrically conductive nanoparticles homogeneously dispersed in an elastomeric matrix, constitute viable alternatives to conductive polymers for use in electronic devices.[14-21] Important advantages of CPNs for these purposes include the use of nanoscale fillers that can vary in size, shape, species, and therefore conductivity; nanofillers generally possessing a large surface-to-volume ratio that favors surface functionalization to promote dispersability within an organic matrix;[22-25] preparation and application methodologies that are both straightforward and cost-effective; and fabrication that extends from free-standing films exhibiting high extensibility to conformal print layers deposited over large, non-uniform areas. Another attractive aspect of CPNs is that the electrical and mechanical properties are composition-tunable,[26] which favors the use of conductive nanofillers possessing a low percolation threshold signaling the onset of a continuous conductive network in the polymer matrix. Excellent examples of nanofillers fulfilling this requirement are carbon black (CB),[27] carbon nanotubes (CNTs),[28-30] graphene (G),[31,32] and carbon nanofibers (CNFs).[10,33] Their high surface-to-volume ratio and correspondingly high surface energy permit surface functionalization to ensure good dispersion and strong matrix-filler bonding.

In this study, we focus on CPNs containing CNF, which possesses high conductivity levels and relatively low percolation thresholds[34] ranging from 0.5 to 2.0 vol%, depending on processing methodology and CNF characteristics.[35-37] These nanofillers are particularly appealing because of their facile dispersability in a wide variety of polymer matrices, as well as their lower cost compared to CNTs. The elastomers utilized in the present work consist of triblock copolymers that, with glassy endblocks and a rubbery midblock, behave as thermoplastic elastomers (TPEs).[38] Due to thermodynamic incompatibility between the chemically-dissimilar sequences, these copolymers microphase-separate[39-41] to form glassy micelles that serve as physical crosslinks to stabilize a molecular network composed of bridged midblocks.[42-44] This elastomer motif extends to TPEs preferentially swollen in a midblock-selective oil, and the phase behavior of, along with the fraction of midblock bridges in, the resulting TPE gels (TPEGs) has been found to depend on copolymer composition, molecular weight, architecture, and concentration.[45,46] Incorporation of CNFs into the TPEs considered here results in CPNs that can be used as piezoresistive sensors capable of relating sensor resistivity to strain state for real-time monitoring of bodily functions[6,47-49] (e.g., respiration and cardiovascular activity) insofar as high-sensitivity sensors possess low strain-cycling hysteresis[50] to maintain superior signal integrity. In one such design, CB-containing TPEs have been reported[51-53] to exhibit either linear or non-linear positive piezoresistance wherein resistance increases with increasing strain. While this phenomenon is typically induced in CPNs by in-plane tensile strain, several efforts have demonstrated that strain-reversible piezoresistivity in which a negative□positive piezoresistivity transition that is repeatable upon strain cycling likewise occurs in CPNs containing anisotropic nanofillers, including G,[54] CNT[55] and CNF.[10] In the present study, we examine the morphological, mechanical, electrical, and electromechanical properties of CNF/TPE(G) CPNs.

3.2. Experimental

3.2.1. Materials

Two poly[styrene-*b*-(ethylene-*co*-butylene)-*b*-styrene] (SEBS) triblock copolymers were employed in this work. The first (SEBS1, Taipol 6151) obtained from TSRC-DEXCO was a conventional TPE with 32 wt% S and a number-average molecular weight (M_n) of 186 kDa (Đ = 1.05), according to in-house gel permeation chromatography performed on a Viscotek Max System. The second (SEBS2, Tuftec H1221) with M_n = 55 kDa (Đ = 1.08) was provided by Asahi KASEI and possessed a significantly lower S content (12 wt%). An aliphatic white mineral oil with a molecular weight of 567 Da and reagent-grade toluene were purchased from A.Ş/Petroyag Lubricants and Merck, respectively, and used as-received. Vapor-grown CNF measuring 130 nm on average in diameter and 20 to 200 nm in length was obtained from Sigma-Aldrich.

3.2.2. Methods

The CPN films examined here were produced according to a 3-step mixing procedure. In the first step, either the SEBS1 copolymer containing 70 wt% mineral oil or the SEBS2 copolymer without mineral oil was dissolved in toluene for 12 h under agitation at ambient temperature. In the second step, a suspension of CNF in toluene was prepared by adding a predetermined mass of CNF to 10 g toluene and then subjecting the mixture to high shear in a Kurabo-Mazerustar KK250 planetary mixer for 90 s. In the final mixing step, the polymer solution was added to the suspension and shear-mixed for an additional 90 s. The resultant suspensions were cast into a Petri dish and dried under vacuum for 12 h at 50 °C. Dried films were melt-pressed at 190 °C for 15 min (TPEG) or 180 °C for 3 min (TPE) to a thickness of 0.8-0.9 mm. Specimens from both CPN series selected for examination by SEM were cryofractured in liquid nitrogen prior to mounting. Images of uncoated CNFs and CPNs were obtained on a field emission JEOL JSM-6400 electron microscope

(Middle East Technical University) and on an ultrahigh-resolution FEI Verios 460L Schottkey emitter electron microscope (North Carolina State University), respectively, both operated at an accelerating voltage of 20 kV. Quasi-static uniaxial tensile strain analysis of the CPNs was performed on a Devotrans DVT universal load frame. For each CPN, 3 rectangular specimens measuring 25 mm x 5 mm were cut from larger films and tested to determine the nominal (engineering) stress as a function of true tensile strain.

The volume resistivity of each CPN was determined with a Keithley Model 6517B electrometer and Model 8009 resistivity chamber in accordance with the ASTM D-257 standard. Before conducting the electrical measurements, specimen thicknesses were discerned using an Asimeto digital thickness meter. At least 5 measurements were collected so that average and standard error values could be calculated. To determine the piezoresistive behavior of the CPNs in the longitudinal direction (parallel to the applied strain), specimens measuring 80 mm x 25 mm were attached to four electrical leads spaced 10 mm apart along the centerline of the specimen parallel to the longitudinal direction. The leads were adhered to each CPN surface with a conductive adhesive containing 40 wt% CB prepared for this purpose. Test specimens were clamped on a customized load frame having the gauge length set at 50 mm and subsequently cycled to 10-50% strain amplitudes at elongation rates of 20 and 100 mm/min to ascertain the effects of strain and stretch rate. Dynamic resistance measurements were simultaneously conducted using a computer-controlled setup consisting of a current source (Keithley 6221) and a nano-voltmeter (Keithley 2182A) under an input current of 1 μA. Resistance was recorded as a function of time, and all CPNs in each series were evaluated for at least ten continuous loading/unloading cycles at a constant crosshead speed.

3.3. Results and Discussion

The present study focuses on the preparation and characterization of soft, low-hysteresis sensory materials that consist of either a neat TPE or an oil-containing TPEG modified with CNF. A representative scanning electron microscopy (SEM) image of the vapor-grown CNFs deposited from suspension is displayed in **Figure 1** and qualitatively confirms the nanofiber dimensions listed by the supplier (see the Experimental section). The enlarged area reveals that some of the nanofibers are at least semi-flexible. To ensure a relatively uniform dispersion of CNF in each of the CPNs investigated here, we have concurrently prepared TPE solutions permitted to reach equilibrium and CNF suspensions exposed to high-shear mixing before combining them and subjecting the resultant suspension to additional high-shear mixing. Further heat treatment during melt-pressing assists in both solvent removal and refinement of the TPE morphology. Although we do not provide electron microscopy images or small-angle scattering data of the TPE or TPEG employed in this work, previous morphological investigations have conclusively established[56-58] that, under the present experimental conditions, both materials consist of a spherical morphology wherein glassy styrenic (S) micelles are arranged on an unspecified lattice. Due to the size of the midblock relative to each of the endblocks in conventional TPEs (typically with 30-33 wt% endblocks), the most commonly observed morphology consists of "hairy" micelles arranged on a body-centered cubic (bcc) lattice. In the presence of a midblock-selective oil that can disrupt long-range order, however, face-centered cubic (fcc) and hexagonal close-packed (hcp) morphologies have also been reported. While the TPE(G) morphology governs property development, the only morphological aspect of interest here is the presence of spherical micelles, which ensure the highest fraction of midblock bridges needed for a highly elastomeric material.

A series of cross-fracture SEM images acquired at two different magnifications (arranged in rows)

from TPEG-based CPNs varying in CNF content from 4 to 6 wt% are provided in **Figure 2**. In these and subsequent images, the CNF appears bright due to its ability to conduct electrons. At 4 wt% CNF in **Figures 2a** and **2d**, the nanofibers possess random trajectories and indicate little evidence of long-range correlation. Some large regions observed in **Figure 2a** appear dark (without CNF), implying that the CNF distribution within these TPEGs is not entirely uniform. As the CNF content is increased to 5 wt% in **Figures 2b** and **2e**, more nanofibers are visible. Interestingly, regions largely devoid of CNF remain evident in **Figure 2b**. At the highest CNF fraction examined here (6 wt%), the nanofibers seen in **Figures 2c** and **2f** are more numerous relative to the earlier images and are more highly correlated. Taken together (**Figures 2a-c** and **Figures 2d-f**), the CNF population and spatial arrangement in these image series can be interpreted to predict that the CPN stiffness (expressed in terms of tensile modulus) and conductivity (expressed in terms of electrical resistance) both increase with increasing CNF content. These properties are considered further below. Similar morphological trends are apparent for the TPE-based CPNs at the same CNF loading levels as in **Figure 3**. An important difference between the images in **Figures 2** and **3** is the absence of relatively large regions that lack CNF in **Figure 3**. At the lowest CNF fraction (4 wt%) in **Figures 3a** and **3d**, nanofibers are isolated but uniformly dispersed. In marked contrast, semi-flexible CNF seems highly connected at 5 wt% in **Figures 3b** and **3e**, and then highly correlated at 6 wt% in **Figures 3c** and **3f**. The

extent to which the CNF appears correlated in **Figures 2c** and **3c** is qualitatively comparable.

Quasi-static tensile tests of CPNs composed of the TPEG and TPE containing CNF are presented in **Figures 4a** and **4b**, respectively, and immediately reveal that the addition of CNF shifts the response curve of each material to progressively higher stresses. This shift is more clearly delineated for the TPEG-based CPNs in **Figure 4a** due to the inherently lower stresses

generated with these soft materials. Since the sensors considered here are not expected to function at very high strain levels, we have not evaluated the ultimate properties of these CPNs at failure (which can exceed 2000% strain for unmodified TPEGs derived from midblock-swollen triblock copolymers). Values of the tensile modulus (E) extracted from response curves such as those displayed in **Figures 4a** and **4b** are included in **Figure 4c** and indicate that E increases with increasing CNF content in both material systems. While the composition dependence of E is routinely expressed in terms of a mixing rule,[23,59-61] the increases in E evident in **Figure 4c** can alternatively be empirically modeled as an exponential function of the form $E = E_0 \exp(\square\square)$,where E_0 ideally represents the modulus of the neat TPE(G) without CNF, $\square$ is a fitted parameter and $\square$ denotes the CNF content (in wt%).[a,b] Values of $\square$ obtained by regression of this expression to the data (with an adjustable E_0) are numerically comparable for TPEG- and TPE-based CPNs. Although such similarity between independent $\square$ values is comforting, this empirical correlation does not imply a fundamental physical relationship. Rather, the primary purpose of these tensile measurements is to discern the extent to which the mechanical properties of the CPNs change in two related polymer matrices upon addition of CNF. Without mineral oil, the TPE (with E = 1.28 MPa) possesses a higher modulus than the TPEG (with E = 0.15 MPa) by about an order of magnitude, confirming that the addition of a midblock-selective diluent can lower the modulus below that of a neat TPE with a higher rubber content. The ability to tune the properties of TPEGs

[a] While mixing rules can be written in many different functional forms, the most successful one employed here is a linear rule given by $\ln E_c = (\phi/100) \ln E_f + (1 - \phi/100) \ln E_p$, where the subscripts c, f and p refer to the nanocomposite, CNF and polymer, respectively. We elect not to use this expression, however, since the extracted values of E_f are inconsistent, varying by orders of magnitude, between the TPE and TPEG datasets. We note that the value of E_f discerned from the TPE tensile data (~93 GPa) is most similar to that reported for CNF in the literature (ranging from about 25 GPa in ref. 59 to about 50 GPa in ref. 60).

[b] Application of the Cox model described in ref. 61 to the two tensile datasets in **Figure 4c** suggests that the aspect ratio of the CNF in the TPE is significantly smaller (< 40) than that in the TPEG (> 100). If real, the most likely cause for such a difference is the mechanical mixing employed to disperse the CNF, since the TPE possesses a higher melt viscosity.

beyond what is achievable with neat TPEs constitutes an important consideration in the development of soft materials.

Since the current materials are being proposed for sensory applications, their static (*i.e.*, deformation-free) electrical properties must be elucidated as a function of CNF content. For this reason, volume resistivity measurements are provided for both TPEG- and TPE-based CPNs in **Figure 5**. Without CNF, the two matrix elastomers exhibit high resistivity levels ranging from about 10^{16} to 10^{18} Ω-cm. As anticipated from prior studies,[62,63] incorporation of CNF improves conductivity by reducing the resistivity by several orders of magnitude. In the case of the TPE-based CPNs, the resistivity undergoes a precipitous drop from *ca*. 3 x 10^{13} to 5 x 10^{6} Ω-cm, indicative of a percolation threshold between 2 and 3 wt%. In addition to percolation theory[64] (which presumes universal behavior on the basis of network characteristics), a variety of theoretical models interpret the percolation threshold by accounting for such factors as random heterogeneities and quantum tunneling.[65,66] In marked contrast, the CNF-induced reduction in resistivity for the TPEG-based CPNs does not display an abrupt change in resistivity. Instead, the decrease is gradual after remaining almost constant up to 1 wt% CNF. This behavior likely reflects the presence of liquid mineral oil, which wets CNF surfaces and thus hinders contact between neighboring nanoparticles. In addition, volume resistivities measured from both CPN series are observed to converge unexpectedly at 7 wt% CNF. The results presented in **Figures 4** and **5** confirm that the addition of CNF to either the TPEG or TPE utilized in this study simultaneously increases both the modulus and conductivity (by reducing the resistivity), which is consistent with the SEM images included in **Figures 2** and **3**. Morphological dissimilarities, coupled with the nontrivial variation in electrical properties evident in **Figure 5**, further suggest that the electromechanical properties of TPEG- and TPE-based CPNs can be expected to differ. These

properties, critically important for sensor performance, are discussed below.

As described in the Experimental section, the extent to which the CPNs are uniaxially strained is investigated in conjunction with the elongation, or stretch, rate. Maximum strain values examined here reflect material limitations regarding either signal quality (TPEGs) or matrix integrity (TPEs) upon strain cycling. Cyclic electrical resistance measurements are provided as a function of time (or strain) for TPEG-based CPNs containing 6 wt% CNF and subjected to 10 and 20% strain in **Figures 6** and **7**, respectively. In each of these figures, panel (a) provides results that are strain-cycled at a stretch rate of 20 mm/min, and panel (b) displays analogous resistance data collected at 100 mm/min. For comparison, resistance measurements acquired during the first and last full strain cycles for each stretch rate are plotted together as a function of dimensionless time (normalized with respect to the cycle time) in panel (c). First, we consider the TPEG strain-cycled to 10% in **Figures 6a** and **6b**. At both 20 and 100 mm/min, the maximum resistances averaged over 50 strain cycles are 1.60 ± 0.01 M□, and 1.57 ± 0.01 M□, respectively, whereas the mean minimum resistances exhibit slightly more variation: 1.20 ± 0.04 M□ at 20 mm/min and 1.27 ± 0.04 M□ at 100 mm/min, respectively. The single-cycle comparisons included in **Figure 6c** reveal several notable features. The most important aspect of these data is that the electrical resistance generally decreases nonlinearly with increasing strain up to the 10% strain limit, at which time it undergoes strain reversal and proceeds to increase with decreasing strain until the cycle is completed. Such behavior identifies the existence of nonlinear negative piezoresistance during the first and final cycles for both stretch rates. Less consistent results are apparent for the same TPEG-based CPNs subjected to 20% strain in **Figure 7**. The maximum and minimum resistance values measured at 20 mm/min in **Figure 7a** are 1.49 ± 0.03 M□ and 0.70 ± 0.07 M□, respectively, while those corresponding to 100 mm/min in **Figure 7b** are 1.21 ± 0.05 M□ and 0.53 ± 0.15 M□,

respectively. In **Figure 7c**, the noisier results imply inferior piezoresistive behavior, as well as overall signal quality.

The single-cycle data collected at 10% strain and 100 mm/min appear relatively smooth in **Figure 6c**, but those corresponding to 20 mm/min are significantly noisier. We attribute the resistance fluctuations visible in these data to dynamically-occurring changes in CNF connectivity. The nanofibers, residing in an oil-swollen rubber matrix, possess greater mobility than in oil-free rubber and can change their position/orientation and, thus, 3D connectivity and corresponding electrical conductivity during tensile deformation. In this scenario, the nanofibers generally become more connected as the CPN is uniaxially strained to yield a reduction in electrical resistance (and a corresponding increase in conductivity). As time (and strain) increase prior to strain reversal at 10% during each strain cycle in which the CPN is stretched at 20 mm/min, the resistance suddenly, but not completely, reverses due to a loss of CNF connectivity as the nanofibers change their position and/or orientation upon further strain. The abruptness of this change in resistance resembles rheological slip encountered[67] in filled polymers during shear deformation. As the strain continues, alternating, but often short-lived, fluctuations in resistance continue until the maximum strain (at 10%) is reached. Beyond this point, the CPN is allowed to relax as the load is gradually released, and the fluctuations in resistance remain but are less pronounced and regular. This behavior manifested during the first strain cycle is retained during the last strain cycle, but an increase in crosshead speed to 100 mm/min completely eliminates these fluctuations in **Figure 6c**. If the strain amplitude is increased to 20% in **Figure 7c**, the fluctuations become more stochastic and the net reduction in resistance prior to strain reversal appears delayed at 20 mm/min. Even the results acquired at 100 mm/min signify the presence of resistance fluctuations due to nanofiber rearrangement. Thus, while TPEGs exhibit relatively negligible

mechanical hysteresis (low irrecoverable strain or set) upon strain cycling, incorporated conductive nanofillers retain unexpectedly high mobility, which serves to deteriorate the quality of the electrical signal.

In marked contrast, the piezoresistance results included for the TPE-based CPNs in **Figures 8** and **9** verify highly stable signal quality, as well as the existence of strain-induced reversible piezoresistivity. At 20% strain in **Figures 8a** (20 mm/min) and **8b** (100 mm/min), the average values of the measured maximum and minimum resistance are 30.4 ± 0.3 and 12.1 ± 0.3 k□, respectively, at 20 mm/min and 39.9 ± 0.3 and 15.2 ± 0.3 k□, respectively, at 100 mm/min. These results confirm much less signal variation than that observed at the same strain amplitude for the TPEG in **Figures 7a** and **7b**. If the strain amplitude is increased to 50% in **Figures 9a** and **9b**, the extent to which the maximum and minimum resistance values vary clearly increases: 97.8 ± 6.6 and 28.4 ± 0.7 k□, respectively, at 20 mm/min and 216 ± 16 and 52.0 ± 4.7 k□, respectively, at 100 mm/min. The single-cycle measurements presented in **Figures 8c** for 20% strain and **9c** for 50% strain reveal two important characteristics. The first is that, at 20 mm/min, results from the first and last cycle are nearly indistinguishable, thereby indicating virtually no electrical hysteresis. At 100 mm/min, the resistance at the point of strain reversal decreases noticeably upon strain cycling. This observation provides indirect evidence that either the CNF permanently changes its position upon cycling or the cycling occurs too fast to permit the CNF to return to its original position (and resistance level). The second noteworthy features is that, in all cases, the resistance initially decreases, exhibits a minimum and then increases prior to strain reversal. We have previously described[10] such strain-reversible piezoresistivity in terms of three distinct stages of strain-induced changes in CNF percolation due to CNF rotation/straightening and translation along the strain axis.

In Stage I, uniaxial strain induces a corresponding reduction in the cross-sectional area of the CPN normal to the strain axis (since the deformation is considered to be isochoric). By doing so, the randomly oriented nanofibers embedded in the polymeric matrix begin to straighten, rotate and align along the strain axis as the glassy micelles formed by the copolymer continue to serve as physical crosslinks to stabilize the TPE matrix. During this typically observed electromechanical process, the 3D connectivity of the nanofibers and, consequently, the conductivity of the CPN concurrently increase so that the measured resistance decreases, resulting in negative piezoresistivity. When the strain level reaches a critical value at Stage II, however, the extent of CNF connectivity becomes briefly independent of strain. Once the CPN enters Stage III, the nanofibers in contact separate due to increased distance along the strain axis, thereby lowering the overall conductivity of the CPN and promoting positive piezoresistivity. Such strain-reversible piezoresistivity is qualitatively consistent with prior reports[68-70] revealing that the maximum conductivity in thermoplastic CPNs containing CNTs occurs at intermediate alignment levels. The unexpected and remarkable aspect of **Figures 8c** and **9c** is that all three stages associated with strain-reversible piezoresistivity are clearly delineated at both of the strain and elongation rate levels examined for the first and final strain cycles.

3.4. Conclusions

Soft strain sensors are of growing technological interest in the fabrication of portable healthcare products and wearable electronic textiles. In this study, we have examined the morphological, mechanical, electrical and electromechanical properties of conductive polymer nanocomposites composed of vapor-grown carbon nanofibers embedded in either a thermoplastic elastomer or a thermoplastic elastomer gel. Comparison of SEM images acquired from representative specimens confirms that the nanofibers expectedly increase in both population density and local correlation

as the nanofiber loading level is increased. This increase in nanofiber content is accompanied by increases in tensile modulus and electrical conductivity. One distinguishing characteristic between the two nanocomposite series is that the one consisting of the neat thermoplastic elastomer matrix exhibits a well-defined percolation threshold, whereas the one with the thermoplastic elastomer gel does not. This behavior is reflected in profound differences observed between the electromechanical properties of the two series. Although thermoplastic elastomer gels are routinely capable of withstanding continuous strain cycling with relatively little mechanical hysteresis or evidence of fatigue, their generally negative piezoresistive properties display significant fluctuations, especially at high strain amplitudes and low stretch rates, due to strain-induced repositioning and reorientation of the conductive nanofibers. At high elongation rates, the degree of apparent fluctuations is substantially reduced. In the presence of the neat thermoplastic elastomer, however, clearly defined strain-reversible piezoresistance is manifested at all strain amplitudes and stretch rates. In this case, electrical resistance initially decreases and then switches and increases prior to strain reversal during strain cycling. At low elongation rates, resistance measurements collected from the first and last strain cycles are nearly indistinguishable, thereby indicating that such materials constitute excellent candidates for strain sensors capable of high sensitivity and repeatability.

3.5. Acknowledgments

This work was supported by Yalova University (Project No. 2018/YL/0006), the NC State University Nonwovens Institute and ABB, Inc. Part of this work was performed in the Analytical Instrumentation Facility (AIF) at North Carolina State University, which is supported by the State of North Carolina and the National Science Foundation (Award No. ECCS-1542015). The AIF is a member of the North Carolina Research Triangle Nanotechnology Network (RTNN), a site in

the National Nanotechnology Coordinated Infrastructure (NNCI).

3.6. References

1. Zhou, Y. H.; Fuentes-Hernandez, C.; Shim, J.. Meyer, J.; Giordano, A. J.; Li, H.; Winget, P.; Papadopoulos, T.; Cheun, H.; Kim, J.; Fenoll, M.; Dindar, A.; Haske, W.; Najafabadi, E.; Khan, T. M.; Sojoudi, H.; Barlow, S.; Graham, S.; Bredas, J. L.; Marder, S. R.; Kahn, A.; Kippelen, B. A Universal Method to Produce Low-Work Function Electrodes for Organic Electronics. Science 2012, 336, 327-332.
2. Zeng, W.; Shu, L.; Li, Q.; Chen, S.; Wang, F.; Tao, X.-M. Fiber-Based Wearable Electronics: A Review of Materials, Fabrication, Devices, and Applications. Adv. Mater. 2014, 26, 5310-5336.
3. Lee, J.; Kwon, H.; Seo, J.; Shin, S.; Koo, J. H.; Pang, C.; Son, S.; Kim, J. H.; Jang, Y. H.; Kim, D. E.; Lee, T. Conductive Fiber-Based Ultrasensitive Textile Pressure Sensor for Wearable Electronics. Adv. Mater. 2015, 27, 2433-2439.
4. Fan, F. R.; Tan, W.; Wang, Z. L. Flexible Nanogenerators for Energy Harvesting and Self-Powered Electronics. Adv. Mater. 2016, 28, 4283-4305.
5. Amjadi, M.; Kyung, K.-U.; Park, I.; Sitti, M. Stretchable, Skin-Mountable, and Wearable Strain Sensors and Their Potential Applications: A Review. Adv. Funct. Mater. 2016, 26, 1678-1698.
6. Khan, Y.; Ostfeld, A. E.; Lochner, C. M.; Pierre, A.; Arias, A. C. Monitoring of Vital Signs with Flexible and Wearable Medical Devices. Adv. Mater. 2016, 28, 4373-4395.
7. Eom, J.; Jaisutti, R.; Lee, H.; Lee, W.; Heo, J.-S.; Lee, J.-Y.; Park, S. K.; Kim, Y.-H. Highly Sensitive Textile Strain Sensors and Wireless User-Interface Devices Using All-Polymeric Conducting Fibers. ACS Appl. Mater. Interfaces 2017, 9, 10190-10197.
8. Yao, S.; Myers, A.; Malhotra, A.; Lin, F.; Bozkurt, A.; Muth, J. F.; Zhu, Y. A Wearable

Hydration Sensor with Conformal Nanowire Electrodes. Adv. Health. Mater. 2017, 6, 1601159.

9. Terán-Jiménez, O.; Rodríguez-Roldán, G.; Hernández-Rivera, D.; Suaste-Gómez, E. Sensors Based on Conducting Polymers for Measurement of Physiological Parameters. IEEE Sensors J. 2017, 17, 2492-2497.
10. Toprakci, H. A.; Kalanadhabhatla, S. K.; Spontak, R. J.; Ghosh, T. K. Polymer Nanocomposites Containing Carbon Nanofibers as Soft Printable Sensors Exhibiting Strain-Reversible Piezoresistivity. Adv. Funct. Mater. 2013, 23, 5536-5542.
11. Munro, B. J.; Campbell, T. E.; Wallace, G. G.; Steele, J. R. The Intelligent Knee Sleeve: A Wearable Biofeedback Device. Sens. Actuator B 2008, 131, 541-547.
12. Yue, B. B.; Wang, C. Y.; Ding, X.; Wallace, G. G. Polypyrrole Coated Nylon Lycra Fabric as Stretchable Electrode for Supercapacitor Applications. Electrochim. Acta 2012, 68, 18-24.
13. Zin, L.; Feng, Z. Q.; Zhu, M. L.; Wang, T.; Leach, M. K.; Jiang, Q. A Novel Fluffy Conductive Polypyrrole Nano-Layer Coated PLLA Fibrous Scaffold for Nerve Tissue Engineering. J. Biomed. Nanotechnol. 2012, 8, 779-785.
14. Benight, S. J.; Wang, C.; Tok, J. B.; Bao, Z. Stretchable and Self-Healing Polymers and Devices for Electronic Skin. Prog. Polym. Sci. 2013, 38, 1961-1977.
15. Amjadi, M.; Pichitpajongkit, A.; Lee, S.; Ryu, S.; Park, I. Highly Stretchable and Sensitive Strain Sensor Based on Silver Nanowire–Elastomer Nanocomposite. ACS Nano 2014, 8, 5154-5163.
16. Liu, H.; Gao, J.; Huang, W.; Dai, K.; Zheng, G.; Liu, C.; Shen, C.; Yan, X.; Guo, J.; Guo, Z. Electrically Conductive Strain Sensing Polyurethane Nanocomposites with Synergistic

Carbon Nanotubes and Graphene Bifillers. Nanoscale 2016, 8, 12977-12989.

17. Liu, H.; Li, Y.; Dai, K.; Zheng, G.; Liu, C.; Shen, C.; Yan, X.; Guo, J.; Guo, Z. Electrically Conductive Thermoplastic Elastomer Nanocomposites at Ultralow Graphene Loading Levels for Strain Sensor Applications. J. Mater. Chem. C 2016, 4, 157-166.
18. Liu, H.; Huang, W.; Yang, X.; Dai, K.; Zheng, G.; Liu, C.; Shen, C.; Yan, X.; Guo, J.; Guo, Z. Organic Vapor Sensing Behaviors of Conductive Thermoplastic Polyurethane–Graphene Nanocomposites. J. Mater. Chem. C 2016, 4, 4459-4469.
19. Wang, M.; Zhang, K.; Dai, X.-X.; Li, Y.; Guo, J.; Liu, H.; Li, G.-H.; Tan, Y.-J.; Zeng, J.-B.; Guo, Z. Enhanced Electrical Conductivity and Piezoresistive Sensing in Multi-Wall Carbon Nanotubes/Polydimethylsiloxane Nanocomposites via the Construction of a Self-Segregated Structure. Nanoscale 2017, 9, 11017-11026.
20. Wei, Y.; Chen, S.; Dong, X.; Lin, Y.; Liu, L. Flexible Piezoresistive Sensors Based on "Dynamic Bridging Effect" of Silver Nanowires Toward Graphene. Carbon 2017, 113, 395-403.
21. Liu, H.; Dong, M.; Huang, W.; Gao, J.; Dai, K.; Guo, J.; Zheng, G.; Liu, C.; Shen, C.; Guo, Z. Lightweight Conductive Graphene/Thermoplastic Polyurethane Foams with Ultrahigh Compressibility for Piezoresistive Sensing. J. Mater. Chem. C 2017, 5, 73-83.
22. Xie, X.; Mai, Y.; Zhou, X. Dispersion and Alignment of Carbon Nanotubes in Polymer Matrix: A Review. Mater. Sci. Eng. R 2005, 49, 89-112.
23. Hussain, F.; Hojjati, M.; Okamoto, M.; Gorga, R. E. Polymer-Matrix Nanocomposites, Processing, Manufacturing, and Application: An Overview. J. Compos. Mater. 2006, 40, 1511-1575.
24. Jiang, M.-J.; Dang, Z.-M.; Xu, H.-P. Giant Dielectric Constant and Resistance-Pressure

Sensitivity in Carbon Nanotubes/Rubber Nanocomposites with Low Percolation Threshold. Appl. Phys. Lett. 2007, 90, 042914.

25. Byrne, M. T.; Gun'ko, Y. K. Recent Advances in Research on Carbon Nanotube-Polymer Composites. Adv. Mater. 2010, 22, 1672-1688.
26. Lin, L.; Liu, S.; Zhang, Q.; Li, X.; Ji, M.; Deng, H.; Fu, Q., Towards Tunable Sensitivity of Electrical Property to Strain for Conductive Polymer Composites Based on Thermoplastic Elastomer. ACS Appl. Mater. Interfaces 2013, 5, 5815-5824.
27. Shintake, J.; Piskarev, E.; Jeong, S. H.; Floreano, D., Ultrastretchable Strain Sensors Using Carbon Black-Filled Elastomer Composites and Comparison of Capacitive Versus Resistive Sensors. Adv. Mater. Technol. 2018, 3, 1700284.
28. Shin, M. K.; Oh, J.; Lima, M.; Kozlov, M. E.; Kim, S. J.; Baughman, R. H., Elastomeric Conductive Composites Based on Carbon Nanotube Forests. Adv. Mater. 2010, 22, 2663-2667.
29. Yamada, T.; Hayamizu, Y.; Yamamoto, Y.; Yomogida, Y.; Izadi-Najafabadi, A.; Futaba, D. N.; Hata, K., A Stretchable Carbon Nanotube Strain Sensor for Human-Motion Detection. Nat. Nanotechnol. 2011, 6, 296-301.
30. Roh, E.; Hwang, B.-U.; Kim, D.; Kim, B.-Y.; Lee, N.-E., Stretchable, Transparent, Ultrasensitive, and Patchable Strain Sensor for Human–Machine Interfaces Comprising a Nanohybrid of Carbon Nanotubes and Conductive Elastomers. ACS Nano 2015, 9, 6252-6261.
31. Boland, C. S.; Khan, U.; Ryan, G.; Barwich, S.; Charifou, R.; Harvey, A.; Backes, C.; Li, Z.; Ferreira, M. S.; Möbius, M. E.; Young, R. J.; Coleman, J. N. Sensitive Electromechanical Sensors Using Viscoelastic Graphene-Polymer Nanocomposites.

Science 2016, 354, 1257-1260.

32. Wang, X.; Meng, S.; Tebyetekerwa, M.; Li, Y.; Pionteck, J.; Sun, B.; Qin, Z.; Zhu, M. Highly Sensitive and Stretchable Piezoresistive Strain Sensor Based on Conductive Poly(styrene-butadiene-styrene)/Few Layer Graphene Composite Fiber. Compos. A: Appl. Sci. Manufact. 2018, 105, 291-299.
33. Wu, S. Y.; Zhang, J.; Ladani, R. B.; Rayindran, A. R.; Mouritz, A. P.; Kinloch, A. J.; Wang, C. H. Novel Electrically Conductive Porous PDMS/Carbon Nanofiber Composites for Deformable Strain Sensors and Conductors. ACS Appl. Mater. Interfaces 2017, 9, 14207-14215.
34. Shante, V. K. S.; Kirkpatrick, S. Introduction to Percolation Theory. Adv. Phys. 1971, 20, 325-357.
35. Jimenez, G. A.; Jana, S. C. Oxidized Carbon Nanofiber/Polymer Composites Prepared by Chaotic Mixing. Carbon 2007, 45, 2079-2091.
36. Allaoui, A.; Hoa, S. V.; Pugh, M. D. The Electronic Transport Properties and Microstructure of Carbon Nanofiber/Epoxy Composites. Compos. Sci. Technol. 2008, 68, 41-416.
37. Al-Saleh, M. H.; Sundararaj, U. A Review of Vapor Grown Carbon Nanofiber/Polymer Conductive Composites. Carbon 2009, 47, 2-22.
38. Drobny, J. G. Handbook of Thermoplastic Elastomers, 2nd ed.; Elsevier: Oxford, 2014.
39. Hamley, I. W. The Physics of Block Copolymers; Oxford University Press: New York, 1998.
40. Matsen, M. W. Effect of Architecture on the Phase Behavior of AB-Type Block Copolymer Melts. Macromolecules 2012, 45, 2161-2165.

41. Bates, C. M.; Bates, F. S. Block Polymers — Pure Potential. Macromolecules 2017, 50, 3–22.
42. Matsen, M. W.; Thompson, R. B. Equilibrium Behavior of Symmetric ABA Triblock Copolymer Melts. J. Chem. Phys. 1999, 111, 7139–7146.
43. Tallury, S. A.; Mineart, K. P.; Woloszczuk, S.; Williams, D. N.; Thompson, R. B.; Pasquinelli, M. A.; Banaszak, M.; Spontak, R. J. Molecular-Level Insights into Asymmetric Triblock Copolymers: Network and Phase Development. J. Chem. Phys. 2014, 141, 121103.
44. Tallury, S. S.; Spontak, R. J.; Pasquinelli, M. A. Dissipative Particle Dynamics of Triblock Copolymer Melts: A Midblock Conformational Study at Moderate Segregation. J. Chem. Phys. 2014, 141, 244911.
45. Woloszczuk, S.; Tuhin, M. O.; Gade, S. R.; Pasquinelli, M. A.; Banaszak, M.; Spontak, R. J. Complex Phase Behavior and Network Characteristics of Midblock-Solvated Triblock Copolymers as Physically-Crosslinked Soft Materials. ACS Appl. Mater. Interfaces 2017, 9, 39940–39944.
46. Tuhin, M. O.; Woloszczuk, S.; Mineart, K. P.; Pasquinelli, M. A.; Sadler, J. D.; Smith, S. D.; Banaszak, M.; Spontak, R. J. Molecular-Level Description of Constrained Chain Topologies in Multiblock Copolymer Gel Networks. J. Chem. Phys. 2018, 148, 231101.
47. Scilingo, E.; Gemignani, A.; Paradiso, R.; Taccini, N.; Ghelarducci, B.; de Rossi, D. Performance Evaluation of Sensing Fabrics for Monitoring Physiological and Biomechanical Variables. IEEE Trans. Inform. Technol. Biomed. 2005, 9, 345-352.
48. Tognetti, A.; Lorussi, F.; Bartalesi, R.; Quaglini, S.; Tesconi, M.; Zupone, G.; de Rossi, D. Wearable Kinesthetic System for Capturing and Classifying Upper Limb Gesture in Post-

Stroke Rehabilitation. J. Neuroeng. Rehab. 2005, 2, 8.

49. Huang, C.; Shen, C.; Tang, C.; Chang, S. A Wearable Yarn-Based Piezo-Resistive Sensor. Sensors Act. A 2008, 141, 396-403.
50. Zhang, X. W.; Pan, Y.; Zheng, Q.; X. Yi, S. Time Dependence of Piezoresistance for the Conductor-Filled Polymer Composites. J. Polym. Sci. B: Polym. Phys. 2000, 38, 2739-2749.
51. Lorussi, F.; Rocchia, W.; Scilingo, E. P.; Tognetti, A; de Rossi, D. Wearable, Redundant Fabric-Based Sensor Arrays for Reconstruction of Body Segment Posture. IEEE Sens. J. 2004, 4, 807-818.
52. Cochrane, C.; Koncar, V.; Lewandowski, M.; Dufour, C. Design and Development of a Flexible Strain Sensor for Textile Structures Based on a Conductive Polymer Composite. Sensors 2007, 7, 473-492.
53. Mattmann, C.; Clemens, F.; Tröster, G. Sensor for Measuring Strain in Textile. Sensors 2008, 8, 3719-3732.
54. Chen, Z. P.; Ren, W. C.; Gao, L. B.; Liu, B. L.; Pei, S. F.; Cheng, H.-M. Three-Dimensional Flexible and Conductive Interconnected Graphene Networks Grown by Chemical Vapour Deposition. Nat. Mater. 2011, 10, 424-428.
55. Fan, Q.; Qin, Z.; Gao, S.; Wu, Y.; Pionteck, J.; Mader, E.; Zhu, M. The Use of a Carbon Nanotube Layer on a Polyurethane Multifilament Substrate for Monitoring Strains as Large as 400%. Carbon 2012, 50, 4085-4092.
56. Shankar, R.; Krishnan, A. S.; Ghosh, T. K.; Spontak, R. J. Triblock Copolymer Organogels as High-Performance Dielectric Elastomers. Macromolecules 2008, 41, 6100-6109.
57. Krishnan, A. S.; Vargantwar, P. H.; Spontak, R. J. Thermorheological Behavior of

Coexisting Physical Networks: Combining SAFIN and SAMIN Organogels. Soft Matter 2012, 8, 12025-12033.

58. Tuhin, M. O.; Ryan, J. J.; Sadler, J. D.; Han, Z.; Lee, B.; Smith, S. D.; Pasquinelli, M. A.; Spontak, R. J. Microphase-Separated Morphologies and Molecular Network Topologies in Multiblock Copolymer Gels. Macromolecules 2018, 51, 5173-5181.
59. Lawrence, J. G.; Berhan, L. M.; Nadarajah, A. Elastic Properties and Morphology of Individual Carbon Nanofibers. ACS Nano 2008, 2, 1230-1236.
60. Inaba, K.; Saida, K.; Ghosh, P.; Matsubara, K.; Subramanian, M.; Hayashi, A.; Hayashi, Y.; Tanemura, M.; Kitazawa, M.; Ohta, R. Determination of Young's Modulus of Carbon Nanofiber Probes Fabricated by the Argon Ion Bombardment of Carbon Coated Silicon Cantilever. Carbon 2011, 49, 4191-4196.
61. Al-Saleh, M. H.; Sundararaj, U. Review of the Mechanical Properties of Carbon Nanofiber/Polymer Composites. Compos. A: Appl. Sci. Manufact. 2011, 42, 2126-2142.
62. Jiang, M.-J.; Dang, Z.-M.; Xu, H.-P. Significant Temperature and Pressure Sensitivities of Electrical Properties in Chemically Modified Multiwall Carbon Nanotube/Methylvinyl Silicone Rubber Nanocomposites. Appl. Phys. Lett. 2006, 89, 182902.
63. Ardanuy, M.; Rodríguez-Perez, M. A.; Algaba, I. Electrical Conductivity and Mechanical Properties of Vapor-Grown Carbon Nanofibers/Trifunctional Epoxy Composites Prepared by Direct Mixing. Compos. B 2011, 42, 675-681.
64. Stauffer, D.; Aharony, A. Introduction to Percolation Theory, 2nd Ed.; Taylor & Francis: London, 1992.
65. Halperin, B. I.; Feng, S.; Sen, P. N. Differences between Lattice and Continuum Percolation Transport Exponents. Phys. Rev. Lett. 1985, 54, 2391-2394.

66. Vionnet-Menot, S.; Grimaldi, C.; Maeder, T.; Strassler, S.; Ryser, P. Tunneling-Percolation Origin of Nonuniversality: Theory and Experiments. Phys. Rev. B 2005, 71, 064201.
67. Tang, H. S.; Kalyon, D. M. Time-Dependent Tube Flow of Compressible Suspensions Subject to Pressure Dependent Wall Slip: Ramifications on Development of Flow Instabilities. J. Rheol. 2008, 52, 1069-1090.
68. Du, F. M.; Fischer, J. E.; Winey, K. I. Effect of Nanotube Alignment on Percolation Conductivity in Carbon Nanotube/Polymer Composites. Phys. Rev. B 2005, 72, 121404.
69. White, S. I.; DiDonna, B. A.; Mu, M.; Lubensky, T. C.; Winey, K. I. Simulations and Electrical Conductivity of Percolated Networks of Finite Rods with Various Degrees of Axial Alignment. Phys. Rev. B 2009, 79, 024301.
70. Bao, W. S.; Meguid, S. A.; Zhu, Z. H.; Meguid, M. J. Modeling Electrical Conductivities of Nanocomposites with Aligned Carbon Nanotubes. Nanotechnol. 2011, 22, 485704.

3.7. Figures

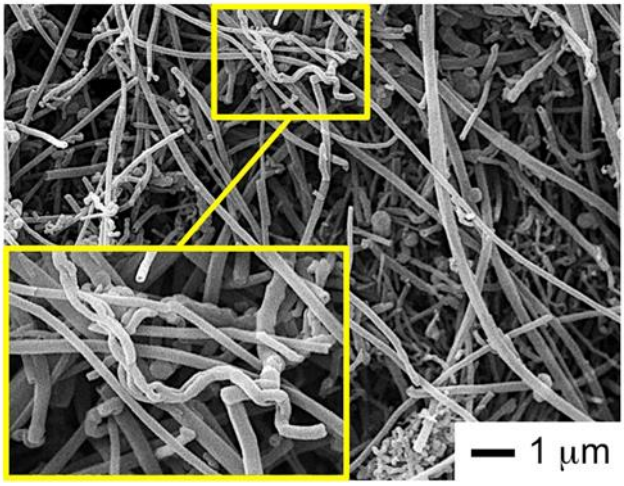

Figure 1. SEM image of the as-received vapor-grown carbon nanofiber (CNF) employed in this study.

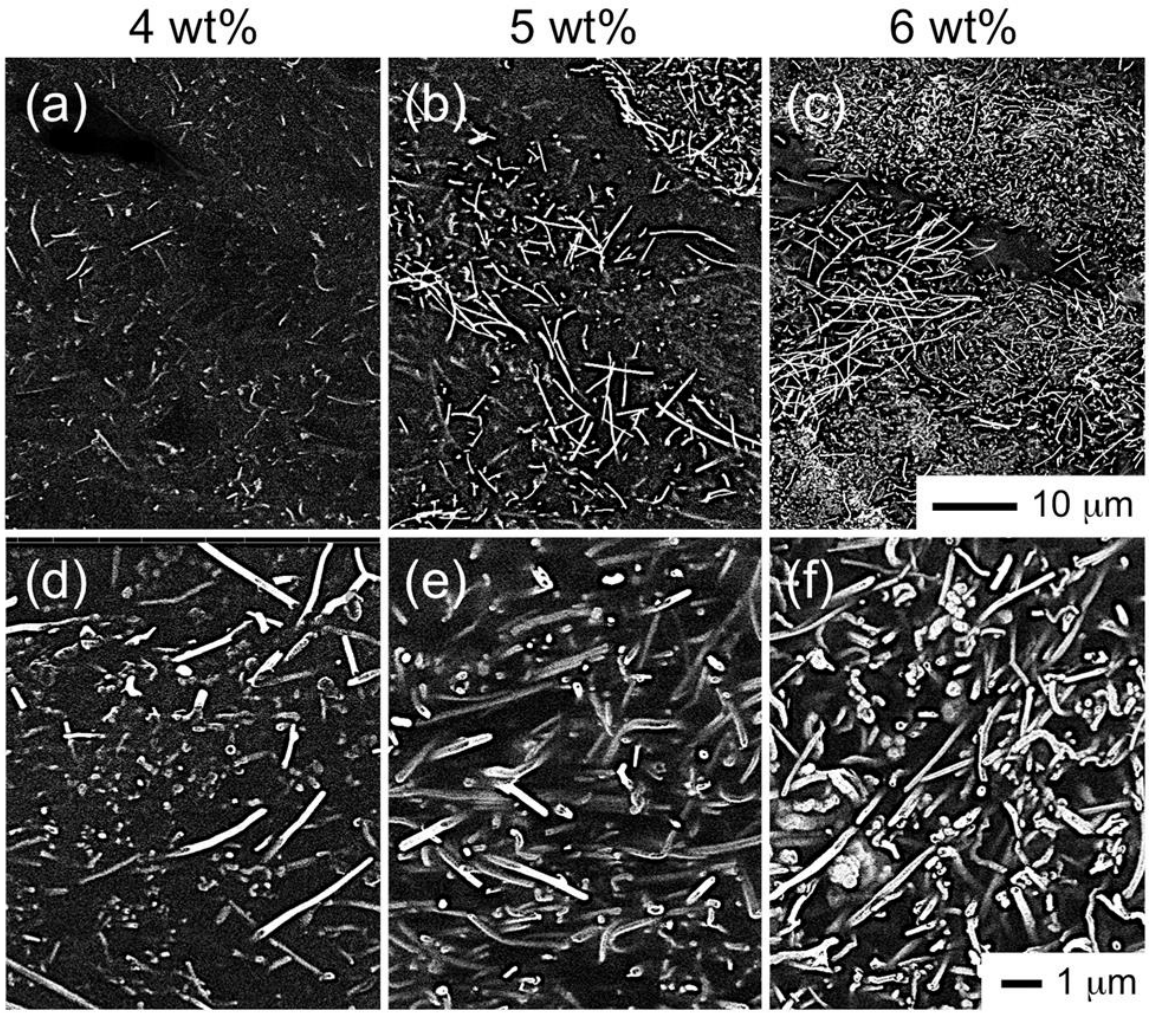

Figure 2. SEM images acquired from uncoated conductive polymer nanocomposites (CPNs) composed of CNF (bright conductive features) embedded in a styrenic thermoplastic elastomer gel (TPEG, dark nonconductive matrix) at three different loading levels (labeled). The scale bar corresponds to all the images in each of the two rows.

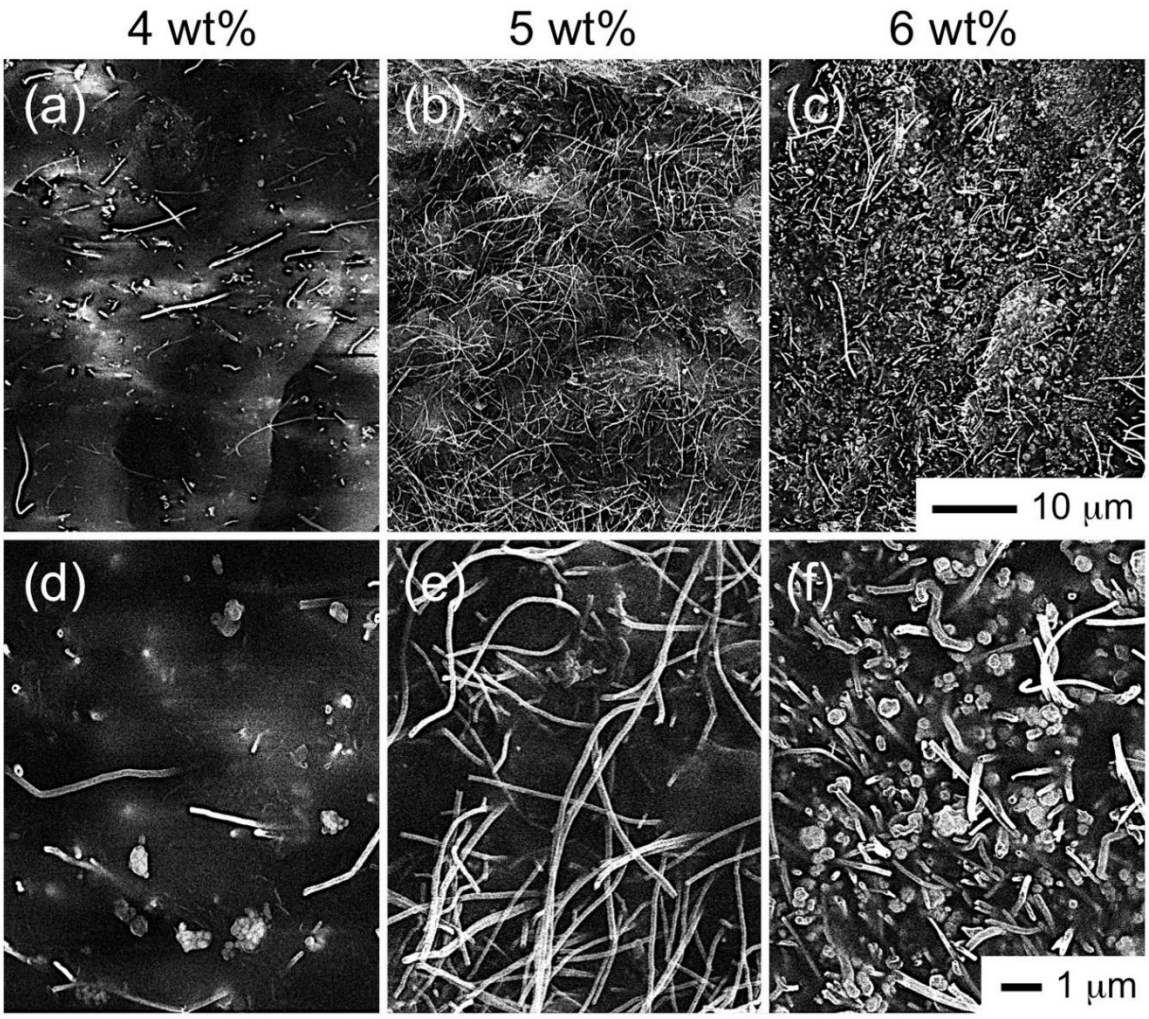

Figure 3. SEM images of uncoated CPNs composed of CNF (bright conductive features) embedded in a neat styrenic thermoplastic elastomer (TPE, dark nonconductive matrix) at three different loading levels (labeled) and presented at two different magnifications in (a-c) and (d-f). Each scale bar corresponds to all the images in its row.

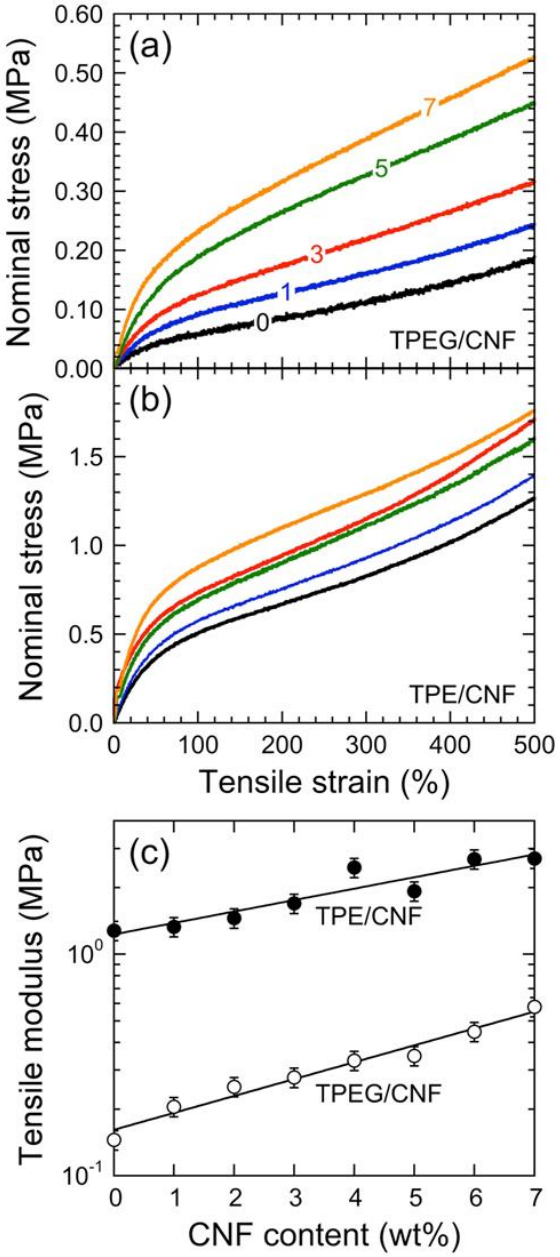

Figure 4. Nominal stress presented as a function of strain at different CNF loading levels (in wt%) during quasi-static uniaxial tensile testing for CPNs composed of (a) TPEG/CNF and (b) TPE/CNF. Results from different loading levels are labeled and color-coded. Tensile moduli extracted from data such as those included in (a) and (b) are included as a function of CNF content in (c) for each series (labeled). The solid lines in (c) represent exponential regressions to the data and serve as guides for the eye.

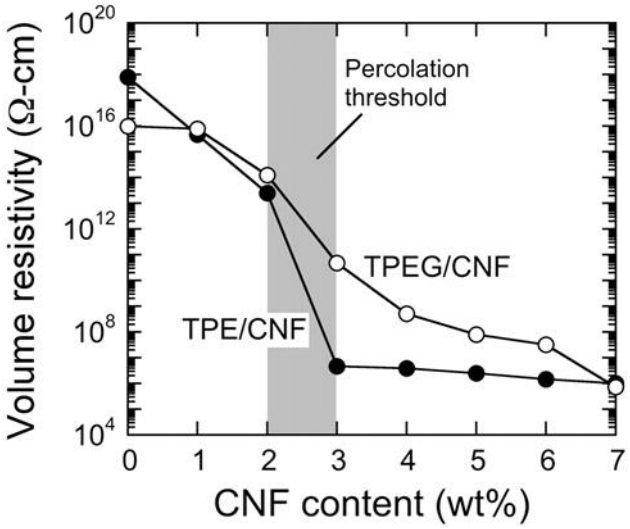

Figure 5. The dependence of volume resistivity measurements on CNF content for two series of CPNs: TPEG/CNF (○) and TPE/CNF (●). The solid lines serve to connect the data, and the percolation threshold for the TPE/CNF materials is displayed as the shaded region.

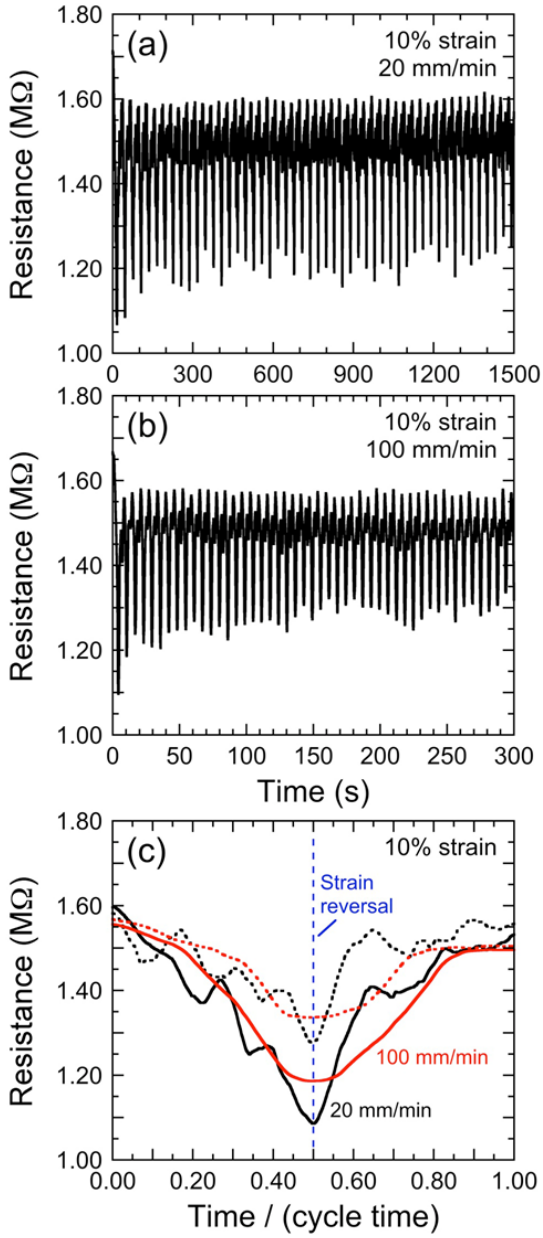

Figure 6. Cyclic electromechanical measurements presented as a function of time normalized with respect to the time of a single cycle for CPNs composed of TPEG/CNF and exposed to 10% strain at two different stretch rates (in mm/min): (a) 20 and (b) 100. In (c), single-cycle results correspond to the first and final cycles (solid and dotted lines, respectively) from tests performed at 20 (black) and 100 (red) mm/min. The dashed line (labeled) identifies the normalized time (at 0.5) corresponding to strain reversal.

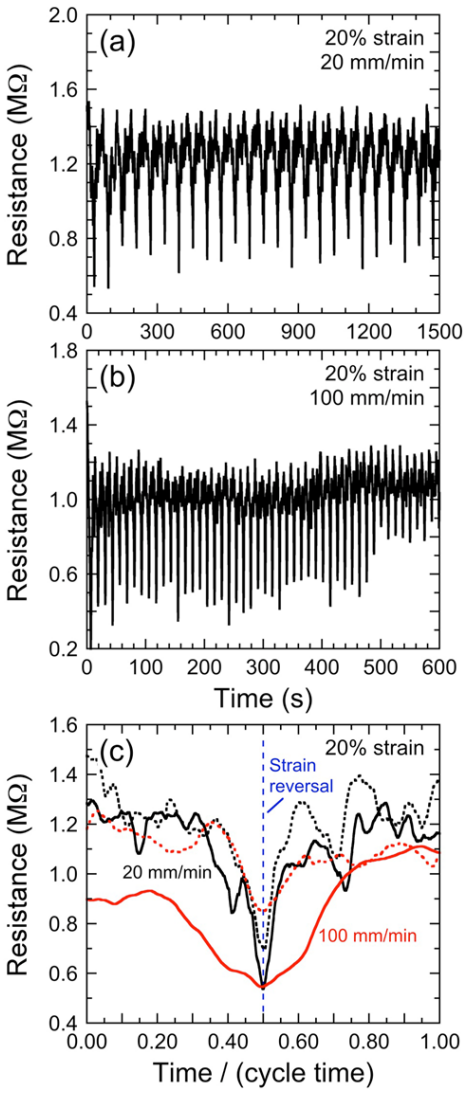

Figure 7. Cyclic electromechanical measurements presented as a function of time normalized with respect to the time of a single cycle for CPNs composed of TPEG/CNF and exposed to 20% strain at two different stretch rates (in mm/min): (a) 20 and (b) 100. In (c), single-cycle results correspond to the first and final cycles (solid and dotted lines, respectively) from tests performed at 20 (black) and 100 (red) mm/min. The dashed line (labeled) identifies the normalized time (at 0.5) corresponding to strain reversal.

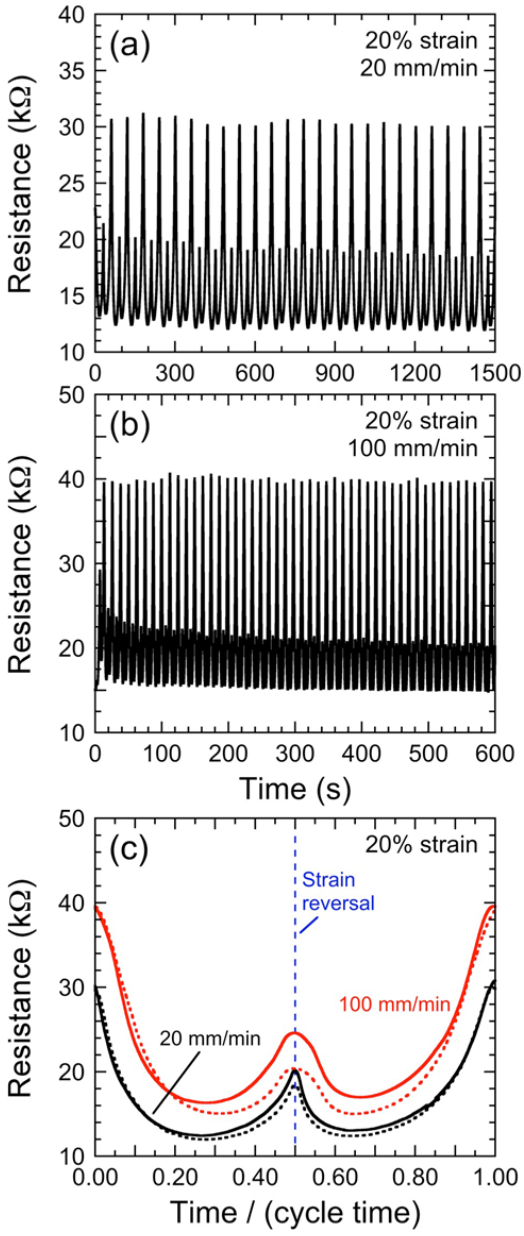

Figure 8. Cyclic electromechanical measurements presented as a function of time normalized with respect to the time of a single cycle for CPNs composed of TPE/CNF and exposed to 20% strain at two different stretch rates (in mm/min): (a) 20 and (b) 100. In (c), single-cycle results correspond to the first and final cycles (solid and dotted lines, respectively) from tests performed at 20 (black) and 100 (red) mm/min. The dashed line (labeled) identifies the normalized time (at 0.5) corresponding to strain reversal.

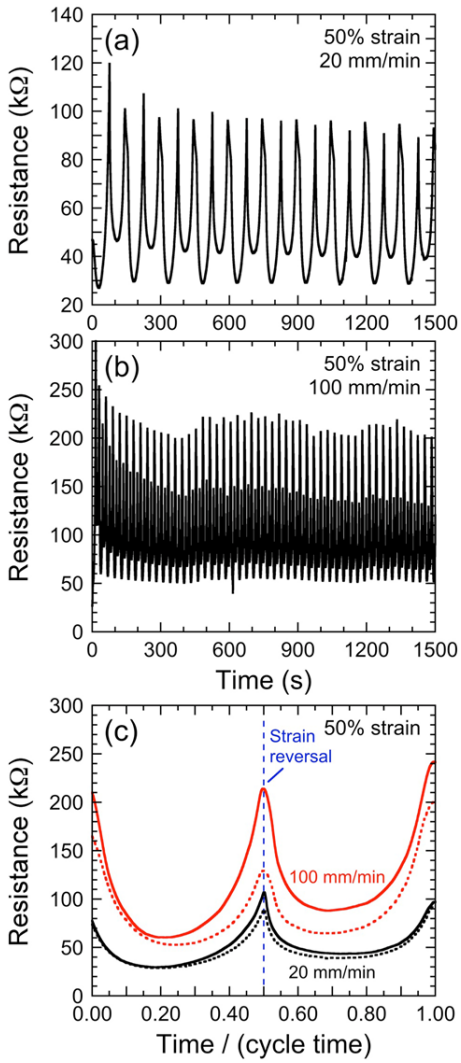

Figure 9. Cyclic electromechanical measurements presented as a function of time normalized with respect to the time of a single cycle for CPNs composed of TPE/CNF and exposed to 50% strain at two different stretch rates (in mm/min): (a) 20 and (b) 100. In (c), single-cycle results correspond to the first and final cycles (solid and dotted lines, respectively) from tests performed at 20 (black) and 100 (red) mm/min. The dashed line (labeled) identifies the normalized time (at 0.5) corresponding to strain reversal.

CHAPTER 4

Complex Phase Behavior and Network Characteristics of Midblock- SolvatedTriblock Copolymers as Physically Cross-Linked Soft Materials**

ABSTRACT

In the presence of a midblock-selective solvent, triblock copolymers not only self-organize but also form a molecular network. Thermoplastic elastomer gels, examples of such materials, serve as sealants and adhesives, as well as ballistic, microfluidic, and electroactive media. We perform Monte Carlo and dissipative particle dynamics simulations to investigate the phase behavior and network characteristics of these materials. Of interest is the existence of a truncated octahedral morphology that resembles the atomic arrangement of various inorganic species. Both simulations quantify the midblock bridges responsible for network development and thus provide a detailed molecular picture of these composition-tunable soft materials.

**This chapter was published in its entirety:

Woloszczuk, S., **Tuhin, M. O**., Gade, S. R., Pasquinelli, M. A., Banaszak, M., & Spontak, R. J. (2017). Complex Phase Behavior and Network Characteristics of Midblock-Solvated Triblock Copolymers as Physically Cross-Linked Soft Materials. *ACS applied materials & interfaces*, *9*(46), 39940-39944.

4.1. Materials, methods, results and discussions

Because of their distinctive ability to spontaneously self-assemble into various nanoscale morphologies,[1,2] block copolymers remain one of the most extensively investigated classes of soft materials to date. Ongoing interest in these macromolecules reflects their unparalleled versatility in applications ranging from blend compatibilization,[3] nano-lithography,[4] and thin-film stabilization[5] to photonic devices,[6]organic photovoltaics,[7] and drug delivery.[8] The simplest AB diblock copolymer architecture consists of two long, chemically dissimilar A and B sequences (or random copolymers thereof[9]). Because of the thermodynamic incompatibility (χN, where χ denotes the Flory−Huggins interaction parameter and N is the number of statistical units along the copolymer backbone) between the blocks, these molecules microphase-separate and, under favorable conditions, order into periodic morphologies that minimize interfacial area and chain packing frustration governed by factors such as molecular composition/architecture[10] and monomer asymmetry/rigidity.[11] Classical ordered morphologies include A(B) spherical micelles on a body- or face-centered cubic lattice (M_k, k = A or B), or cylindrical micelles on a hexagonal lattice (HPC_k), in a continuous B(A) matrix, as well as alternating lamellae (L). In contrast, the

42 bicontinuous gyroid (G) with $Ia\bar{3}d$ symmetry[12] and the O^{70} phase with Fddd symmetry[13] are more spatially complex. Most of these morphologies are observed in blends of AB diblock copolymers with either a parent homopolymer,[14] a second copolymer[15] or a solvent.[16]

Bicomponent ABA triblock copolymers likewise order into comparable morphologies but, depending on relative end block sizes,[17] form B-networks stabilized by A-microdomains. This molecular design constitutes the basis for first-generation thermoplastic elastomers (TPEs) wherein the soft midblock is rubbery and the rigid end blocks are glassy or semicrystalline.[18,19] The most ubiquitous TPEs, which consist of styrenic end blocks and a polydiene/olefin midblock,

account for ~1/3 of all TPEs manufactured globally.[20] Independent efforts intended to quantify the midblock bridging fraction (υ) by experimental,[21] theoretical[22] and simulation[23– 25] means have sought to correlate bulk properties with network characteristics. The properties of such technologically valuable materials can be enhanced through the incorporation of midblock-selective solvents, such as low-volatility organic oils. Resultant TPE gels (or TPEGs), employed in applications such as ballistic media,[26] pressure-sensitive adhesives,[27] dielectric elastomers,[28] microfluidic devices,[29] and shape-memory materials,[30] can also self-organize and, in so doing, form molecular networks whose (electro)mechanical properties are composition-tunable tunable. Limited experimental[31] and simulation[32] attempts to elucidate the phase behavior of TPEGs confirm that these soft materials can self-organize into several ordered morphologies. In the present study, we perform Monte Carlo (MC) and dissipative particle dynamics (DPD) simulations to generate a comprehensive picture of TPEG phase behavior and the effects of copolymer and blend composition on network development (i.e., υ).

The MC simulations utilize a cooperative motion algorithm on a face-centered cubic lattice, as described elsewhere.[33] In this arrangement, movement of one segment mandates cooperative motion of adjacent segments. The size of each simulation box, filled with chain segments (each ~1 kDa) and solvent (S), is chosen so that fully extended copolymer chains fit completely inside the box. The pairwise interaction energy between species i and j (i,j = A, B, or S) is designated as ε_{ij} with $\varepsilon_{AA} = \varepsilon_{BB} = \varepsilon_{SS} = \varepsilon_{BS} = 1$ and $\varepsilon_{AB} = \varepsilon_{AS} = 2 = \chi kT/(z - 2)$, where k is the Boltzmann constant, T denotes absolute temperature, and z (=12) is the lattice coordination number. Each simulation is run to equilibrium (lowest free energy) at T* (= kT/ε), and parallel

tempering[34] overcomes local free energy traps. Although DPD simulations have also been conducted to explore the morphological characteristics of TPEs, we use this approach to compare

values of υ (with MC simulations) in systems containing 100−1000 ABA chains, each composed of 100 connected ∼1 kDa beads. For this purpose, the system parameters discussed[24] for neat ABA copolymers is utilized in the Large-Scale Atomic/Molecular Massively Parallel Simulator (LAMMPS) software suite.[35] In similar fashion as above and to ensure self-organization of the copolymer in the presence of midblock-selective S, we set $\varepsilon_{AA} = \varepsilon_{BB} = \varepsilon_{SS} = \varepsilon_{BS} = 25kT$ and $\varepsilon_{AB} = \varepsilon_{AS} = 50kT$. After equilibration at $2kT/\varepsilon$, a density-based cluster-recognition algorithm[24] distinguishes among chain conformations (bridges, loops, dangles, and unsegregated chains). In both simulation series, morphologies and transitions are identified by visual inspection and heat capacities, respectively.

From MC simulations, we first consider the phase behavior of four ABA copolymers possessing 40 segments and varying in the fraction of A segments (f): 0.2 (4−32−4), 0.4 (8−24−8), 0.6 (12−16−12), and 0.8 (16−8−16). In the limit of high solvent fraction (ϕ_S), micellar coronae transition from hairy at low f to crewcut at high f. The binary $T^*-\phi_S$ phase diagrams generated for these relatively simple, nonpolar systems are displayed in Figure 1 and reveal complex phase behavior. Although these morphologies are reproducible, and equilibrium is expected for nearly all the conditions examined, metastable morphologies might develop at low temperatures due to long relaxation times, in which case caution is recommended in interpreting results near $T^* = 1$. The subscript listed on each morphological designation identifies the minority block. In Figure 1a, the neat copolymer ($\phi_S = 0$) possesses f = 0.2 and, as such, is expected to self-organize into either a dispersed M_A or HPC_A morphology. Both morphologies appear stable at different temperatures, with the HPC_A morphology disordering −disorder transition (ODT) is into M_A as the order approached. At intermediate temperatures, long A channels (CH_A, i.e., curved cylinders) that appear either discrete or continuous ($1C_A$) develop, along with the possibility of A

rods (R_A) that resemble short, wormlike cylinders. Because these morphologies are dispersed with curved interfaces, the addition of midblock-selective solvent, which increases the volume fraction of the B-rich matrix, is unable to produce a wide variety of different morphologies. At temperatures below the ODT, conversion of all morphologies to M_A is observed between $0.6 < \phi_S < 0.8$. (We only consider morphological shapes and do not classify them on the basis of lattice symmetry.)

The copolymer selected in Figure 1a is representative of commercial TPEs, since dispersed morphologies are expected[28] to possess the highest υ and mechanical properties that come closest to chemically cross-linked rubber. An increase in f to 0.4 in Figure 1b shifts the neat copolymer morphology to L over all temperatures examined. At temperatures below the ODT, increasing ϕ_S initially results in the formation of perforated A layer (PL_A) and bicontinuous (B, most likely G) morphologies that gradually give way to cylindrical (although not necessarily hexagonally packed) morphologies and finally to A micelles at high ϕ_S. This morphological progression has been experimentally verified[48] upon incorporation of a midblock-selective oil into a styrenic TPE. In a symmetric block copolymer phase diagram, the L morphology typically extends from $f \approx 0.35$ to f 0.65, in which case it is reasonable that not only the neat copolymer with f = 0.6 but also corresponding blends with 20− 30% solvent exhibit lamellae in Figure 1c. In this system, however, the transition from L to PL_A and bicontinuous nanostructures becomes substantially more temperature-dependent at lower f (in Figures 1a, b), and the cylindrical morphologies display less order. At high solvent levels ($\phi_S > 0.6$), spherical micelles, as well as elongated micelles (M_{Ae}) and cubically packed A cylinders (CPC_A), are observed. Whereas deformed micelles are not surprising under these conditions, the CPC_A morphology, which has not been experimentally validated, is unexpected at such high solvent levels. This spatial arrangement has, however, been postulated for the keratin filaments comprising mammalian stratum cornea.[36]

As anticipated, the copolymer with f = 0.8 exhibits the most complex phase diagram of the series in Figure 1d, because the midblock-selective solvent systematically swells the minority B microphase, which consists of a minority B morphology (HPC_B) without solvent. Although the morphologies at $\phi_S > 0$ contain a mixture of B + S, the designations only list B for clarity. As ϕ_S is increased, complex morphologies such as PL_B, $1C_B$, B_B, and CH_B develop as the A/B interface becomes increasingly less curved, especially at higher temperatures. The existence of a previously unobserved bicontinuous block copolymer morphology, A and B truncated octahedral networks (OCT_A and OCT_B, respectively), is also established by both MC and DPD simulations. The characteristics of this morphology are discussed below. Increasing ϕ_S first yields the L morphology with flat interfaces and then inverted morphologies with curved interfaces and minority A micro-phases. Additional complex nanostructures, including the OCT_A morphology, are again visible at solvent levels beyond those responsible for the L morphology. Interestingly, discrete crewcut A micelles with a relatively thin B corona only appear to be stable at very high ϕ (>0.85). Although no experimental studies have been performed to date on TPEGs under these conditions, existing evidence confirms[31] that coronal size does influence micellar packing in TPEGs. Although micelles possessing a thick corona (due to a long B midblock common in most commercial TPEs with 20−35 wt % A) self-organize on a body-centered cubic lattice, those with a thin corona (due to a short B midblock) can order on an atypical face-centered cubic lattice.

Although structural details of the double-channel network comprising the truncated octahedron morphology are pre-sented in Figure 2 with solid (Figure 2a) and interfacial (Figure 2b) cutaway images to illustrate its spatial complexity (solvent-swollen B midblocks are colored red and gold to indicate the nonintersecting nature of their cubic networks, B-selective solvent molecules are blue and the A end blocks are transparent), a more in-depth analysis of its origin and stability

limits in TPEGs, as well as other copolymer systems, is forthcoming. Suffice it to say that, unlike the bicontinuous G morphology (observed in linear bicomponent block copolymer systems at compositions of 30−35 wt % of one species and yielding nonintersecting channel networks in a continuous matrix), the truncated octahedron arrangement of ABA copolymer molecules reflects symmetric (i.e., isochoric) microphase separation, as is evident from Figure 2c. In Figure 2d, e, the channels and nodes of the mutually exclusive B networks appear hollow to accommodate the midblock-selective solvent, the spatial distribution of which is more clearly seen in Figure 2f. Nanostructures possessing this spatial symmetry occur in numerous inorganic systems, including natural minerals (e.g., clay, talc, and mica), mineral-organic polyhedra,[37] and powder catalysts.[38] Although an octahedron

morphology has not been previously reported for self-organized block copolymer systems at mesoscale dimensions, block copolymers have been used to generate nanoparticles with this spatial symmetry.[39]

In addition to their surprisingly rich phase behavior, TPEGs form physically cross-linked molecular networks that hold promise as flesh-like, stimuli-responsive, sealable, and recyclable soft materials for use in a wide variety of technologies. Although the contribution of interpenetrating looped midblocks, while not considered here, should not be discounted, midblock bridges are primarily responsible for network properties. Fractions of midblock conformations (i.e., bridges, loops, dangles, and unsegregated chains, depicted in Figure 3a) as determined from DPD simulations are presented in Figure 3b for blends in which f = 0.2 and 0.4 and ϕ_S varies from 0.0 to 1.0. Results indicate that, at the selected incompatibility and composition levels, midblock bridging dominates with negligible unsegregated chains and dangles discernible only at high ϕ_S. Because network formation due to midblock bridging in

TPEGs is of paramount interest in the development of their hyperelastic (electro)mechanical properties, values of υ evaluated from MC simulations are provided as a function of ϕ_S in Figure 4 for three of the parent ABA copolymers identified in Figure 1 and a fourth evaluated at f = 0.5 (to avoid the inverted morphologies at f = 0.8). These results confirm that υ changes with morphology and, hence, interfacial area as the blends become increasingly solvent-rich. The red dots included in Figure 4a, b for B-rich copolymers identify order−order transitions in Figures 1a, b, respectively. Unexpectedly, υ is observed in Figure 4a to attain a maximum value of 76%, which is higher than previously reported for microphase-ordered ABA copolymers.[22,24,32]

This combined MC and DPD simulations study of midblock-solvated ABA triblock copolymers differing in copolymer composition (f) and gel concentration (ϕ_S) establishes that these soft, network-forming materials can, depending on f, exhibit a broad range of temperature-dependent morphologies,[40] including some that have not yet been experimentally reported due to the absence of copolymers with suitable compositions. By themselves, A-rich ABA copolymers with a relatively short midblock would behave more like rubber-reinforced thermoplastics than conventional TPEs. Insofar as macrophase separation does not occur, incorporation of a B-selective solvent is expected to cause discrete B microdomains to swell and ultimately transform into a continuous B+solvent matrix. During this sequence of morphological transitions, a bicontinuous truncated octahedron morphology has been identified. Detailed examination of this morphology reveals that solvent molecules locate within the B-rich channels and nodes of the nonintersecting cubic networks. Experimental investigation of this mesoscale morphology is forthcoming, and the properties associated with this dual-network morphology are expected to yield an elevated modulus and continuous diffusive pathways. Although the morphologies reported here are not compared directly with experimental findings, results from a previous MC simulation

study[41] of selectively solvated AB diblock copolymers compare favorably with available experimental data. At the molecular level, evaluation of the midblock conformational fractions indicates that the bridging fraction, which is largely responsible for the elastic behavior required in the broad assortment of technological applications presently employing TPEGs, is sensitive to morphological changes as f (at $\phi_S = 0$) or ϕ_S (at constant f) is changed. Because TPEGs are becoming increasingly useful in a diverse range of technologies, an improved understanding of their concomitant phase and network behavior is warranted. The present study confirms that these materials, while technologically relevant, are also scientifically interesting as examples of self-assembled soft matter with highly tunable morphologies and network-dependent properties.

4.2. Acknowledgments

This work was supported by the Polish National Science Centre (NCN Grant DEC-2012/07/B/ST5/00647), the NC State University Nonwovens Institute, and ABB, Inc. Simulations were conducted at the Poznan Computer and Networking Center and NC State High-Performance Computing Center.

4.3. References

1. Hamley, I. W. The Physics of Block Copolymers; Oxford University Press: New York, 1998.
2. Bates, C. M.; Bates, F. S. Block Polymers Pure Potential. Macromolecules 2017, 50, 3−22.
3. Ruzette, A. V.; Leibler, L. Block Copolymers in Tomorrow's Plastics. Nat. Mater. 2005, 4, 19−31.
4. Bita, I.; Yang, J. K. W.; Jung, Y. S.; Ross, C. A.; Thomas, E. L.; Berggren, K. K. Graphoepitaxy of Self-Assembled Block Copolymers on Two-Dimensional Periodic Patterned Templates. Science 2008, 321,939−943.
5. Gozen, A. O.; Zhou, J. J.; Roskov, K. E.; Shi, A.-C.; Genzer, J.; Spontak, R. J. Block Copolymer Self-Organization vs. Interfacial Modification in Bilayered Thin-Film Laminates. Soft Matter 2011, 7, 3268−3272.
6. Boyle, B. M.; French, T. A.; Pearson, R. M.; McCarthy, B. G.; Miyake, G. M. Structural Coloring for Additive Manufacturing: 3D-Printed Photonic Crystals from Block Copolymers. ACS Nano 2017,11, 3052−3058.
7. Guo, C. H.; Lin, Y. H.; Witman, M. D.; Smith, K. A.; Wang, C.; Hexemer, A.; Strzalka, J.; Gomez, E. D.; Verduzco, R. Conjugated Block Copolymer Photovoltaics with Near 3% Efficiency through Microphase Separation. Nano Lett. 2013, 13, 2957−2963.
8. Mura, S.; Nicolas, J.; Couvreur, P. Stimuli-Responsive Nano-carriers for Drug Delivery. Nat. Mater. 2013, 12, 991−1003.
9. Ashraf, A. R.; Ryan, J. J.; Satkowski, M. M.; Lee, B.; Smith, S. D.; Spontak, R. J. Bicomponent Block Copolymers Derived from One or More Random Copolymers as an

Alternative Route to Controllable Phase Behavior. Macromol. Rapid Commun. 2017, 38, 1700207.

10. Matsen, M. W. Effect of Architecture on the Phase Behavior of AB-Type Block Copolymer Melts. Macromolecules 2012, 45, 2161−2165.
11. Chen, J. T.; Thomas, E. L.; Ober, C. K.; Mao, G. P. Self-Assembled Smectic Phases in Rod-Coil Block Copolymers. Science 1996, 273, 343−346.
12. Hajduk, D. A.; Harper, P. E.; Gruner, S. M.; Honeker, C. C.; Kim, G.; Thomas, E. L.; Fetters, L. J. The GyroidA New Equilibrium Morphology in Weakly Segregated Diblock Copolymers. Macromolecules 1994, 27, 4063−4075.
13. Tyler, C. A.; Morse, D. C. Orthorhombic Fddd Network in Triblock and Diblock Copolymer Melts. Phys. Rev. Lett. 2005, 94, 208302.
14. Matsen, M. W. Phase-Behavior of Block-Copolymer Homopolymer Blends. Macromolecules 1995, 28, 5765−5773.
15. Spontak, R. J.; Patel, N. P. Phase Behavior of Block Copolymer Blends. In Block Copolymer Science and Technology; Hamley, I. W., Ed.; Wiley: New York, 2004; pp 159−212.
16. Lodge, T. P.; Pudil, B.; Hanley, K. J. The Full Phase Behavior for Block Copolymers in Solvents of Varying Selectivity. Macromolecules 2002, 35, 4707−4717.
17. Tallury, S. A.; Mineart, K. P.; Woloszczuk, S.; Williams, D. N.; Thompson, R. B.; Pasquinelli, M. A.; Banaszak, M.; Spontak, R. J. Molecular-Level Insights into Asymmetric Triblock Copolymers: Network and Phase Development. J. Chem. Phys. 2014, 141, 121103.

18. Holden, G.; Kricheldorf, H. R.; Quirk, R. P. Thermoplastic Elastomers, 3rd ed.; Hanser: Munich, Germany, 2004.
19. Drobny, J. G. Handbook of Thermoplastic Elastomers, 2nd ed.; Elsevier: Oxford, U.K., 2014.
20. TPE Market Approaches Maturity. Plastics Rubber Weekly; October 18, 2016.
21. Watanabe, H.; Sato, T.; Osaki, K. Concentration Dependence of Loop Fraction in Styrene-Isoprene-Styrene Triblock Copolymer Solutions and Corresponding Changes in Equilibrium Elasticity. Macromolecules 2000, 33, 2545−2550 and the references cited therein.
22. Matsen, M. W.; Thompson, R. B. Equilibrium Behavior of Symmetric ABA Triblock Copolymer Melts. J. Chem. Phys. 1999, 111, 7139−7146.
23. Sliozberg, Y. R.; Andzelm, J. W.; Brennan, J. K.; Vanlandingham, M. R.; Pryamitsyn, V.; Ganesan, V. Modeling Viscoelastic Properties of Triblock Copolymers: A DPD Simulation Study. J. Polym. Sci., Part B: Polym. Phys. 2010, 48, 15−25.
24. Tallury, S. S.; Spontak, R. J.; Pasquinelli, M. A. Dissipative Particle Dynamics of Triblock Copolymer Melts: A Midblock Conformational Study at Moderate Segregation. J. Chem. Phys. 2014, 141, 244911.
25. Xu, Z.; Lin, J.; Zhang, Q.; Wang, L.; Tian, X. Theoretical Simulations of Nanostructures Self-Assembled from Copolymer Systems. Polym. Chem. 2016, 7, 3783−3811.
26. Mrozek, R. A.; Leighliter, B.; Gold, C. S.; Beringer, I. R.; Yu, J. H.; VanLandingham, M. R.; Moy, P.; Foster, M. H.; Lenhart, J. L. The Relationship between Mechanical Properties and Ballistic Penetration Depth in a Viscoelastic Gel. J. Mech. Behavior Biomed. Mater. 2015, 44,109−120.

27. Flanigan, C. M.; Crosby, A. J.; Shull, K. R. Structural Development and Adhesion of Acrylic ABA Triblock Copolymer Gels. Macromolecules 1999, 32, 7251−7262.
28. Shankar, R.; Ghosh, T. K.; Spontak, R. J. Electroactive Nanostructured Polymers as Tunable Actuators. Adv. Mater. 2007,19, 2218−2223.
29. Sudarsan, A. P.; Wang, J.; Ugaz, V. M. Thermoplastic Elastomer Gels: An Advanced Substrate for Microfluidic Chemical Analysis Systems. Anal. Chem. 2005, 77, 5167−5173.
30. Mineart, K. P.; Tallury, S. S.; Li, T.; Lee, B.; Spontak, R. J. Phase-Change Thermoplastic Elastomer Blends for Tunable Shape Memory by Physical Design. Ind. Eng. Chem. Res. 2016, 55, 12590−12597.
31. Krishnan, A. S.; Smith, S. D.; Spontak, R. J. Ternary Phase Behavior of a Triblock Copolymer in the Presence of an Endblock- Selective Homopolymer and a Midblock-Selective Oil. Macromolecules 2012, 45, 6056−6067.
32. Chantawansri, T. L.; Sirk, T. W.; Sliozberg, Y. R. Entangled Triblock Copolymer Gel: Morphological and Mechanical Properties. J. Chem. Phys. 2013, 138, 024908.
33. Woloszczuk, S.; Banaszak, M.; Spontak, R. J. Monte Carlo Simulations of the Order-Disorder Transition Depression in ABA Triblock Copolymers with a Short Terminal Block. J. Polym. Sci., Part B: Polym. Phys. 2013, 51, 343−348.
34. Beardsley, T. M.; Matsen, M. W. Monte Carlo Phase Diagram for Diblock Copolymer Melts. Eur. Phys. J. E: Soft Matter Biol. Phys. 2010, 32, 255−264.
35. Plimpton, S. Fast Parallel Algorithms for Short-Range Molecular-Dynamics. J. Comput. Phys. 1995, 117, 1−19.

36. Norlen, L.; Al-Amoudi, A. Stratum Corneum Keratin Structure, Function, and Formation: The Cubic Rod-Packing and Membrane Templating Model. J. Invest. Dermatol. 2004, 123, 715−732.
37. Tranchemontagne, D. J.; Ni, Z.; O'Keeffe, M.; Yaghi, O. M. Reticular Chemistry of Metal-Organic Polyhedra. Angew. Chem., Int. Ed. 2008, 47, 5136−5147.
38. Huang, W. Oxide Nanocrystal Model Catalysts. Acc. Chem. Res. 2016, 49, 520−527.
39. Cho, K. Y.; Yeom, Y. S.; Seo, H. Y.; Kumar, P.; Lee, A. S.; Baek, K.-Y.; Yoon, H. G. Molybdenum-Doped PdPt@Pt Core-Shell Octahedra Supported by Ionic Block Copolymer-Functionalized Graphene as a Highly Active and Durable Oxygen Reduction Electrocatalyst. ACS Appl. Mater. Interfaces 2017, 9, 1524−1535.
40. Sugimoto, M.; Sakai, K.; Aoki, Y.; Taniguchi, T.; Koyama, K.; Ueda, T. Rheology and Morphology Change with Temperature of SEBS/Hydrocarbon Oil Blends. J. Polym. Sci., Part B: Polym. Phys. 2009, 47, 955−965.
41. Woloszczuk, S.; Banaszak, M.; Knychala, P.; Radosz, M. Monte Carlo Phase Diagram of Symmetric Diblock Copolymer in Selective Solvent. Macromolecules 2008, 41, 5945−5951.

4.4. Figures

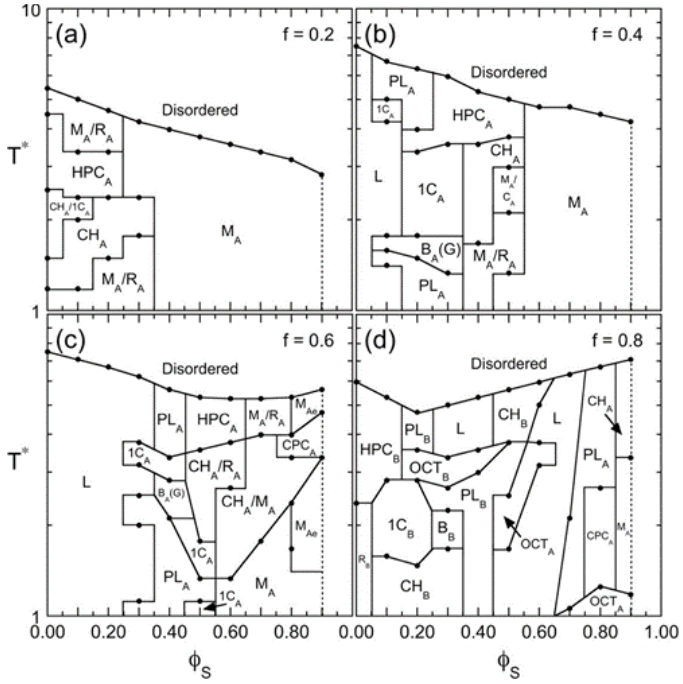

Figure 1. Reduced temperature−gel concentration ($T^*-\phi_S$) phase diagrams generated by MC simulations of midblock-solvated ABA triblock copolymers differing in f: (a) 0.2, (b) 0.4, (c) 0.6, and (d) 0.8. The solid lines correspond to interpolated order−order transition boundaries between data points. Morphological abbreviations are defined in the text.

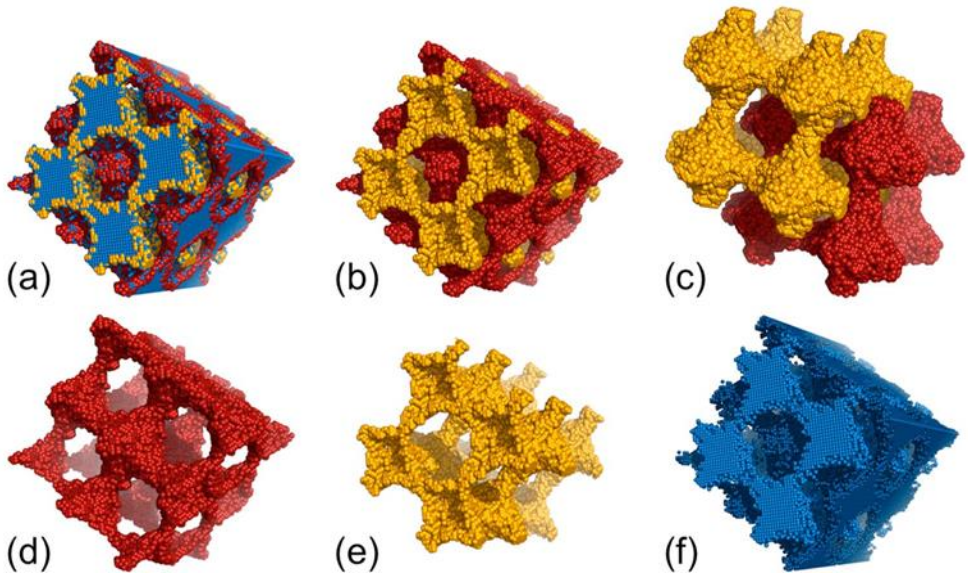

Figure 2. MC simulation snapshots of the truncated octahedron (OCT_A) morphology encountered for midblock-solvated ABA copolymers in Figure 1d. Here, the B blocks form nonintersecting networks (red and gold) that contain solvent (blue) in a continuous (transparent) matrix composed of A blocks. Cutaway images for a representative blend (f = 0.8 and ϕ_S = 0.3) are displayed (a) for the solid and (b) along the interface, and (c) the two coexisting networks are shifted to be more clearly visible. (d, e) Separating nonintersecting B networks, and (f) the spatial distribution of solvent.

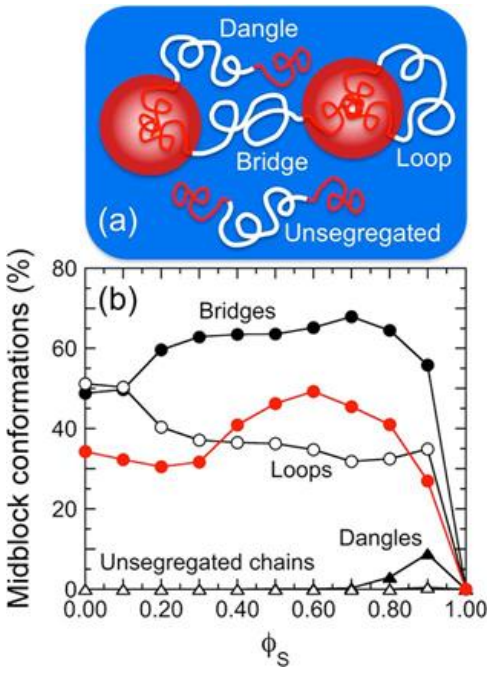

Figure 3. (a) Schematic illustration of ABA triblock copolymer molecules that self-organize into spherical micelles. Midblock conformations are labeled as bridges, loops, dangles, and unsegregated. (b) Results from DPD simulations indicating the dependence of the midblock fractions, bridges (●), loops (○), dangles (▲), and unsegregated chains ( ), on ϕ_S for 2 midblock-solvated ABA triblock copolymers differing in f: 0.2 (black) and 0.4 (red). The solid lines serve to connect the data.

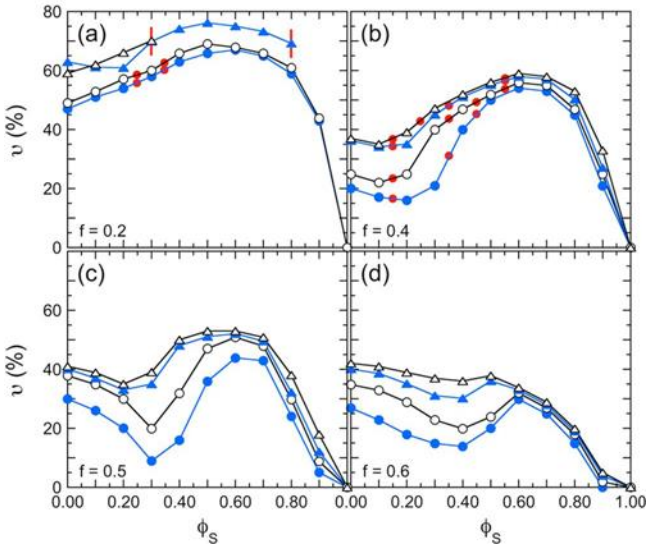

Figure 4. Midblock bridging fraction (υ) determined from MC simulations and presented as a function of ϕ_S for four ABA triblock copolymers differing in f, (a) 0.2, (b) 0.4, (c), 0.5, and (d) 0.6, at four different values of T*, 1 (●), 2 (○), 3 (▲), and 4 ( ). The solid lines serve to connect the data, and the vertical red lines indicate the last point accessible before crossing the ODT. (a, b) Red dots in the B-rich copolymer systems identify order−order transitions from the corresponding phase diagrams displayed in Figure 1.

CHAPTER 5

Microphase-Separated Morphologies and Molecular Network Topologies in Multiblock Copolymer Gels**

ABSTRACT

Strong physical gels derived from thermoplastic elastomeric ABA triblock copolymers solvated with a midblock-selective oil continue to find use in increasingly diverse applications requiring highly elastic and mechanically robust soft materials with tunable properties. In this study, we first investigate the morphological characteristics of thermoplastic elastomer gels (TPEGs) derived from a homologous series of linear $A(BA)_n$ multiblock copolymers composed of styrene and hydrogenated isoprene repeat units and possessing comparable molecular weight, but varying in the number of B-blocks: 1 (triblock), 2 (pentablock) and 3 (heptablock). Small-angle X-ray scattering performed at ambient temperature confirms that (*i*) increasing hydrogenation reduces the microdomain periodicity of the neat copolymers and (*ii*) increasing the oil concentration of the TPEGs tends to swell the nanostructure (increasing the periodicity), but concurrently decrease the size of the styrenic micelles, to different extents depending on molecular architecture. Complementary dissipative particle dynamics simulations reveal the extent to which midblock bridging, which is primarily responsible for the elasticity in this class of materials, is influenced by both oil concentration and molecular architecture. Since constrained topological complexity increases with increasing block number, we introduce a midblock conformation index that facilitates systematic classification of the different topologies involved in nearest-micelle bridge formation. Those possessing at least one bridged and one looped midblock with no dangling ends are found to be the most predominant topologies in the pentablock and heptablock networks.

**This chapter has been published in its entirety:

Tuhin, M. O., Ryan, J. J., Sadler, J. D., Han, Z., Lee, B., Smith, S. D., ... & Spontak, R. J. (2018). Microphase-Separated Morphologies and Molecular Network Topologies in Multiblock Copolymer Gels. Macromolecules.

5.1. Introduction

Block copolymers continue to attract significant attention from the academic and industrial communities due principally to their intriguing ability to self-assemble into a wide range of soft nanostructures[1,2] that are precisely suitable for a diverse range of uses within the scope of a broad technological platform.[3-8] Due to the thermodynamic incompatibility between the covalently-linked blocks, these copolymers are capable of spontaneously self-organizing into several classical morphologies (*e.g.*, micelles on a body- or face-centered cubic lattice, cylinders on a hexagonal lattice or alternating lamellae), as well as more spatially complex morphologies (*e.g.*, double helices,[9] the gyroid,[10-12] the O^{70},[13,14] and the Frank-Kasper σ phase[15]). Of the many block copolymer archetypes that are commercially available, triblock copolymers that behave as thermoplastic elastomers[16] (TPEs) with hard (glassy or semicrystalline) endblocks and a soft (rubbery) midblock constitute an important and recyclable alternative to chemically cross-linked elastomers due to their ability to form a molecular network composed of bridged midblocks that physically connect neighboring microdomains (*cf.* Figure 1).[17] For this reason, they serve as soft materials capable of affording both scientific insight and application versatility through customizable properties, and independent experimental,[18-21] theoretical[22,23] and simulation[25,26] efforts focused on quantifying the fraction of bridged midblocks (υ) have been reported. Studies relating molecular arrangement to morphological and property development in bicomponent TPEs prepared from melt or solution processing are not, however, restricted to triblock copolymers, since both randomly-coupled[26-28] and perfectly-alternating[29-35] linear multiblock copolymers have also been synthesized and investigated in this broad copolymer family.

In the same fashion as a parent homopolymer,[37-39] incorporation of a selective solvent into an ordered block copolymer can elicit several responses, including microdomain swelling, one or

more order-order transitions or microdomain dissolution at the order-disorder transition. These responses depend on the thermodynamic incompatibility of the copolymer, the copolymer concentration and temperature. Experimental studies[40] of midblock-solvated triblock copolymers with and without an endblock-selective additive verify that these systems exhibit the same phase behavior observed[41] with selectively-solvated diblock copolymers. A recent simulation investigation[41] of midblock-solvated triblock copolymers furthermore indicate that unique morphologies, such as the truncated octahedron, can likewise develop. In the specific case of triblock copolymer TPEs, addition of a midblock-selective diluent such as a nonpolar oligomeric oil yields tunably compliant thermoplastic elastomer gels (TPEGs) for use as dielectric[43-47] and phase-change[48-50] elastomers, pressure-sensitive adhesives,[51] and substrates for microfluidics[52] and flextronics.[53] This paradigm naturally extends to include polar diluents such as water[54] and ionic liquids[55] in the case of triblock or higher-order multiblock copolymers possessing hydrophobic endblocks and a hydrophilic midblock. These functional soft materials are of interest in the fabrication of proteinaceous hydrogels,[56] Li-ion batteries,[57] soft robotics,[58] organic photovoltaics,[59,60] and water-treatment[61,62] or amphoteric gas-separation[63] membranes. An especially attractive attribute of TPEGs is their ability to be (electro)mechanically strain-cycled with little, if any, hysteresis.[64] Moreover, these materials are capable of avoiding dynamic fatigue and achieving ultrahigh elongations, with some reaching strains of ≈4000% prior to failure.[65]

The illustration provided in Figure 1 displays rigid micelles that are responsible for connecting swollen soft midblocks and thus stabilizing the molecular network in conventional TPEGs. In the case of TPEGs derived from ABA triblock copolymers, a single copolymer molecule can at most physically connect two micelles. In the case of $A(BA)_n$ multiblock copolymers with $n > 1$, however, a single molecule can form multiple bridges and connect up to n+1 micelles. While

previous studies of TPEGs have focused primarily on triblock copolymers, the objective of this study is to elucidate the morphological characteristics and constrained chain topologies responsible for network formation in TPEGs composed of multiblock copolymers. In this spirit, we have synthesized a homologous series of perfectly-alternating linear multiblock copolymers with constant molecular weight (M) and investigated their morphologies as functions of copolymer architecture and solvent concentration by small-angle X-ray scattering (SAXS). In addition, dissipative particle dynamics (DPD) simulations have been performed to identify the molecular conformations responsible for soft-midblock bridging and, hence, network formation. Due to the topological complexity introduced with multiblock copolymers, a conformation-based classification index is proposed and used to compare the relative influence of all nearest-micelle bridge conformations.

5.2. Experimental

5.2.1. Materials

For the synthesis of the three model multiblock copolymers, cyclohexane (HPLC grade) was obtained from VWR, whereas isoprene and styrene were supplied by Aldrich. Both the cyclohexane and isoprene were used as-received, but the styrene required purification to remove by-products. This was achieved by first degassing the styrene with N_2, followed by titration with dibutylmagnesium (Aldrich) to a yellow end point and then column chromatography. In addition to *sec*-butyllithium (Aldrich), Irganox-1010 (Ciba-Geigy) and ultrahigh-purity hydrogen (Matheson), methanol, 2,3-dimethyl-3-pentanol (DMP), nickel(II) bis(2-ethylhexanoate), triethyl aluminum (1 M solution in heptane), hydrochloric acid (HCl), and sodium bicarbonate ($NaHCO_3$) were purchased from Aldrich and used as-received. The diluent was a primarily aliphatic mineral oil (MO, Hydrobrite 380, Sonneborn). Copolymers consisting of styrenic (S) endblocks and 1-3

isoprenic (I) midblocks separated by S blocks (with $M_{S,midblock} = 2M_{S,endblock}$ to account for the extension difference between an endblock tail and a midblock bridge/loop) were synthesized in the presence of *sec*-butyllithium and cyclohexane at 60°C by living anionic polymerization.[32] The composition of each copolymer was fixed at 20 wt% S, and the number-average M and polydispersity (Đ) values ranged from 293 to 303 kDa and 1.05 to 1.14, respectively, as determined by size-exclusion chromatography and ^{1}H NMR spectroscopy (performed on a GE QE-300 spectrometer), respectively. Copolymer designations (including I midblock number and block masses, in kDa) are as follows: TBC (n = 1, $S_{30}I_{240}S_{30}$), PBC (n = 2, $S_{15}I_{120}S_{30}I_{120}S_{15}$) and HBC (n = 3, $S_{10}I_{80}S_{20}I_{80}S_{20}I_{80}S_{10}$). Polyisoprene (PI) in all copolymers was 95-99% hydrogenated to yield ethylene-*alt*-propylene (EP) rubber, as described elsewhere.[66]

5.2.2. Methods

The copolymers were co-dissolved with the mineral oil as the EP-selective midblock diluent, ranging in solvent weight percent (φ_S) from 0 to 96%, and 1.0 wt% Irganox 1010 in reagent-grade toluene at a solution concentration of 4% w/v. Resultant solutions were cast into Teflon molds and dried for 8-9 days at ambient temperature to yield films measuring 1.2-1.5 mm thick. These films were heated to 120°C for 6 h under vacuum, quiescently cooled for 12 h, carefully removed from the molds and wrapped in Al foil, and then stored in a plastic container at ambient temperature and pressure until testing. Subsequent SAXS analysis was conducted at ambient temperature on beam-line 12-ID-B at the Advanced Photon Source (Argonne National Laboratory). The sample-to-detector distance and beam spot size were 2 m and 0.5 x 0.025 mm^2, respectively, and the 14 keV beam provided a wavelength (λ) of 0.087 nm and a flux of ~10^{12} photons/s. Two-dimensional SAXS patterns collected on a 2-D Pilatus 2M detector were azimuthally integrated to yield intensity profiles expressed as a function of the scattering vector (q), where $q = (4\pi/\lambda)\sin\theta$ and θ

is half the scattering angle.

5.3. Simulations

The DPD simulations performed here conform to the procedures previously detailed,[25] and we provide an abbreviated overview below. Since the coarse-grained beads in DPD simulations behave as soft (compressible) spheres, they can remain discrete in the case of diluent molecules or they can be linked together to mimic polymer chains as bead-spring equivalents. Each bead is coarse-grained to 1 kDa, and so the ~300 kDa copolymer chains described above correspond to 300 beads, where a single A bead represents ~10 S repeat units and a B bead accounts for ~14 EP repeat units. Since the molecular weight of the MO is ~0.5 kDa, one solvent bead accounts for ~2 solvent molecules. The net force (f_i) that bead *i* (*i* = A, B or S) experiences at position r_i is expressed as the summation of all forces accounting for pairwise interactions with all other (*j*) beads within a characteristic radius (R_C) typically set to unity, and is written as

$$f_i = \sum_{j \neq i} (F_{ij}^C + F_{ij}^D + F_{ij}^R + F_{ij}^S) \qquad (1)$$

where F_{ij}^C represents the conservative (repulsive) force given by

$$F_{ij}^C = \begin{cases} a_{ij}\left(1 - \frac{r_{ij}}{R_C}\right)\hat{r}_{ij} & \text{for } (r_{ij} < R_C) \\ 0 \end{cases} , \qquad (2)$$

and α_{ij} corresponds to the pair-repulsion potential between beads *i* and *j*, $\hat{\mathbf{r}}_{ij} = r_{ij}/|r_{ij}|$, and $r_{ij} = |r_{ij}|$ is the scalar distance between beads. The spring force (F_{ij}^S) only exists between connected beads comprising the polymer chains and is represented by $-k_s(r_{ij} - r_0)\,\hat{\mathbf{r}}_{ij}$, where $k_s = 4.0$ and $r_0 = 0.8$. The dissipative (F_{ij}^D) and random (F_{ij}^R) forces in Eq. 1 retain their usual meanings, and values of the various parameters and number bead density ($\rho = 3$) required in these terms are selected to

ensure consistency with prior DPD studies[67] of block copolymers. Similarly, the like pair-repulsion parameters (α_{AA}, α_{BB} and α_{SS}) are calculated from 75 kT/ρ, where k is the Boltzmann constant and T denotes absolute temperature (kT = 1 at a system thermostat set equal to 373 K so that $\alpha_{AA} = \alpha_{BB} = \alpha_{SS} = 25$). We presume that the solvent is B-selective so that $\alpha_{BS} = \alpha_{BB}$. In contrast, the value of the unlike pair-repulsion parameters involving A (α_{AB} and α_{AS}) are determined[68] from $\alpha_{AA} + 3.27(1 + 3.9/N^{0.51})\chi$, where N is the number of beads per chain and χ is the Flory-Huggins interaction parameter estimated from the solubility parameters for PS and EP.

The DPD simulations were performed with the Large-scale Atomic/Molecular Massively Parallel Simulator (LAMMPS) software package[68] under the conditions of a microcanonical ensemble to ensure constant mass, volume and energy so that the total number of beads representing both solvent and copolymer molecules was held constant in a cubic cell measuring 23 R_c on each side to ensure that at least 100 copolymer chains would be in the most dilute system. The *chain.py* routine was used to build the copolymer chains and to distribute them randomly with the solvent beads in the simulation box. Each system was then equilibrated up to 5×10^5 steps with a time step of 0.05 and periodic boundary conditions using *nve* integrator. It is important to note here that doubling the cell size or reducing the time step (to 0.02 or 0.04) did not generate any statistically different results. Production runs, on the other hand, were performed for an additional 5×10^5 steps. All simulations were performed on the Henry2 cluster at the NC State High Performance Computing Center. The discrete microdomains of neat $A(BA)_n$ copolymers and their selectively-swollen gels were systematically identified from snapshots of the simulation trajectories using a versatile density-based clustering algorithm (DBSCAN),[69] which does not presume a particular microdomain shape *a priori;* its application to particle simulation trajectories has been described elsewhere.[25] We adapted DBSCAN, which employs the *flexible procedures for clustering* (fpc)

package within the R statistical software suite, to be used in conjunction with an in-house algorithm so that periodic boundary conditions could be considered when counting midblock conformations. Constrained topologies identified for each $A(BA)_n$ chain by the existence of nearest-neighbor soft-midblock bridges were classified here according to a midblock conformation index (MCI) of the form [mbld], where m is the number of connected micelles, and b, l and d represent the number of B bridges, B loops and A dangling ends, respectively. Schematic illustrations and corresponding MCI designations of conformations encountered for TBCs (n=1), PBCs (n=2) and HBCs (n=3) are presented in Figure 2 and reveal that the level of topological complexity quickly increases with increasing n.

5.4. Results and Discussion

5.4.1. Morphological Characteristics

5.4.1.1. Neat Copolymers

Since the multiblock copolymers initially consist of isoprenic midblocks, we first examine the neat (diluent-free) copolymers to ascertain the effects of molecular architecture (n) and hydrogenation on morphology at constant M. The corresponding SAXS profiles are provided in Figure 3 and confirm that the 3 copolymers are microphase-ordered, displaying a well-defined principal peak at q* and at least two higher-order reflections. Although the peaks are quite broad, the position of the second-order peak (at q_2) relative to q* varies from 1.76 to 1.82, suggesting that the morphology consists of S cylinders or spheroids poorly arranged on a hexagonal lattice (for which $q_2/q^*=1.72$) in a continuous EP-rich matrix. At the constant copolymer composition (20 wt% S), however, spheroidal or ellipsoidal micelles are more intuitively expected. Important considerations that might be responsible for the results displayed in Figure 3 include the copolymer molecular weight coupled with a large chemical difference between the block species and the multiblock

architectures. The first two factors contribute to a high thermodynamic incompatibility (χN) and slow diffusion, while the third results in a downward shift and flattening of the ordered block copolymer envelope as n is increased, according to self-consistent field theory predictions.[70] Thus, under the current experimental conditions, a polydisperse spheroidal morphology is reasonable and moreover consistent with the scattering results included (and modeled in terms of the form factor) in Figure 4. The apparent shift in the form factor to higher q with increasing n indicates that the micelles become smaller, which is a direct consequence of increasing n at constant M. Two additional observations included in the inset of Figure 3 indicate that the microdomain periodicity ($D = 2\pi/q^*$) decreases with increasing n and with increasing hydrogenation. The first finding is attributed to the reduction in block sizes associated with increasing n, and can, in the strong-segregation limit, be described by $D \sim (n + 1)^{-2/3}$. Soft-midblock hydrogenation, which serves to increase χN, likewise promotes a marginal reduction in D at constant n. This result is, however, contrary to that predicted from strong-segregation theory,[71] as well as experimentally reported,[66] for unconstrained (*i.e.*, non-networked) diblock copolymers and clearly warrants further investigation.

5.4.1.2. Swollen Copolymers

Three series of SAXS profiles acquired from TPEGs varying in φ_S from 0 to 80% in 20% increments are presented in Figure 4 for oil-swollen multiblock copolymers differing in molecular architecture: n=1 (TBC, Figure 4a), n=2 (PBC, Figure 4b) and n=3 (HBC, Figure 4c). The model fits included in Figure 4 represent the form factor for polydisperse spheres and favorably match the SAXS data at moderate to high q. In all of the cases examined, an ordered morphology reminiscent of that in the neat copolymers remains discernible, in agreement with previous[72,73] examples of TPEGs. Most prior studies of TPEGs composed of styrenic triblock copolymers with

either an EP or ethylene-*co*-butylene (EB) midblock and aliphatic mineral oil possess a body-centered-cubic (bcc) spherical morphology,[74] although the face-centered-cubic (fcc) morphology has likewise been reported for block copolymers.[40,75,76] The relative signature peak positions (expressed as q_2/q^*) of the SAXS profiles in Figure 4 signify that a hexagonal-close packed morphology persists in all the TPEGs considered. Mean values of q_2/q^* are 1.76 ± 0.01 for n=1 (Figure 4a), 1.74 ± 0.02 for n=2 (Figure 4b) and 1.76 ± 0.02 for n=3 (Figure 4c). Values of the structure factor, S(q), extracted[77] from the triblock copolymer and several associated TPEGs are provided as a function of q normalized with respect to q* in Figure 5 and, despite the broad scattering peaks, confirms that the spherical micelles are not arranged on a bcc or fcc lattice. At higher φ_S (90% and above), the TPEGs approach their critical gel fraction below which the population of copolymer molecules becomes insufficient to form a molecular network. Detailed examination of this regime by dynamic rheology and mesoscale simulations reveals[78] that the critical gel fraction is sensitive to copolymer attributes such as molecular weight, composition and architecture. In Figure 6, long-range order appears lost when $\varphi_S > 90\%$ in the case of n=1 (Figure 6a), but is retained for the remaining two copolymers up to $\varphi_S = 92\%$ at least in Figures 6b ($q_2/q^*=1.76$ for n=2) and 6c ($q_2/q^*=1.78$ for n=3) even though the block masses become smaller with increasing n. Model fits corresponding to hexagonal close-packed and 2D hexagonal spheres are included in Figure 6 and verify that the spheres are loosely positioned on a hexagonal lattice with relatively short-range order (no distinction is made here between the two lattice types). We do not discount the possibility of fcc ordering since this lattice with numerous stacking faults and non-correlated {111} planes yields broad second peaks and resembles the 2D hexagonal arrangement.

Two important nanostructural dimensions extracted from the SAXS profiles provided in Figures

4 and 6 are the periodicity (D) and spherical radius (R), which are included as functions of □S and n in Figures 7a and 7b, respectively. On one hand, as anticipated from the results presented in Figure 3 for the neat copolymers and the fact that the block masses systematically decrease with increasing n at constant N, D consistently decreases with increasing n over the entire range of φ_S examined in Figure 7a. For each copolymer series, an increase in φ_S from 0 to ~60% generally promotes a modest (10-14%) increase in D. Above 60% oil, however, D increases sharply (by as much as ~100% relative to the neat copolymer in the case of the HBC series). Values of R have been modeled as both monodisperse and polydisperse spherical micelles from the form factor at intermediate q values (model fits for polydisperse spheres are included in Figure 4) and are displayed in Figure 7b. Although R expectedly decreases with increasing n due to the accompanying change in block mass (estimated values of the unperturbed gyration diameter for the S blocks in the neat TBC, PBC and HBC specimens are 9.7, 6.9 and 5.6 nm, respectively), it is sensitive to polydispersity below φ_S = 40%. At and beyond this dilution level, R appears to depend less on polydispersity and decrease monotonically with increasing φ_S. The results included in Figure 7 reveal that the S-rich microdomains become not only more separated (from D) but also physically smaller (from R) as φ_S increases. Volume-fraction estimates derived from R and D confirm that the S micelles are spherical and not cylindrical. Corresponding values of D/R for monodisperse spheres up to φ_S = 60% average 3.5 ± 0.1 over all n. At higher φ_S, D/R more than doubles to 8.1. In the next section, we use DPD simulations to determine if changes in TPEG morphology influence the midblock conformations responsible for network formation.

5.4.2. Conformational Analysis

To begin, final snapshots collected from equilibrated DPD simulation trajectories representing multiblock-based TPEGs with n = {1, 2, 3}, each collected at 4 different values of φ_S, are portrayed

for comparison in Figure 8. Three important features of these results warrant discussion at this juncture. First, in the solvent-free systems (φ_S = 0%), the discrete microdomains visible in Figure 8 appear elongated, which is consistent with the existence of distorted spheres. As φ_S is increased, however, most of the microdomains become less elongated and more spherical in shape. This observation supports the conclusion based on the SAXS form factor analyses in Figure 4 that the micelles in these TPEGs are spheroidal. Second, the microdomains in the simulations do not possess obvious evidence of long-range order, as implied by the SAXS data. Third, an increase in φ_S is accompanied by an increase in separation distance (which relates to D) and a reduction in microdomain size (which relates to R). Corresponding values of D/R are 3.3 ± 0.1 over all φ_S and n. Thus, we conclude that the DPD simulations capture several, but not all, of the important characteristics of the TPEGs investigated in this study. The most likely reason for differences is either the length required for each bead to be coarse-grained to 1 kDa or the total number of chains, as each simulation was conducted with 100-1000 copolymer chains, excluding the solvent beads. Once the simulations are run beyond equilibration and the microdomains are subsequently identified by the DBSCAN cluster algorithm, individual chain conformations are analyzed and organized according to the MCI classifications described earlier.

Before discussing the chain topologies derived from DPD simulations, the MCI classification scheme proposed here is examined on the basis of its two assumptions and potential drawbacks. The first assumption is that at least two micelles must be connected by a single copolymer chain so that a network can form. Since the index requires the number of connected micelles (m), we note that m_{min}=2, thereby precluding consideration of single micelles with numerous loops or dangling ends. Since b_{max}=n for a fully extended chain occupying the maximum number of micelles possible, m_{max}=n+1 at the opposite extreme. The second assumption is that only chain

conformations responsible for connecting nearest-neighbor micelles are considered. As an example of a conformation that would not be included, consider an extended ABABA PBC molecule similar to the one classified as [3200] in Figure 2. If the A midblock is not contained within a micelle (and behaves as a dangling midblock), then m=2 and the two A endblocks would ultimately immobilize the entire chain but at a much lower crosslink density than the other PBC conformations. In the spirit of chemically-crosslinked elastomers, the conformations included in the MCI classification scheme require that the molecular mass between physical crosslinks (*i.e.*, the rigid micelles) must equal the mass of the soft midblocks. Another consideration to be addressed regarding the proposed MCI scheme is degeneracy; that is, the possibility that a given designation corresponds to more than one conformation. An example of such degeneracy is the [2210] conformation for n=3 included in Figure 2. Insofar as we are aware, this is the only case of degeneracy in all the cases examined here. While the extent to which degeneracy occurs is expected to increase further with n > 3, we elect to combine results obtained for conformations assigned to the same MCI.

The fraction of copolymer bridges ascertained from DPD simulations of TBC- and PBC-based TPEGs analogous to the experimental analogs is provided as functions of ϕ_s and MCI designation in Figure 9. In the case of the TBC materials with n=1, only one conformation classified as [2100] contributes to network formation (*cf.* Figure 2). It is important to recognize that all other conformations are taken into account to extract each value of υ furnished in this section. Results provided for the TBC-based TPEGs are numerically comparable to those reported[42,77] elsewhere from both DPD and Monte Carlo simulations. In the case of TPEGs derived from PBCs (with n=2), the four conformations illustrated in Figure 2 must be analyzed. The fully extended conformation connecting the maximum number of micelles (m_{max}=3) is designated as [3200] and

accounts for about 20-30% of all conformations. Interestingly, υ associated with the [2110] conformation connecting two micelles and possessing one B-midblock bridge and one B-midblock loop ranges from 40 to 50% over the entire range of φ_S examined. In marked contrast, the most compact topology ([2200]) only contributes 5-10%, whereas the [2101] designation, constituting the only conformation with a thermodynamically unfavorable dangling end, is negligible, adding only 0-1%. The total bridging fraction afforded by PBC-based TPEGs, obtained by summing the results from all the individual MCI designations, is ≈85%, which is considerably higher than the maximum υ (≈68%) afforded by TBC-based TPEGs due to the greater topological complexity inherent in PBCs.

The substantial increase in topological complexity in TPEGs derived from HBCs is immediately evident from Figure 10 wherein conformations responsible for connecting 4 (the maximum number possible) or 3 micelles are displayed in Figure 10a and those connecting only 2 micelles (the minimum number considered) are included in Figure 10b. Although υ corresponding to the fully extended [4300] conformation appears to increase with increasing φ_S, it is important to recognize that this conformation at most accounts for ≈16% of all possible topologies. Values of υ for the alternative, less extended conformation that likewise possesses 3 B-midblock bridges/molecule, designated as [3300], remain comparable to those of the [4300] conformation up to $\varphi_S \approx 50\%$ and then decrease as φ_S is increased further. The dominant conformation visible in Figure 10a is designated as [3210], as it connects 3 micelles with 2 B-midblock bridges and possesses a single B-midblock loop. In this case, υ increases from about 21 to 40% as φ_S is increased from 0 to 90%. As with the PBC-based TPEGs in Figure 9, values of υ determined for the counterpart to this conformation with a dangling end instead of a B-midblock loop ([3201]) are insignificant (<1%). In Figure 10b, the highly deleterious effects (responsible for low υ) of one

or two dangling ends (*i.e.*, the [2201] and [2111] topologies or the [2102] topology, respectively) and compaction (*i.e.*, the [2300] topology) are apparent. While the most prominent conformation connecting 2 micelles and possessing a nearly constant bridging fraction (≈29%) is designated as [2120] with 1 B-midblock bridge and 2 B-midblock loops, its analog described as having 2 bridges and 1 loop ([2210]) provides a more modest contribution that generally decreases monotonically from 16% in the neat copolymer to about 6% when φ_S = 90%. Upon summing all the values of υ in Figure 10 for HBC-based TPEGs, over 90% of the copolymer molecules are found to participate in network development via B-midblock bridging.

5.5. Conclusions

In this study, we have investigated the morphological characteristics and chain topologies of TPEGs composed of linear multiblock copolymers custom-synthesized by living anionic polymerization to possess comparable composition and molecular weight but different molecular architecture, and selectively hydrogenated from PI to EP. According to analysis of the form factor in SAXS profiles, the morphologies of the neat and solvated copolymers are generally classified as spheroidal, which agrees with results from accompanying DPD simulations. From the relative scattering peak positions, 2D or 3D hexagonal close-packed spheres appear to persist as the copolymers are solvated up to 92% in the case of the PBC- and HBC-containing systems. These findings will be compared to transmission electron microscopy results in a forthcoming publication. As the TPEGs become increasingly solvated, the microdomain periodicity initially increases slowly and then sharply at relatively high solvent levels (> 80%). Corresponding spherical radii extracted from scattering form factors are sensitive to polydispersity at low φ_S (< 40%) and then become nearly monodisperse (and decrease nearly linearly) at high φ_S. By introducing a midblock conformation index (MCI) as a means by which to develop a molecular-

level classification scheme of the network,[79,80] we can systematically categorize the various molecular conformations that contribute to network formation in these TPEGs. Since topological complexity increases significantly with an increase in the number of blocks along the copolymer backbone, this index is anticipated to augment existing theoretical treatments[81,82] of block copolymer self-assembly and network formation in solution. In the cases of the PBC- and HBC-based systems, the likelihood of chains being fully extended so as to connect the maximum number of micelles possible is less than that of chains possessing at least one swollen midblock loop. Since these copolymer molecules are highly incompatible, conformations with a dangling endblock are negligible. The objective of this study is to elucidate the nanostructural characteristics and detailed chain topologies of TPEGs derived from linear multiblock copolymers so that conformation-structure-property relationships can be developed in this remarkably versatile and tunable class of soft and elastic materials.

5.6. Acknowledgments

This work was supported by the NC State Nonwovens Institute and DFG Grant EXC 1027 Bild Wissen Gestaltung. This research used resources of the Advanced Photon Source, a U.S. Department of Energy (DOE) Office of Science User Facility operated for the DOE Office of Science by Argonne National Laboratory under Contract No. DE-AC02-06CH11357.

5.7. References

1. Hamley, I. W. *The Physics of Block Copolymers*; Oxford University Press: New York, 1998.
2. Abetz, V.; Simon, P. F. W. Phase Behaviour and Morphologies of Block Copolymers. In *Block Copolymers I* (Ed.: V. Abetz); Springer: Berlin, 2005; pp. 125–212.
3. Park, C.; Yoon, J.; Thomas, E. L. Enabling Nanotechnology with Self Assembled Block Copolymer Patterns. *Polymer* 2003, *44*, 6725–6760.
4. Guo, C. H.; Lin, Y. H.; Witman, M. D.; Smith, K. A.; Wang, C.; Hexemer, A.; Strzalka, J.; Gomez, E. D.; Verduzco, R. Conjugated Block Copolymer Photovoltaics with Near 3% Efficiency through Microphase Separation. *Nano Lett*. 2013, *13*, 2957–2963.
5. Chan, E. P.; Walish, J. J.; Urbas, A. M.; Thomas, E. L. Mechanochromic Photonic Gels. *Adv. Mater*. 2013, *25*, 3934–3947.
6. Boyle, B. M.; French, T. A.; Pearson, R. M.; McCarthy, B. G.; Miyake, G. M. Structural Coloring for Additive Manufacturing: 3D-Printed Photonic Crystals from Block Copolymers. *ACS Nano* 2017, *11*, 3052–3058.
7. Müller-Buschbaum, P. (Ed.) Forum on Block Copolymers for Nanotechnology Applications. *ACS Appl. Mater. Interfaces* 2017, *9* 31213–32412.
8. Bates, C. M.; Bates, F. S. Block Polymers — Pure Potential. *Macromolecules* 2017, *50*, 3–22.
9. Jinnai, H.; Kaneko, T.; Matsunaga, K.; Abetz, C.; Abetz, V. A Double Helical Structure Formed from an Amorphous, Achiral ABC Triblock Terpolymer. *Soft Matter* 2009, *5*, 2042–2046.
10. Hajduk, D. A.; Harper, P. E.; Gruner, S. M.; Honeker, C. C.; Kim, G.; Thomas, E. L.;

Fetters, L. J. The Gyroid — A New Equilibrium Morphology in Weakly Segregated Diblock Copolymers. *Macromolecules* 1994, *27*, 4063–4075.

11. Laurer, J. H.; Hajduk, D. A.; Fung, J. C.; Sedat, J. W.; Smith, S. D.; Gruner, S. M.; Agard, D. A.; Spontak, R. J. Microstructural Analysis of a Cubic Bicontinuous Morphology in a Neat SIS Triblock Copolymer. *Macromolecules* 1997, *30*, 3938–3941.
12. Jinnai, H.; Nishikawa, Y.; Spontak, R. J.; Smith, S. D.; Agard, D. A.; Hashimoto, T. Direct Measurement of Interfacial Curvature Distributions in a Bicontinuous Block Copolymer Morphology. *Phys. Rev. Lett.* 2000, *84*, 518–521.
13. Tyler, C. A.; Morse, D. C. Orthorhombic *Fddd* Network in Triblock and Diblock Copolymer Melts. *Phys. Rev. Lett*. 2005, *94*, 208302.
14. Takenaka, M.; Wakada, T.; Akasaka, S.; Nishitsuji, S.; Saijo, K.; Shimizu, H.; Kim, M. I.; Hasegawa, H. Orthorhombic *Fddd* Network in Diblock Copolymer Melts. *Macromolecules* 2007, *40*, 4399–4402.
15. Lee, S.; Bluemle, M. J.; Bates, F. S. Discovery of a Frank-Kasper Phase in Sphere-Forming Block Copolymer Melts. *Science* 2010, *330*, 349–353.
16. Drobny, J. G. *Handbook of Thermoplastic Elastomers*, 2nd ed.; Elsevier: Oxford, 2014.
17. Hamersky, M. W.; Smith, S. D.; Gozen, A. O.; Spontak, R. J. Phase Behavior of Triblock Copolymers Varying in Molecular Asymmetry. *Phys. Rev. Lett*. 2005, *95*, 168306.
18. Watanabe, H. Slow Dielectric-Relaxation of a Styrene-Isoprene-Styrene Triblock Copolymer with Dipole Inversion in the Middle Block – A Challenge to a Loop-Bridge Problem. *Macromolecules* 1995, *28*, 5006–5011.
19. Karatasos, K.; Anastasiadis, S. H.; Pakula, T.; Watanabe, H. On the Loops-to-Bridges Ratio in Ordered Triblock Copolymers: An Investigation by Dielectric Relaxation

Spectroscopy and Computer Simulations. *Macromolecules* 2000, *33*, 523–541.

20. Watanabe, H.; Sato, T.; Osaki, K. Concentration Dependence of Loop Fraction in Styrene-Isoprene-Styrene Triblock Copolymer Solutions and Corresponding Changes in Equilibrium Elasticity. *Macromolecules* 2000, *33*, 2545–2550.
21. Kane, L.; Norman, D. A.; White, S. A.; Matsen, M. W.; Satkowski, M. M.; Smith, S. D.; Spontak, R. J. Molecular, Nanostructural and Mechanical Characteristics of Lamellar Triblock Copolymer Blends: Effects of Molecular Weight and Constraint. *Macromol. Rapid Commun.* 2001, *22*, 281–296.
22. Matsen, M. W.; Schick, M. Lamellar Phase of a Symmetrical Triblock Copolymer. *Macromolecules* 1994, *27*, 187–192.
23. Matsen, M. W.; Thompson, R. B. Equilibrium Behavior of Symmetric ABA Triblock Copolymer Melts. *J. Chem. Phys.* 1999, *111*, 7139–7146.
24. Tallury, S. A.; Mineart, K. P.; Woloszczuk, S.; Williams, D. N.; Thompson, R. B.; Pasquinelli, M. A.; Banaszak, M.; Spontak, R. J. Molecular-Level Insights into Asymmetric Triblock Copolymers: Network and Phase Development. *J. Chem. Phys.* 2014, *141*, 121103.
25. Tallury, S. S.; Spontak, R. J.; Pasquinelli, M. A. Dissipative Particle Dynamics of Triblock Copolymer Melts: A Midblock Conformational Study at Moderate Segregation. *J. Chem. Phys.* 2014, *141*, 244911.
26. Fredrickson, G. H.; Milner, S. T.; Leibler, L. Multicritical Phenomena and Microphase Ordering in Random Block Copolymer Melts. *Macromolecules* 1992, *25*, 6341–6354.
27. Park, C. H.; Lee, C. H.; Guiver, M. D.; Lee, Y. M. Sulfonated Hydrocarbon Membranes for Medium-Temperature and Low-Humidity Proton Exchange Membrane Fuel Cells

(PEMFCs). *Prog. Polym. Sci*. 2011, *36*, 1443–1498.

28. Denisova, Y. I.; Gringolts, M. L.; Krentsel, L. B.; Shandryuk, G. A.; Peregudov, A. S.; Finkelshtein, E. S.; Kudryavtsev, Y. V. *Polym. Sci. Ser. B* 2017, *59*, 412–420.
29. Spontak, R. J.; Smith, S. D.; Satkowski, M. M.; Ashraf, A.; Zielinski, J. M. Synthesis and Morphological Studies of $(AB)_n$ Multiblock Copolymers. In Polymer Solutions, Blends, and Interfaces (Eds: I. Noda and D. N. Rubingh), Elsevier: Amsterdam, 1992, pp. 65–88.
30. Smith, S. D.; Spontak, R. J.; Satkowski, M. M.; Ashraf, A.; Lin, J. S. Microdomain Contraction in Microphase-Separated Multiblock Copolymers. *Phys. Rev. B* 1993, *47*, 14555–14558.
31. Smith, S. D.; Spontak, R. J.; Satkowski, M. M.; Ashraf, A.; Heape, A. K.; Lin, J. S. Microphase-Separated Poly(styrene-*b*-isoprene)$_n$ Multiblock Copolymers with Constant Block Lengths. *Polymer* 1994, *35*, 4527–4536.
32. Spontak, R. J.; Smith, S. D. Perfectly-Alternating Linear $(AB)_n$ Multiblock Copolymers: Effect of Molecular Design on Morphologies and Properties. *J. Polym. Sci. B: Polym. Phys.* 2001, *39*, 947–955.
33. Wu, L. F.; Cochran, E. W.; Lodge, T. P.; Bates, F. S. Consequences of Block Number on the Order-Disorder Transition and Viscoelastic Properties of Linear $(AB)_n$ Multiblock Copolymers. *Macromolecules* 2004, *37*, 3360–3368.
34. Lee, I.; Bates, F. S. Synthesis, Structure, and Properties of Alternating and Random Poly(styrene-*b*-butadiene) Multiblock Copolymers. *Macromolecules* 2013, *46*, 4529–4539.
35. Eagan, J. M.; Xu, J.; Di Girolamo, R.; Thurber, C. M.; Macosko, C. W.; LaPointe, A. M.; Bates, F. S.; Coates, G. W. Combining Polyethylene and Polypropylene: Enhanced

Performance with PE/iPP Multiblock Polymers. *Science* 2017, *355*, 814–816.

36. Bates, F. S.; Hillmyer, M. A.; Lodge, T. P.; Bates, C. M.; Delaney, K. T.; Fredrickson, G. H. Multiblock Polymers: Panacea or Pandora's Box? *Science* 2012, *336*, 434–440.
37. Winey, K. I.; Thomas, E. L.; Fetters, L. J. Isothermal Morphology Diagrams for Binary Blends of Diblock Copolymer and Homopolymer. *Macromolecules* 1992, *25*, 2645–2650.
38. Matsen, M. W. Phase-Behavior of Block-Copolymer Homopolymer Blends. *Macromolecules* 1995, *28*, 5765–5773.
39. Spontak, R. J.; Patel, N. P. Phase Behavior of Block Copolymer Blends. In: *Block Copolymer Science and Technology*, (Ed: I. W. Hamley), Wiley: New York, 2004, pp. 159–212.
40. Krishnan, A. S.; Smith, S. D.; Spontak, R. J. Ternary Phase Behavior of a Triblock Copolymer in the Presence of an Endblock-Selective Homopolymer and a Midblock-Selective Oil. *Macromolecules* 2012, *45*, 6056–6067.
41. Lodge, T. P.; Pudil, B.; Hanley, K. J. The Full Phase Behavior for Block Copolymers in Solvents of Varying Selectivity. *Macromolecules* 2002, *35*, 4707–4717.
42. Woloszczuk, S.; Tuhin, M. O.; Gade, S. R.; Pasquinelli, M. A.; Banaszak, M.; Spontak, R. J. Complex Phase Behavior and Network Characteristics of Midblock-Solvated Triblock Copolymers as Physically-Crosslinked Soft Materials. *ACS Appl. Mater. Interfaces* 2017, *9*, 39940–39944.
43. Shankar, R.; Ghosh, T. K.; Spontak, R. J. Electroactive Nanostructured Polymers as Tunable Actuators. *Adv. Mater.* 2007, *19*, 2218–2223.
44. Shankar, R.; Ghosh, T. K.; Spontak, R. J. Dielectric Elastomers as Next-Generation Polymeric Actuators. *Soft Matter* 2007, *3*, 1116–1129.

45. Kim, B.; Park, Y. D.; Min, K.; Lee, J. H.; Hwang, S. S.; Hong, S. M.; Kim, B. H.; Kim, S. O.; Koo, C. M. Electric Actuation of Nanostructured Thermoplastic Elastomer Gels with Ultralarge Electrostriction Coefficients. *Adv. Funct. Mater*. 2011, *21*, 3242–3249.
46. Vargantwar, P. H.; Ozcam, A. E.; Ghosh, T. K.; Spontak, R. J. Prestrain-Free Dielectric Elastomers Based on Acrylic Thermoplastic Elastomer Gels: A Morphological and (Electro)Mechanical Property Study. *Adv. Funct. Mater*. 2012, *22*, 2100–2113.
47. Armstrong, D. P.; Spontak, R. J. Designing Dielectric Elastomers over Multiple Length Scales for 21st-Century Soft Materials Technologies. *Rubber Chem. Technol*. 2017, *90*, 207–224.
48. Song, S.; Feng, J.; Wu, P. A New Strategy to Prepare Polymer-based Shape Memory Elastomers. *Macromol. Rapid Commun.* 2011, *32*, 1569–1575.
49. Zhang, Q.; Song, S.; Feng, J.; Wu, P. A New Strategy to Prepare Polymer Composites with Versatile Shape Memory Properties. *J. Mater. Chem.* 2012, *22*, 24776–24782.
50. Mineart, K. P.; Tallury, S. S.; Li, T.; Lee, B.; Spontak, R. J. Phase-Change Thermoplastic Elastomer Blends for Tunable Shape Memory by Physical Design. *Ind. Eng. Chem. Res.* 2016, *55*, 12590–12597.
51. Creton, C.; Hu, G. J.; Deplace, F.; Morgret, L.; Shull, K. R. Large-Strain Mechanical Behavior of Model Block Copolymer Adhesives. *Macromolecules* 2009, *42*, 7605–7615.
52. Sudarsan, A. P.; Wang, J.; Ugaz, V. M. Thermoplastic Elastomer Gels: An Advanced Substrate for Microfluidic Chemical Analysis Systems. *Anal. Chem*. 2005, *77*, 5167–5173.
53. Mineart, K. P.; Lin, Y.; Desai, S. C.; Krishnan, A. S.; Spontak, R. J.; Dickey, M. D. Ultrastretchable, Cyclable and Recyclable 1- and 2-Dimensional Conductors Based on Physically Cross-Linked Thermoplastic Elastomer Gels. *Soft Matter* 2013, *9*, 7695–7700.

54. Alexandridis, P.; Olsson, U.; Lindman, B. A Record Nine Different Phases (Four Cubic, Two Hexagonal, and One Lamellar Lyotropic Liquid Crystalline and Two Micellar Solutions) in a Ternary Isothermal System of an Amphiphilic Block Copolymer and Selective Solvents (Water And Oil). *Langmuir* 1998, *14*, 2627–2638.
55. He, Y. Y.; Boswell, P. G.; Buhlmann, P.; Lodge, T. P. Ion Gels by Self-Assembly of a Triblock Copolymer in an Ionic Liquid. *J. Phys. Chem. B* 2007, *111*, 4645–4652.
56. Shen, W.; Zhang, K .C.; Kornfield, J. A.; Tirrell, D. A. Tuning the Erosion Rate of Artificial Protein Hydrogels through Control of Network Topology. *Nat. Mater*. 2006, *5*, 153–158.
57. Hallinan, D. T.; Balsara, N. P. Polymer Electrolytes. *Ann. Rev. Mater. Res*. 2013, *43*, 503–525.
58. Vargantwar, P. H.; Roskov, K. E.; Ghosh, T. K.; Spontak, R. J. Enhanced Biomimetic Performance of Ionic Polymer–Metal Composite Actuators Prepared with Nanostructured Block Ionomers. *Macromol. Rapid Commun.* 2012, *33*, 61–68.
59. Al-Mohsin, H. A.; Mineart, K. P.; Spontak, R. J. Highly Flexible Aqueous Photovoltaic Elastomer Gels Derived from Sulfonated Block Ionomers. *Adv. Energy Mat.* 2015, *8*, 1401941.
60. Al-Mohsin, H. A.; Mineart, K. P.; Armstrong, D. P.; El-Shafei, A.; Spontak, R. J. Quasi-Solid-State Dye-Sensitized Solar Cells Containing a Charged Thermoplastic Elastomeric Gel Electrolyte and Hydrophilic/phobic Photosensitizers. *Sol. RRL* 2018, 1700145.
61. Geise, G. M.; Freeman, B. D.; Paul, D. R. Characterization of a Sulfonated Pentablock Copolymer for Desalination Applications. *Polymer* 2010, *51*, 5815–5822.
62. Fan, Y.; Zhang, M.; Moore, R. B.; Cornelius, C. J. Structure, Physical Properties, and

Molecule Transport of Gas, Liquid, and Ions within a Pentablock Copolymer. *J. Membr. Sci.* 2014, *464*, 179−187.

63. Ansaloni, L.; Dai, Z.; Ryan, J. J.; Mineart, K. P.; Saud, K. T.; Yu, Q.; Hägg, M.-B.; Spontak, R. J.; Deng, L. Base- and Acid-Gas Transport through Solvent-Templated Block Ionomers: Effect of Humidity on Ammonia and Carbon Dioxide Permeation. *Adv. Mater. Interfaces* 2017, 1700854.
64. Shankar, R.; Krishnan, A. S.; Ghosh, T. K.; Spontak, R. J. Triblock Copolymer Organogels as High-Performance Dielectric Elastomers. *Macromolecules* 2008, *41*, 6100−6109.
65. Armstrong, D. P.; Mineart, K. P.; Lee, B.; Spontak, R. J. Olefinic Thermoplastic Elastomer Gels: Combining Polymer Crystallization and Microphase Separation in a Selective Solvent. *ACS Macro Lett*. 2016, *5*, 1273−1277.
66. Ashraf, A.; Ryan, J. J.; Satkowski, M. M.; Smith, S. D.; Spontak, R. J. Effect of Systematic Hydrogenation on the Phase Behavior and Nanostructural Dimensions of Block Copolymers. *ACS Appl. Mater. Interfaces* 2018, *10*, 3186−3190.
67. Qian, H.; Lu, Z.; Chen, L.; Li, Z.; Sun, C. Computer Simulation of Cyclic Block Copolymer Microphase Separation. *Macromolecules* 2005, *38*, 1395−1401.
68. Groot, R. D.; Madden, T. J.; Tildesley, D. J. On the Role of Hydrodynamic Interactions in Block Copolymer Microphase Separation. *J. Chem. Phys.* 1999, *110*, 9739−9749.
69. Plimpton, S. Fast Parallel Algorithms for Short-Range Molecular-Dynamics. *J. Comput. Phys*. 1995, *117*, 1−19.
70. Matsen, M. W. Effect of Architecture on the Phase Behavior of AB-Type Block Copolymer Melts. *Macromolecules* 2012, *45*, 2161–2165.
71. Semenov, A. N. Theory of Block-Copolymer Interfaces in the Strong Segregation Limit.

Macromolecules 1993, *26*, 6617–6621.

72. Kleppinger, R.; Mischenko, N.; Theunissen, E.; Reynaers, H. L.; Koch, M. H. J.; Almdal, K.; Mortensen, K. Shear-Induced Single Crystalline Mesophases in Physical Networks of Gel-Forming Triblock Copolymer Solutions. *Macromolecules* 1997, *30*, 7012–7014.
73. Mortensen, K.; Theunissen, E.; Kleppinger, R.; Almdal, K.; Reynaers, H. Shear-Induced Morphologies of Cubic Ordered Block Copolymer Micellar Networks Studied by in Situ Small-Angle Neutron Scattering and Rheology. *Macromolecules* 2002, *35*, 7773–7781.
74. Krishnan, A. S.; van Zanten, J. H.; Seifert, S.; Lee, B.; Spontak, R. J. Selectively-Solvated Triblock Copolymer Networks under Biaxial Strain. *Appl. Phys. Lett*. 2011, *99*, 101908.
75. Park, M. J.; Bang, J.; Harada, T.; Char, K.; Lodge, T. P. Epitaxial Transitions among FCC, HCP, BCC, and Cylinder Phases in a Block Copolymer Solution. *Macromolecules* 2004, *37*, 9064–9075.
76. Bang, J.; Lodge, T. P. On the Selection of FCC and BCC Lattices in Poly(styrene-b-isoprene) Copolymer Micelles. *Macromol. Res*. 2008, *16*, 51–56.
77. Senesi, A. J.; Lee, B. Small-Angle Scattering of Particle Assemblies. *J. Appl. Crystallog.* 2015, *48*, 1172–1182.
78. Chantawansri, T. L.; Sirk, T. W.; Sliozberg, Y. R. Entangled Triblock Copolymer Gel: Morphological and Mechanical Properties. *J. Chem. Phys*. 2013, *138*, 024908.
79. Li, S.; Chen, J.; Xu, D.; Shi, T. Topological Constraints of Network Chains in Telechelic Associative Polymer Gels. *J. Chem. Phys*. 2015, *143*, 244902.
80. Zhong, M.; Wang, R.; Kawamoto, K.; Olsen, B. D.; Johnson, J. A. Quantifying the Impact of Molecular Defects on Polymer Network Elasticity. *Science* 2016, *353*, 1264–1268.
81. Bras, R. E.; Shull, K. R. Self-Consistent Field Theory of Gelation in Triblock Copolymer

Solutions. *Macromolecules* 2009, *42*, 8513–8520.

82. Zhang, Q.; Lin, J.; Wang, L.; Xu, Z. Theoretical Modeling and Simulations of Self-Assembly of Copolymers in Solution. *Prog. Polym. Sci*. 2017, *75*, 1–30.

5.8. Figures

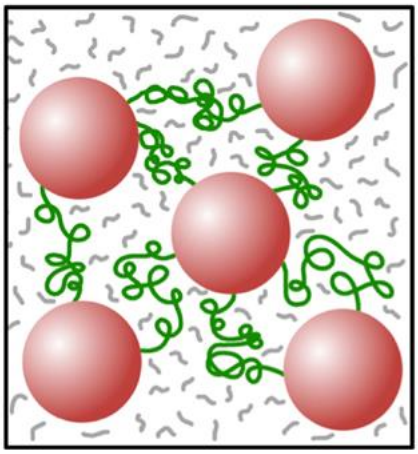

Figure 1. Illustration depicting the rigid micelles (red) that serve as physical crosslinks in TPEGs. $A(BA)_n$ multiblock copolymers can possess up to n soft-block bridges (green) that are selectively swollen by the added diluent (gray) and physically connect up to n+1 micelles.

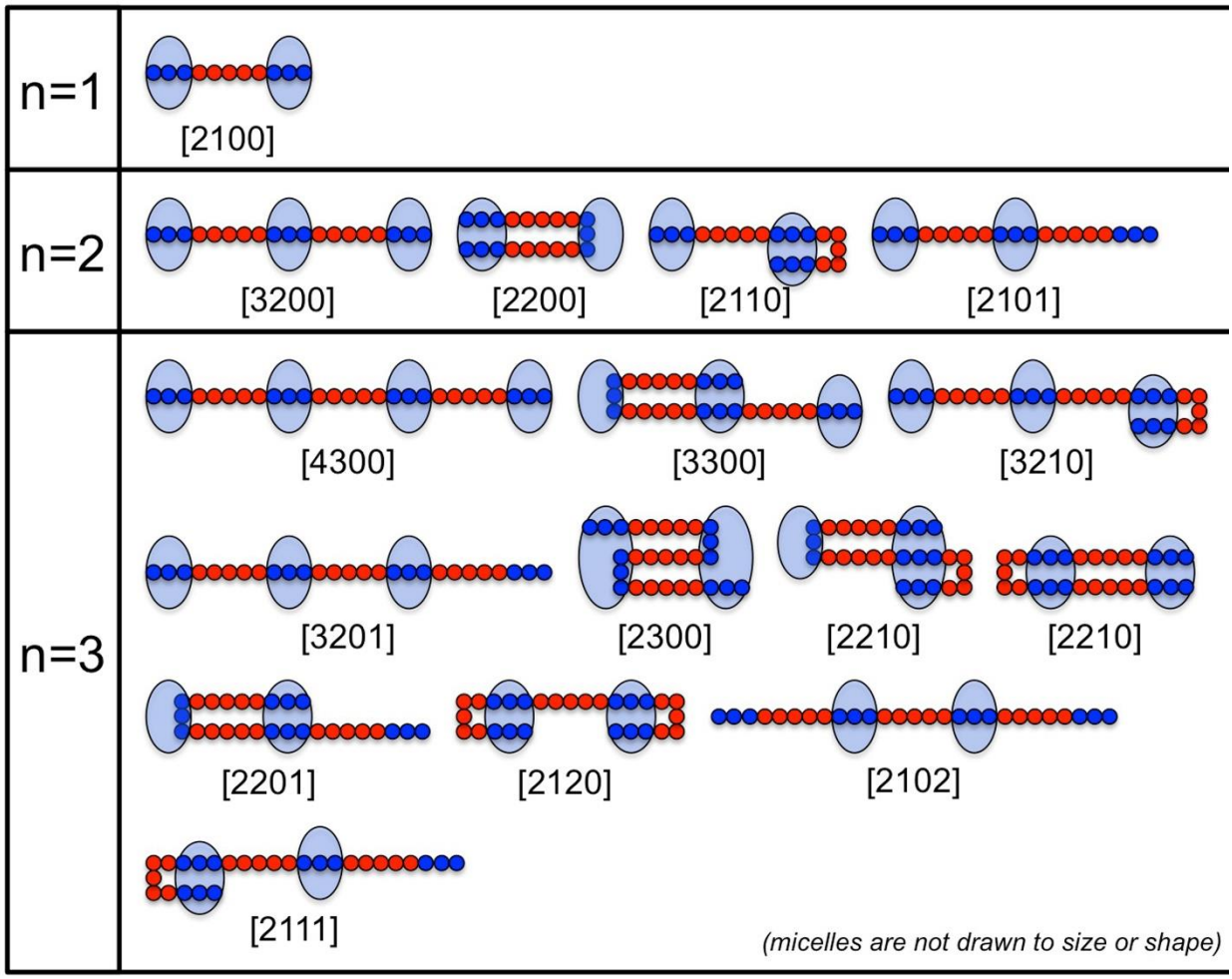

Figure 2. Schematic diagram of the various molecular conformations responsible for networks composed of linear $A(BA)_n$ multiblock copolymers varying in the number of swollen soft-midblocks (n, red): 1 (TBC), 2 (PBC) and 3 (HBC). Rigid blocks (dark blue) are able to self-organize into micelles (light blue), and the only conformations considered here possess soft-midblocks that bridge nearest-neighbor micelles. Corresponding MCI designations of the form [#micelles, #bridges, #loops, #dangles] are included for each conformation that connects at least 2 micelles and confirm that little degeneracy exists up to n=3.

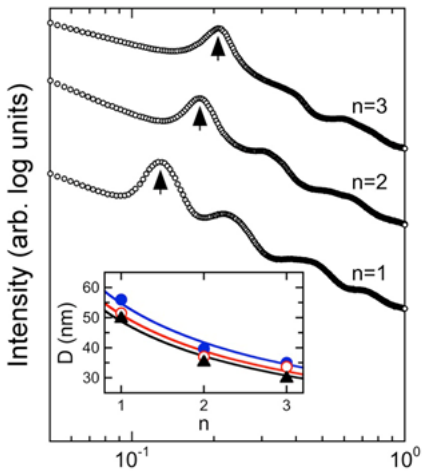

Figure 3. SAXS intensity profiles measured from neat multiblock copolymers varying in n (labeled). Each arrow identifies the principal peak at q*. In the inset, D (=2π/q*) is included as a function of n for all three copolymers at different degrees of hydrogenation (in mol%): 0 (blue), 50 (red) and ≈97 (black). The color-coded lines correspond to the scaling relation in the text.

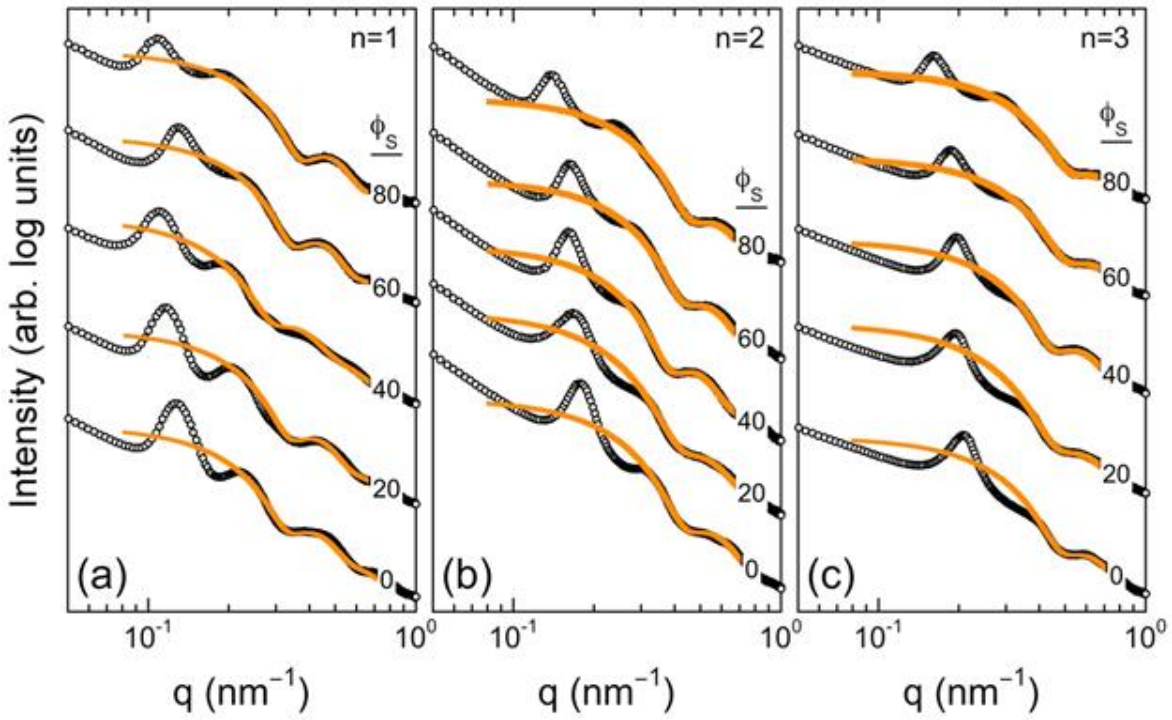

Figure 4. SAXS profiles acquired from TPEGs varying in molecular architecture (n) — (a) 1, (b) 2 and (c) 3 — at different φ_S (labeled, in %). The position of the second peak relative to q* suggests that all of these systems possess hexagonal close-packed S spheres. The curve fits (gold) correspond to the form factor for polydisperse spheres.

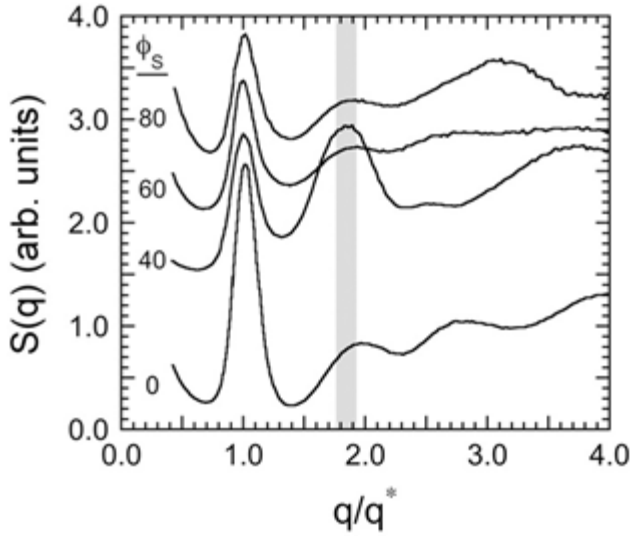

Figure 5. Structure factor, S(q), values extracted from the SAXS data in Figure 4 for several swollen TPEGs varying in φ_S (labeled, in %) with n=1, and vertically shifted to facilitate viewing. The shaded region identifies the range of the second maximum, confirming that the spherical morphologies are not bcc or fcc.

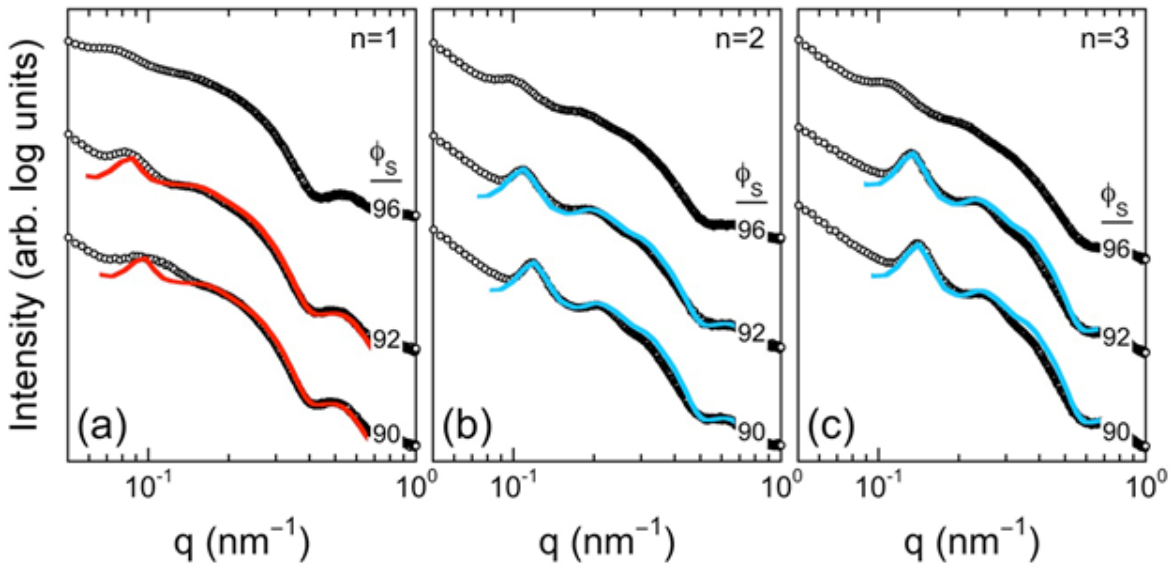

Figure 6. SAXS profiles measured from TPEGs varying in molecular architecture (n) — (a) 1, (b) 2 and (c) 3 — at different φ_S (labeled, in %). The position of the second peak relative to q* indicates that the PBC- and HBC-based TPEGs possess hexagonal close-packed S spheres in an oil-swollen EP matrix up to φ_S=92%. The red and blue curves represent model fits for hexagonal close-packed and 2D hexagonal spheres, respectively.

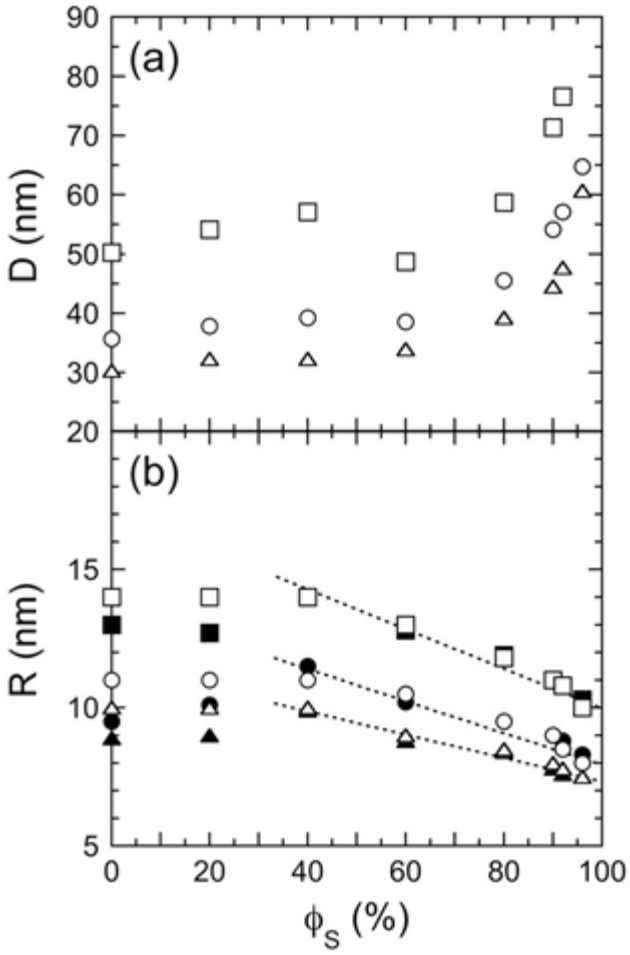

Figure 7. Values of (a) D and (b) R extracted from SAXS profiles for TPEGs varying in copolymer architecture (n) — 1 (squares), 2 (circles) and 3 (triangles) — as a function of φ_S. In (b), the open and filled symbols correspond to monodisperse and polydisperse spheres, respectively. The dotted lines in (b) serve as guides for the eye and indicate the range over which R decreases nearly linearly upon matrix swelling.

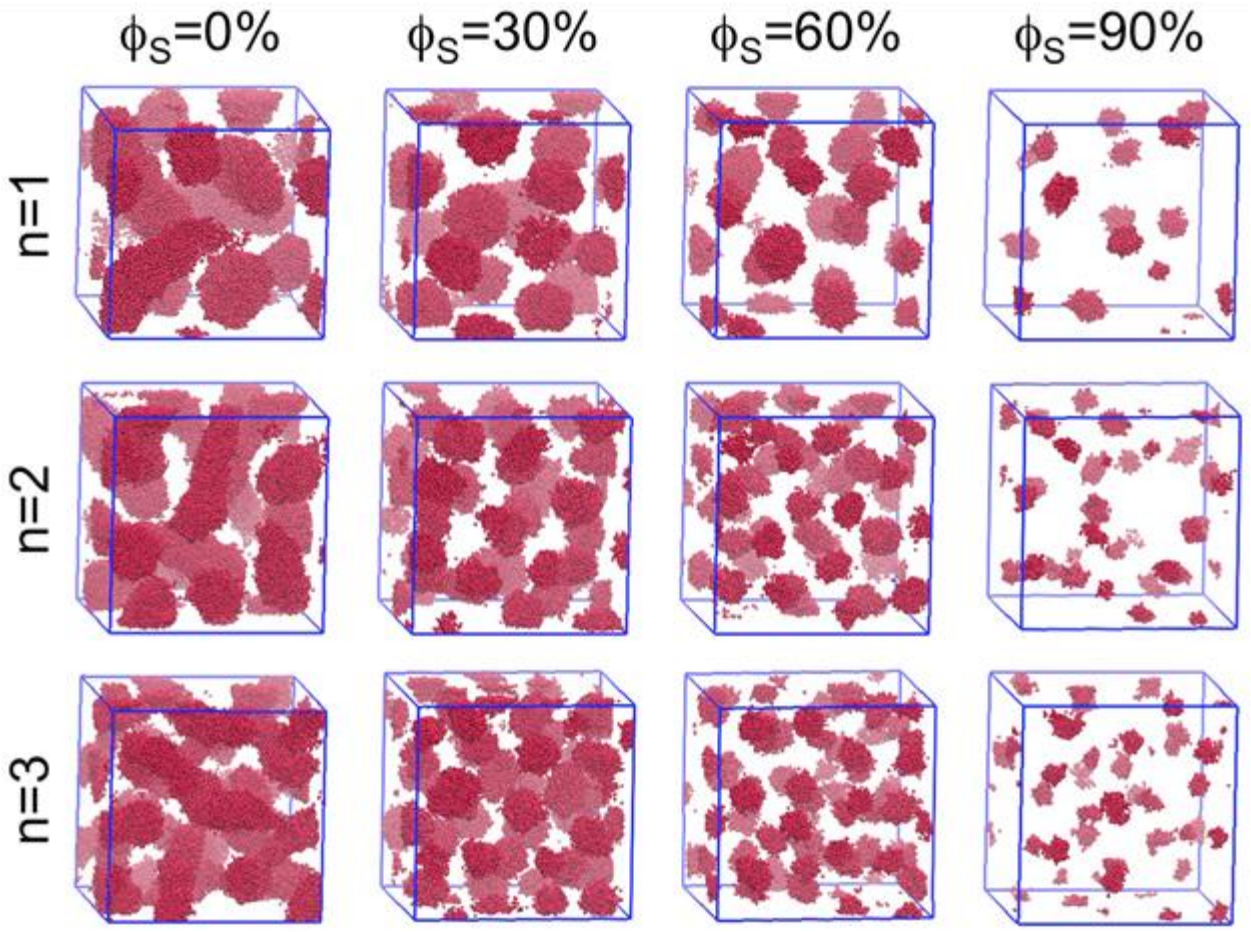

Figure 8. Equilibrated DPD simulation trajectory snapshots acquired from selectively-solvated linear multiblock copolymers varying in molecular architecture (n) and solvent content (φ_S), as labeled.

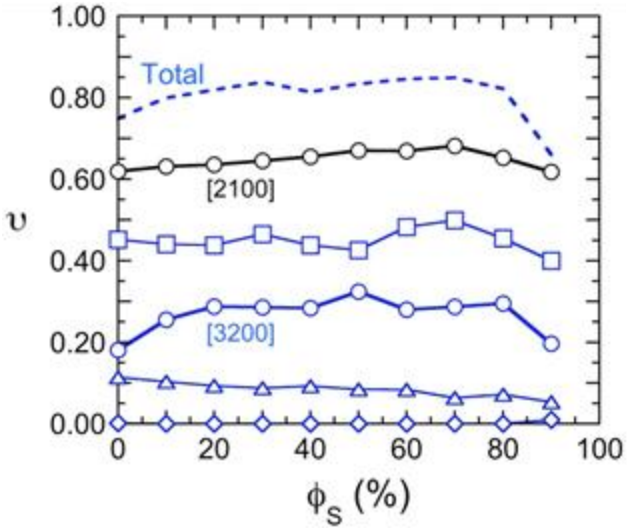

Figure 9. Values of the bridging fraction (υ) presented as a function of φ_S for selectively-solvated TBCs (black) and PBCs (blue). MCI designations include [2200] (△), [2110] (□) and [2101] (◇). Solid lines serve to connect the data, and bold lines identify the fully extended conformations with $m=m_{max}$. The dashed line is the total bridging fraction obtained by summing all the individual conformational contributions.

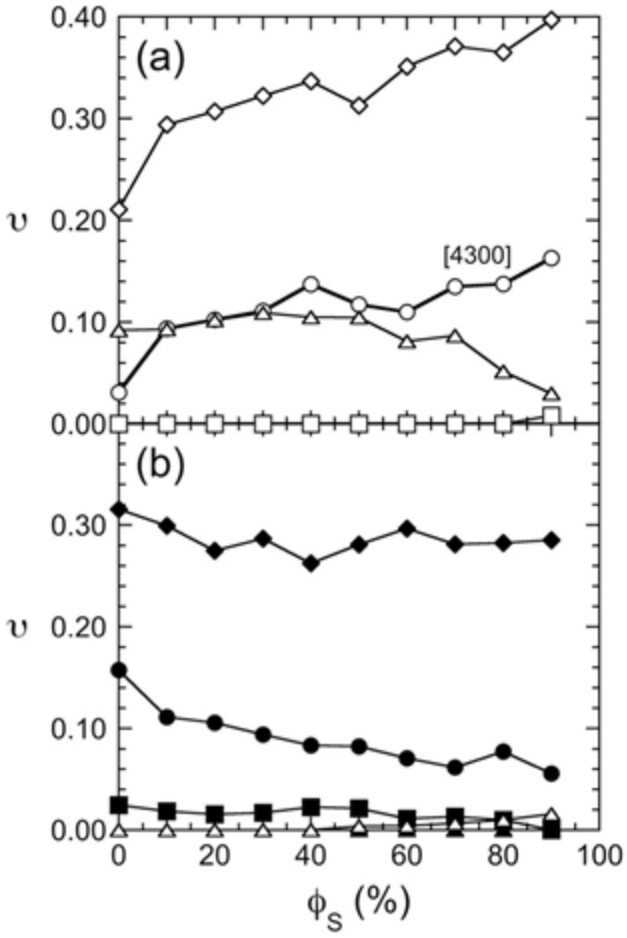

Figure 10. Values of υ as a function of φ_S for selectively-solvated HBCs in which m = 3 or 4 in (a) or m = 2 in (b). MCI designations in (a) include [3300] (△), [3210] (◇) and [3201] (□). Those in (b) include [2300] (■), [2210] (●), [2201] (▲), [2120] (◆), and [2111] (△). Solid lines serve to connect the data, and the bold line identifies the fully extended conformation with $m=m_{max}$.

CHAPTER 6

6.1. Introduction

Block copolymers have long been used in myriad fields of applications, predominantly, because of their capability of being self-assembled into nanostructures.[1-3] While forming the self-assembled organizations, the constituent molecules form different molecular conformations if the molecules contain two or more components having more than or equal to three polymeric blocks connected by covalent bonds.[4] In case of linear triblock copolymer, the simplest class of such block copolymers, molecules can connect the self-assembled microdomains by forming bridge, can be the part of same domain by forming loop, or can leave one end block hanging while another one being part of a microdomain and thus forming dangles.[5] The loops from neighboring domains can also interlock with each other and thus can form bridge type connection out of loops. While these are the known molecular conformations in triblock copolymers, increasing the number of midblocks can further extend the possibility due to the increased number of molecular conformations with myriad variations of multiblock copolymers.[6] Two of such kind, linear pentablock and heptablock copolymers were studied for their molecular conformations at equilibrium and were detailed enumerated for their molecular conformations in both melt and constituent gels.[7]

The molecular conformations, especially the bridges connecting the microdomains play vital role in determining the mesoscale properties of the constituent systems of block copolymers either in melt or in their gel structure. The bridges were found to predominantly influence the elastic response of the materials as was reported in previous studies of triblock copolymer gels.[8-9] Linear pentablock and heptablock copolymer gels around the terminal region of gelation were also studied and it was found that total bridge fraction increases as the number of midblock segments increases

from 1 (triblock copolymer) to 2 (heptablock copolymer). The linear multiblock copolymer gels were further investigated for their elastic response within linear viscoelastic region and it was observed that for the same composition of the multiblock copolymer gel, higher number of midblock provided higher degree of elastic response.[10] The same study also reported that pentablock and heptablock copolymers retain the gel characteristics beyond the minimum quantity of triblock copolymer composition that depict the gel formation where the added solvent, mineral oil, was midblock selective in all constituent gels. Such difference in the elastic response of the gels around the terminal point of gelation network was attributed to the difference in bridge fraction formed by the multiblock copolymers.

While previous study[10] focused on the influence of molecular conformations around the terminal point of gelation in linear multiblock copolymer gels, one objective of this study is to explore the correlation of elastic nature as a function of the architectural variation in multiblock copolymers at the farther distance from terminal points of gelation. Another objective is to investigate the influence of change in chemistry of the constituent blocks, thus leading to the difference in incompatibility among the constituent blocks, on the viscoelastic response of the multiblock copolymer gels. For that purpose, while the component of endblocks were consistently made up of polystyrene, the midblocks were varied from isoprenic midblocks to ethylene-*alt*-propylene based midblocks where hydrogenation of isoprenic midblocks yielded the ethylene-*alt*-propylene based midblocks. Perfectly alternating multiblock copolymers were synthesized with fixed molecular weight (M) and the isoprenic blocks, denoted as 0 % hydrogenated multiblock in the current study, were hydrogenated upto 50 % and 100 % to obtain the series of multiblock copolymers. Thus, the study encompasses 70-90 wt% addition of midblock selective solvent,

mineral oil, into three series of linear multiblock copolymers: 0 % hydrogenated series, ~50 % hydrogenated series and ~100 % hydrogenated series.

6.2. Experimental Section

Materials: The details of the diluent component, mineral oil, and the synthesis methods of model multiblock copolymer were elaborated elsewhere[7] including their architectures. In the 0 % hydrogenated series, the midblocks were constituted of polyisoprene (PI) while the endblocks remained polystyrene (PS). The hydrogenated series of the block copolymers were obtained for two series: via 50 % hydrogenation of the midblocks having partial conversion of the PI blocks into ethylene-*alt*-propylene (EP) and via ~100 % conversion of the midblocks into EP rubber as described elsewhere[11].

Methods: The block copolymer/mineral oil gels were prepared via solvent casting route using Teflon mold following the detail method elaborated elsewhere[7]. However, the prepared films in these series were slightly thinner (~1.3 mm) than the films used in Ref. 7. The prepared films were carefully extracted from the mold, wrapped inside aluminum (Al) foil and preserved for testing. Afterwards, the rheological measurements for dynamic moduli were carried out within the linear viscoelastic region (LVE) of the gel samples using Anton Paar parallel plate rheometer, MCR 302. In order to evaluate the LVE region, strain sweep tests were performed at the angular frequency of 0.1 rad/s and the strain within the plateau region was chosen for subsequent tests of viscoelastic moduli (G', G") for the subjects in this study. The frequency sweep for the evaluation of G' and G" was chosen from 0.01 to 100 rad/s, from the lower range to higher range of frequency while testing the gel films. Considering how soft the gels are, in addition to their nature of elasticity and adhesion, the samples, once placed within the plates, were left for 3-5 mins to provide sufficient time so that the samples can relax back to viscoelastically stable state before applying for

frequency sweep at constant strain within LVE region. The reproducible characteristics of the trends reported in this study were confirmed by testing, at least, 2-3 samples for each data set. All rheological experiments were carried out at constant temperature of 25^0 C.

6.3. Results and Discussion

Isoprenic midblock copolymers: All hydrogenated series of block copolymers of different degree of hydrogenation, from 50% to 100%, were obtained from the structurally analogous block copolymers containing isoprenic-midblock. Hence, it's convenient to follow characteristic changes in these parent block copolymer-oriented gels (isoprenic-gels) to understand the comparable changes in properties. The viscoelastic properties, G' and G", of these isoprenic-gels are presented in figure 1. The moduli representations in figure 1 for triblock (a), pentablock (b) and heptablock (c) depicts that elastic modulus, G', is plateau throughout the range of angular frequency used for these tests. However, the viscous modulus, G", for the gel compositions of above 80 wt% depict slightly downward curve for all three architectures. This decrease in G" can be attributed to the relaxation of polymer molecules. At higher quantity of solvent addition, the polymer can get enough time for relaxation as the shear takes longer time at the lower range of frequency. Such change in G" was observed throughout the whole range of composition for pentablock (b) and heptablock (c) copolymer gels, whereas in triblock copolymer gels, such relaxation is evident only after 85 wt% of solvent addition. Such behavior can be attributed to the difference in length of polymer segments in each of the chain. Considering that the polystyrene endblock forms self-assembled micelles, and, as a result of selectivity towards midblock, diluents solvate the midblock occupied area in the gels, the molecular relaxation in the gel matrix can be attributed to the characteristics of the midblock segments. Since, endblocks entangled into micelles are less likely to be mobile while the midblock can be relatively easier to have molecular level

mobility under stress. As the midblock of the triblock copolymers are longer than those in pentablock and heptablock copolymers, the relaxation time for the triblock copolymer chains will be longer than that of pentablock and heptablock copolymer chains. While longer chain tends to increase the relaxation time, the higher the quantity of solvent the less time it should take for the relaxation. Thus, at equal or above 85 wt% of solvent composition, triblock copolymers also tend to show the relaxation behavior at lower range of frequency. The upward directional curve G" at higher range of frequency, above 10 rad/s, can be ascribed to the fact that both material inertia and instrument inertia starts to kick in and thus may contribute to the results of G". However, such inertia is not expected to have countable impact on the elastic response of these gels.

The average G' at lower range of frequency was considered to compare the elastic responses of these isoprenic block copolymers as function of their architecture (figure 1) (d). The values were chosen at the lower range considering that any potential contribution of the instrument inertia is expected to have no impact at this range of frequency. Throughout the range of solvent addition, block copolymers with higher number of midblock depicted higher values of G'. Both pentablock and heptablock copolymer gels depicted power-law behavior upto 80 wt% addition of solvent while triblock copolymer was found to show that at first two compositions only starting from 70 wt%. While G' decreases slowly for all three architectures upto 85 wt% of solvent addition, the triblock copolymer depicted sudden drop in G' at the composition of 90 wt% of solvent addition. Such behavior can be explained using the result of midblock conformations of triblock, pentablock and heptablock copolymer gels reported elsewhere [7,10] for the similar gels where the midblocks were ethylene-*alt*-propylene. The elastic modulus, G' is dictated by the molecular conformations connecting self-assembled microdomains of block copolymers. The dissipative particle dynamics simulation results of Ref. 7,10 depicted that while the quantity of bridge fractions in triblock

copolymers decrease steeply, the midblock conformations connecting the microdomains retain inter-domain connection and thus, such connections decrease slowly in case of pentablock and heptablock copolymer gels. Although, the G' depicted in figure 1(d) belongs to isoprenic block copolymers of similar architecture, similar trend of molecular connectivity as was reported for ethylene-*alt*-propylene midblock is expected to form as a function of different segmental architecture of the block copolymers. The abrupt drop of G' in case of triblock copolymer gels can be the signature of the drop in the quantity of bridge fraction at higher quantity of midblock selective solvent addition.

50% hydrogenated midblock copolymers: The dynamic shear moduli of gels containing 50% hydrogenated midblock are presented in the plots of figure 2. The G' follows the similar trend of being plateau irrespective of the solvent composition and architecture as was observed in the isoprenic-gels. However, the trends of G'' illustrate the change at the lower range of frequency. The downward fall of the G" curve, the signature of molecular relaxation, is evident only at 90 wt% composition in case of both triblock and pentablock copolymer gels. Even in heptablock copolymer gels, the relaxation behavior is observed at and above 80 wt% of solvent addition, unlike the isoprenic-gels. Such behavior can be explained in the context of change in incompatibility between dissimilar blocks of the copolymers. The increase in hydrogenation of midblock in these copolymers is analogous to the increase in incompatibility between dissimilar blocks, which is expected to yield relatively stronger segregation. As the result of such increase in incompatibility, the polymer molecules will have relatively greater tendency to expand. Such expansion is expected to provide multiple scenario at molecular level. Because of such tendency of expansion, the midblock segments are also expected to expand leading endblock segments expand and be part of self-assembled microdomains. Because of further extension of midblock,

there will be less molecular entropy at the vicinity of midblock occupied areas leading relatively less room for relaxation of the molecules, which is observed in lower frequency G" in figures 2 (a), (b) & (c). Such tendency is also expected to increase the inter domain connectivity leading in increase of elastic response of the materials expressed with the G' values in current studies. Further comparison of the material properties of the multiblock copolymer gels as a function of hydrogenation can corroborate such hypothesis, which will be described in the subsequent sections.

The changes in G' as a function of solvent composition for 50% hydrogenated series is presented in the plot of figure 2(d). The gels composed of triblock and pentablock copolymers depict power-law behavior upto 85 wt% of solvent composition, whereas the gels of heptablock copolymer were found to show power-law behavior from 75-85 wt% of solvent composition. Comparing with the values of G' in isoprenic-gels at 70 wt% composition, the 50 % hydrogenated heptablock copolymer has relatively lower value of G' than what was observed for triblock and pentablock copolymer gels. Such findings lead to the assumption that the increase in interblock incompatibility induced enhancement in G' is more dominant in triblock and pentablock copolymer gels than the extent of it is in case of the heptablock copolymer gels at relatively lower solvent composition. The changes in the elastic responses, G', in all three architectures of the block copolymers in their corresponding gels as a function of the degree of hydrogenation can further illustrate how that influences the change in elastic behavior of multiblock copolymer gels, which will be discussed in the subsequent sections.

100% hydrogenated midblock copolymers: The linear viscoelastic responses of multiblock copolymer gels containing ~100% hydrogenated block copolymers are presented in figure 3 for triblock copolymer gels (a), pentablock copolymer gels (b), heptablock copolymer gels (c) and the

comparable average G' at lower range of frequency the gels were examined for all three architectures (d).

The trend in G' remained plateau in the gel compositions of ~100% hydrogenated gels as was in the previous series of 0% and 50% hydrogenated series. The change in G" at lower range of frequency became more pronounced as the hydrogenation induced incompatibility is increased. While the pentablock copolymer gel depicts slight sign of molecular relaxation at 90 wt% solvent composition, such relaxation is totally absent in the series of the triblock copolymer gels in all solvent composition. Heptablock copolymer gels depicted the signature of molecular relaxation induced G" at lower range of frequency only at the 90 wt% solvent composition. Such gradual change in the G" at lower range of frequency at different degree of hydrogenation bolsters the assumption that the hydrogenation induced incompatibility between dissimilar blocks dictates the molecular relaxation.

The average G' plotted in figure 3 (d) depicts the power-law behavior for all architecture at different solvent compositions: 70-80 wt% for triblock, 70-85 wt% for pentablock and 75-85 wt% for heptablck copolymer gels. The reverse trend of values in G' with increase in midblock number at 70 wt% of solvent composition corroborates the assumption that increase in hydrogenation has the least impact on heptablock copolymer chains among all three architectures yielding the lowest value of average G'.

Influence if hydrogenation on G': Influence of hydrogenation can be observed from the plots in figure 4. Comparing the average G' in triblock and pentablock copolymer gels with those of heptablock copolymer gels illustrate that the hydrogenation has the least influence on elastic properties of the heptablock architectures. While addition of increased quantity of midblock selective diluent gradually decreases the influence of hydrogenation on elastic responses of

triblock and pentablock copolymer gels, that in analogous heptablock copolymer gels appear to be significantly less effected.

6.4. Conclusion

In this study, we used linear multiblock copolymer and midblock-selective solvent, mineral oil, to examine the change in viscoelastic properties within LVE region of the materials using a parallel plate rheometer at 25^0C. The gels were investigated as a function of binary aspects of multiblock copolymers: one, the architectural difference induced change in viscoelastic properties; and two, the change in the chemistry of midblock induced interblock incompatibility dictated changes in the viscoelastic properties. All linear multiblock copolymers used in the study were custom-synthesized using living anionic polymerization in a way that the molecular weight of the polymer chains was kept constant while changing architecture of the block copolymer chains for investigating the architectural impact of the block copolymers on designated properties of gels. Similarly, both length and architecture of the chains were kept constant while obtaining different degree of hydrogenation in midblock segments of the linear copolymer chains in order to examine the influence of variation in incompatibility of polystyrene block-to-midblock. The evaluation of the property depicted that dynamic moduli (G' and G") decrease with the increase in the quantity of mineral oil into gel in case of all multiblock copolymers used in this study irrespective of their difference in chain architecture and degree of hydrogenation of midblock in those copolymer chains. For the nonhydrogenated series, the average values of G' at lower range of frequency depicted that G' of the gels decreases as the number of midblock increases in series. As the midblocks are hydrogenated, either 50% or 100%, the gels at the higher end of the copolymer i.e. 70 wt% of mineral addition to the studied series was observed to reverse the tendency of change in G'. However, as the solvent quantity was increased beyond 75 wt% of the gel, the change in G'

decreases as the number of midblock decreases. The impact of hydrogenation depicted that as the block incompatibility increase, the elastic response of the gels also follows similar suit i.e. increment of the quantity, irrespective of the chain architecture or the composition of the gels. The evaluation of these structure-property and chemistry-property relationship of the gels are expected to bring about useful insights in the context of application of soft and tunable multiblock copolymer gels.

6.5. References

1. Letchford, K., & Burt, H. (2007). A review of the formation and classification of amphiphilic block copolymer nanoparticulate structures: micelles, nanospheres, nanocapsules and polymersomes. *European journal of pharmaceutics and biopharmaceutics*, *65*(3), 259-269.
2. Blanazs, A., Armes, S. P., & Ryan, A. J. (2009). Self-assembled block copolymer aggregates: from micelles to vesicles and their biological applications. *Macromolecular rapid communications*, *30*(4-5), 267-277.
3. Mai, Y., & Eisenberg, A. (2012). Self-assembly of block copolymers. *Chemical Society Reviews*, *41*(18), 5969-5985.
4. Takahashi, Y., Song, Y., Nemoto, N., Takano, A., Akazawa, Y., & Matsushita, Y. (2005). Effect of loop/bridge conformation ratio on elastic properties of the sphere-forming ABA triblock copolymers under uniaxial elongation. *Macromolecules*, *38*(23), 9724-9729.
5. Tallury, S. S., Spontak, R. J., & Pasquinelli, M. A. (2014). Dissipative particle dynamics of triblock copolymer melts: A midblock conformational study at moderate segregation. *The Journal of chemical physics*, *141*(24), 244911.
6. Bates, F. S., Hillmyer, M. A., Lodge, T. P., Bates, C. M., Delaney, K. T., & Fredrickson, G. H. (2012). Multiblock polymers: panacea or Pandora's box?. *Science*, *336*(6080), 434-440.
7. Tuhin, M. O., Ryan, J. J., Sadler, J. D., Han, Z., Lee, B., Smith, S. D., ... & Spontak, R. J. (2018). Microphase-Separated Morphologies and Molecular Network Topologies in Multiblock Copolymer Gels. *Macromolecules*.

8. Takano, A., Kamaya, I., Takahashi, Y., & Matsushita, Y. (2005). Effect of loop/bridge conformation ratio on elastic properties of the sphere-forming ABA triblock copolymers: Preparation of samples and determination of loop/bridge ratio. *Macromolecules*, *38*(23), 9718-9723.

9. Sliozberg, Y. R., Andzelm, J. W., Brennan, J. K., Vanlandingham, M. R., Pryamitsyn, V., & Ganesan, V. (2010). Modeling viscoelastic properties of triblock copolymers: a DPD simulation study. *Journal of Polymer Science part B: polymer physics*, *48*(1), 15-25.

10. Tuhin, M. O., Woloszczuk, S., Mineart, K. P., Pasquinelli, M. A., Sadler, J. D., Smith, S. D., ... & Spontak, R. J. (2018). Communication: Molecular-level description of constrained chain topologies in multiblock copolymer gel networks. *The Journal of Chemical Physics*, *148*(23), 231101.

11. Ashraf, A. R., Ryan, J. J., Satkowski, M. M., Smith, S. D., & Spontak, R. J. (2018). Effect of Systematic Hydrogenation on the Phase Behavior and Nanostructural Dimensions of Block Copolymers. *ACS applied materials & interfaces*, *10*(4), 3186-3190.

6.6. Figures

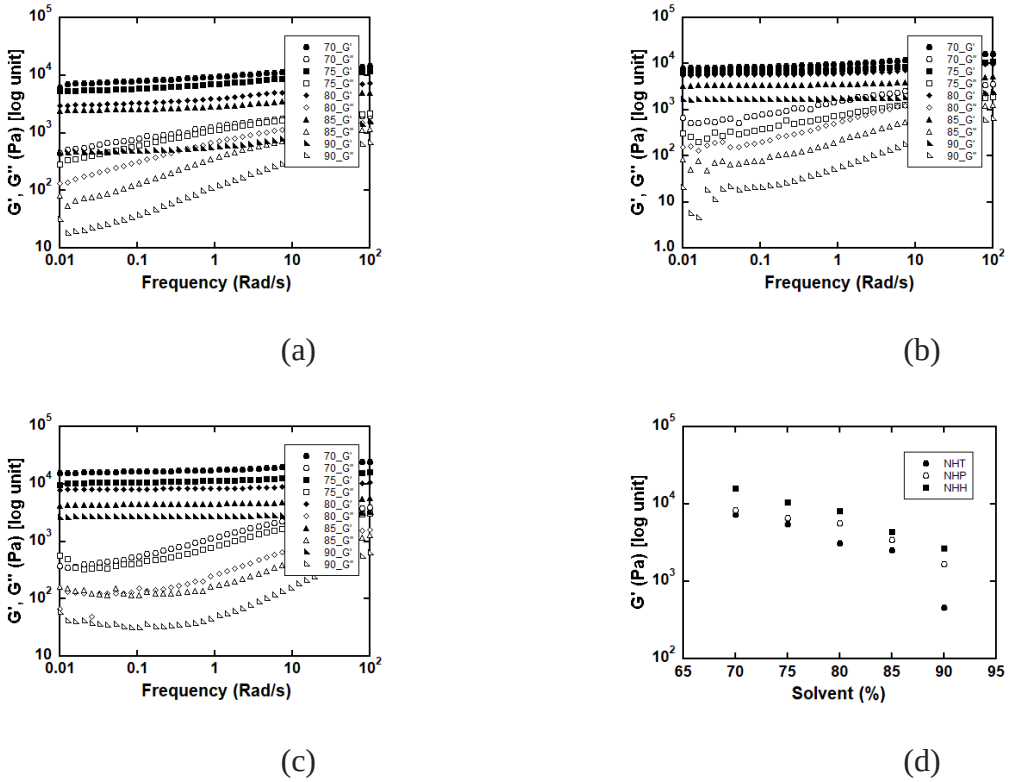

Figure 1. Frequency spectra of dynamic shear moduli (G', filled markers; G", open markers) from selectively swollen multiblock copolymers having polyisoprene midblocks for triblock copolymers, pentablock copolymers and heptablock copolymers in figure (a), (b) & (c), respectively. The composition of the block copolymers, 30-10 wt%, are mentioned on each graph as the addition of added quantity of midblock selective solvent, mineral oil. For example, 70_G' denotes that the elastic response was obtained from the gel containing 70 wt% mineral oil and 30 wt% of block copolymers. Similar naming designation is applicable for the open markers denoting the viscous responses of the block copolymer gels. The elastic modulus, G', in figure (d) represents the average G' at the lower range of frequency, from 0.01 to 0.1 (rad/s), for triblock (filled cirlces), pentablock (open circles) and heptablock (filled squares) copolymers.

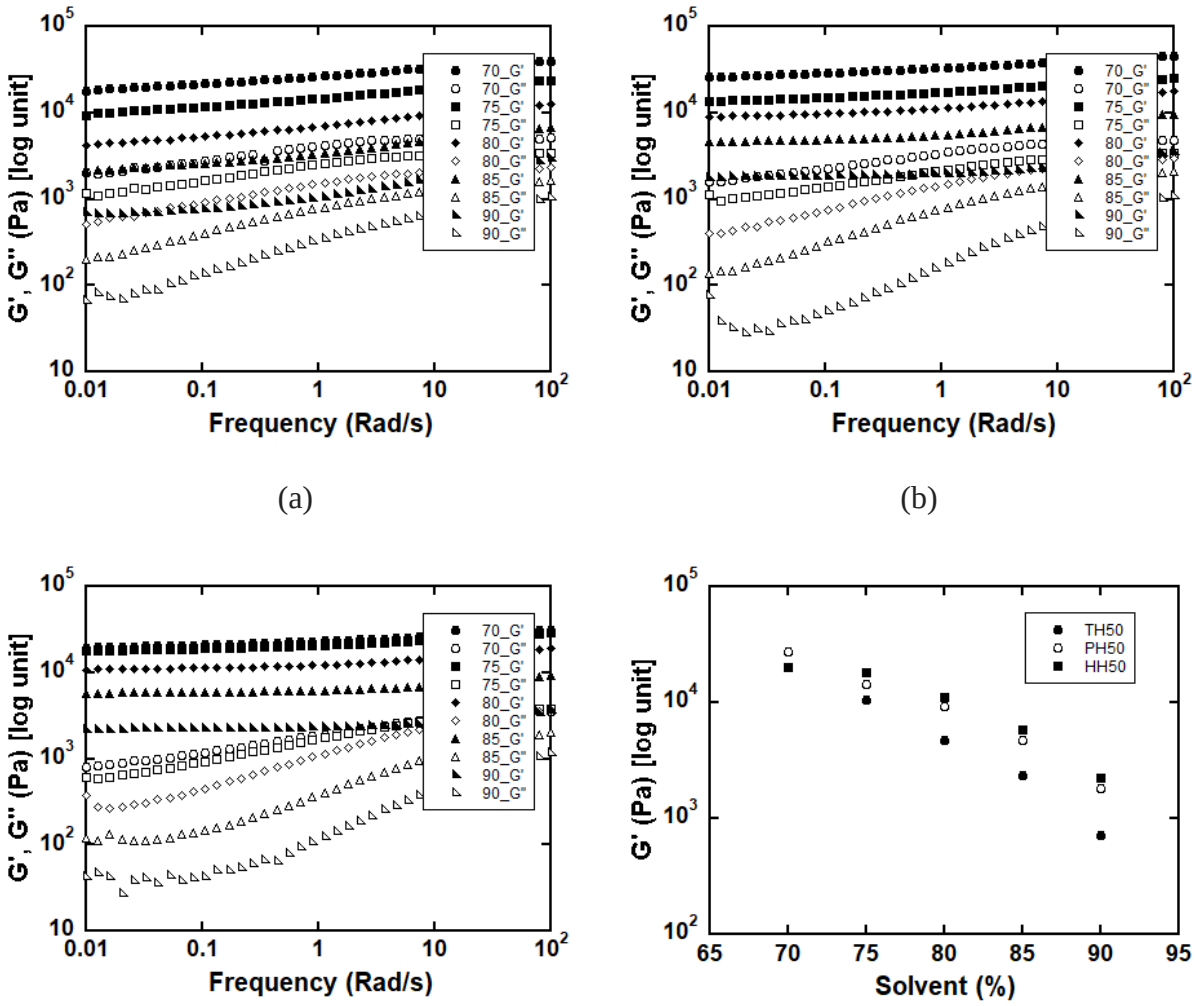

Figure 2. (a), (b) & (c) dynamic shear moduli (G', filled markers; G", open markers) as a function of frequency sweep for triblock, pentablock and heptablock copolymer gels. In these figures, the block copolymers were obtained as a result of ~50% hydrogenation of isoprenic midblocks. The frequency spectra in (d) denotes the average G' at lower range of frequency. The detail nomenclature is similar to that of the representation of shear moduli mentioned in figure 1.

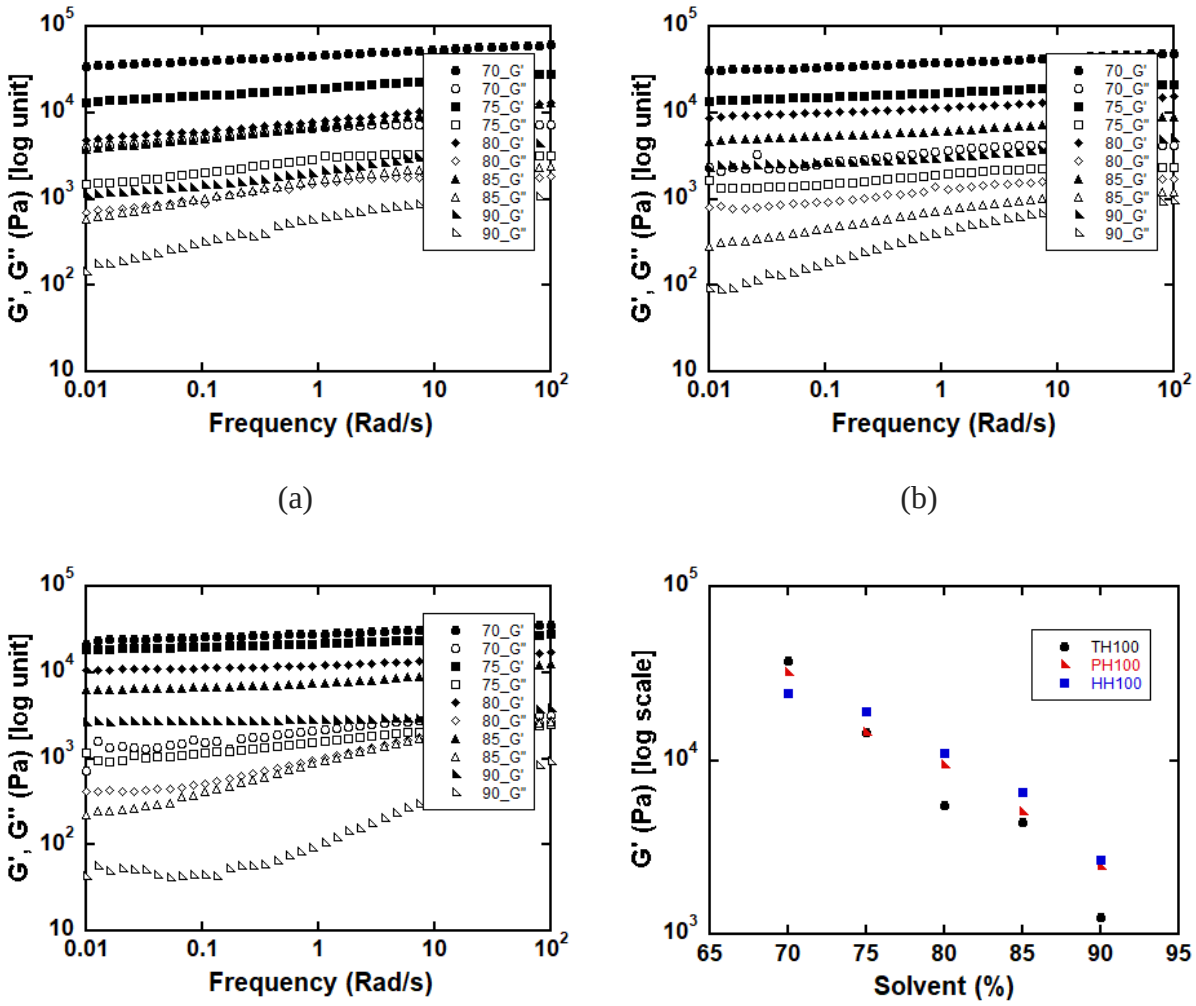

Figure 3. (a), (b) & (c) dynamic shear moduli (G', filled markers; G", open markers) as a function of frequency sweep for triblock, pentablock and heptablock copolymer gels. In these figures, the block copolymers were obtained as a result of ~100% hydrogenation of isoprenic midblocks. The frequency spectra in (d) denotes the average G' at lower range of frequency for triblock (filled circles), pentablock (filled triangle) and heptablock (filled square) copolymer gels. The detail nomenclature is similar to that of the representation of shear moduli mentioned in figure 1.

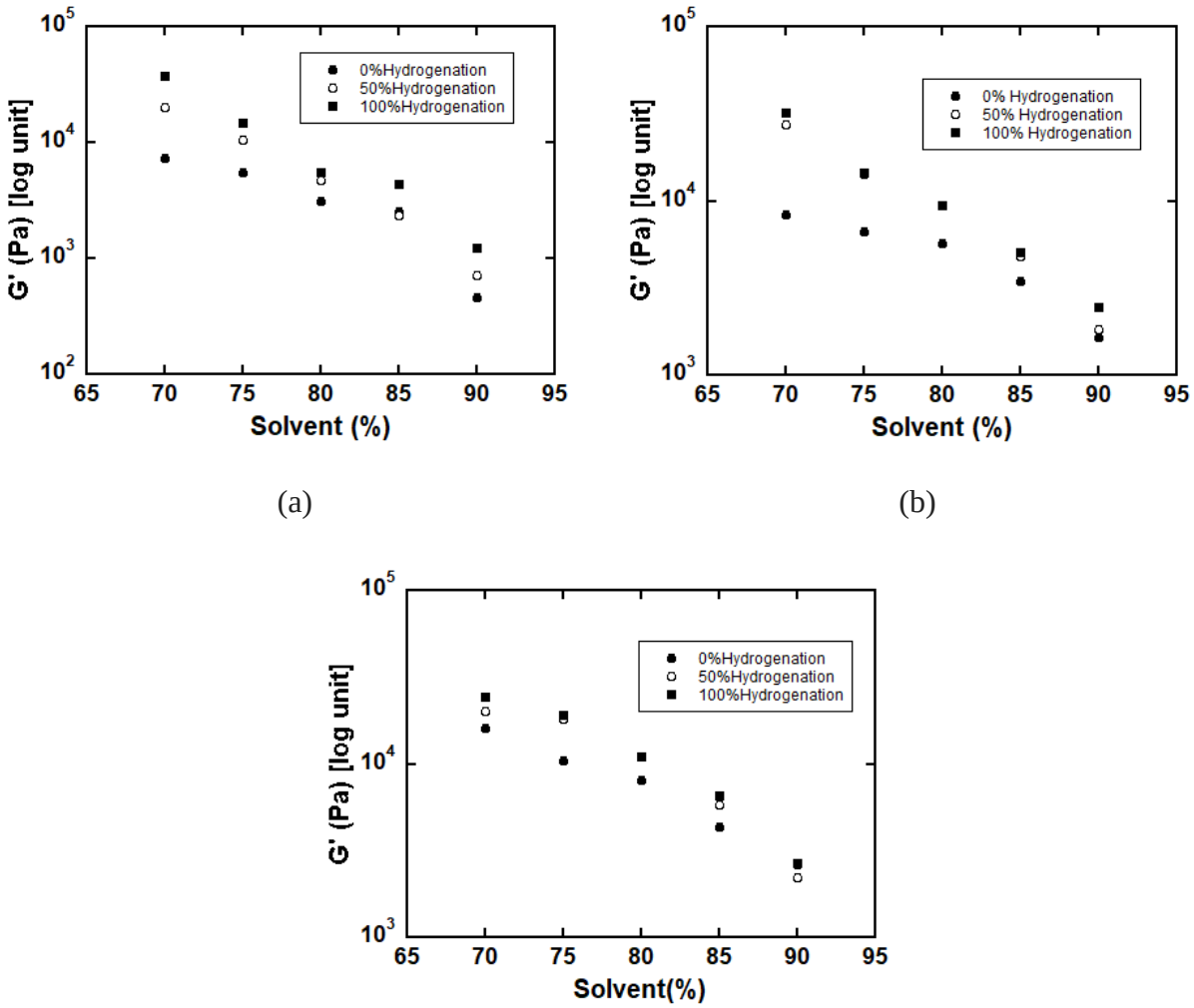

Figure 4. Influence of different degree of hydrogenation on the elastic response of multiblock copolymer gels. The figures in (a), (b) and (c) depict the average elastic modulus, G', at the lower range of frequency spectra, 0.01-0.1 rad/s, where the block copolymer gel contains 10-30 wt% of midblock selective solvent, mineral oil. Gels obtained from the block copolymers with three degrees of hydrogenation, 0 % (filled circles), ~50 % (open circles) and ~100 % (filled square) were plotted together for comparison.

CHAPTER 7

Molecular-Level Description of Constrained Chain Topologies in Multiblock Copolymer Gel Networks**

ABSTRACT

Network characteristics in physical gels composed of solvated block copolymers varying in molecular design are examined here by dynamic rheology and computer simulations. In two triblock copolymer series, one with chain length (N) varied at constant copolymer composition (f) and the other with f varied at constant N, we discern the dependence of equilibrium network metrics on both N and f. Increasing the block number in a linear multiblock series at constant N and f escalates conformational complexity, which dominates network connectivity classified according to a midblock conformation index.

**This chapter has been published in its entirety:

Tuhin, M. O., Woloszczuk, S., Mineart, K. P., Pasquinelli, M. A., Sadler, J. D., Smith, S. D., ... & Spontak, R. J. (2018). Communication: Molecular-level description of constrained chain topologies in multiblock copolymer gel networks. *The Journal of Chemical Physics*, *148*(23), 231101.

7.1. Materials, methods, results and discussion

Block copolymers (BCPs) constitute an extensively studied class of macromolecules due to their unique ability to spontaneously self-assemble into various nanostructures.[1,2] By combining long chemical sequences with different properties as covalently-linked building blocks, BCPs expedite soft materials design, which explains their ubiquitous function in a broad range of (nano)technologies.[3,4] While BCPs in the melt typically microphase-order into classic morphologies (i.e., spherical, cylindrical and lamellar), they can also produce spatially complex gyroid,[5,6] *Fddd*[7] and double-helix[8] morphologies. Moreover, insofar as the copolymer molecules consist of one or more midblocks that can connect, or bridge, adjacent microdomains, a BCP can likewise form a transient molecular network. The simplest copolymer architecture to display such network development is the bicomponent ABA triblock archetype composed of A and B repeat units. If the minority A endblocks are hard (glassy) and the majority B midblock is soft (rubbery), the BCP behaves as a thermoplastic elastomer (TPE). Since BCPs retain their ability to undergo natural[9,10] or directed[11,12] self-assembly in the presence of a selective solvent, midblock-swollen TPEs possess tunable thermomechanical properties for use as dielectric elastomers in soft robotics,[13,14] moldable substrates in microfluidics[15] and 192lextronics,[16] pressure-sensitive adhesives for biomedical applications,[17] and phase-change elastomers for shape-memory media.[18,19] Under favorable conditions, such midblock-solvated ABA copolymers can also order into bicontinuous truncated octahedra.[20]

While the examples above refer to nonpolar BCPs modified with a nonpolar diluent, triblock (telechelic) and higher-order multiblock copolymers, copolypeptides or ionomers containing one or more hydrophilic midblocks and hydrophobic endblocks likewise undergo self-assembly in the presence of water, various glycols or ionic liquids.[21,22] Such materials are of contemporary interest

in the development of Li-ion batteries,[23] proteinaceous hydrogels,[24] organic photovoltaics,[25,26] and water-treatment/carbon-capture membranes.[27,28] An important characteristic responsible for the performance of these soft materials is the existence of an elastic network that allows these solvated copolymers to behave as highly stretchable and strong physical organogels (hereafter simply referred to as gels). A molecular-level description of polymeric networks enables property predictions,[29] and the critical gel concentration (*cgc*) constitutes a fundamental metric signaling the population of copolymer molecules required to induce network formation in the presence of a selective solvent.[17,30,31] Dynamic shear rheology has been previously proposed[32] as a means by which to measure the onset of gelation due to concentration/temperature changes or reaction progression from the point where the frequency (ω) spectra of the storage (G') and loss (G") moduli become ω-independent. While theoretical[33] and simulation[34] efforts have quantified the number fraction of copolymer midblocks that form bridges (υ) between neighboring micelles in solvent-free, bicomponent BCPs as functions of chain length (N, or the molecular weight, M), composition ($f = N_A/N$, where $N = N_A + N_B$) and architecture (n, the number of blocks/molecule) at equilibrium, relationships between these copolymer attributes, molecular topology and network formation in multiblock copolymer gels remain lacking. Previously, we have identified[35,36] the molecular-level network-forming transition in molecularly asymmetric A_1BA_2 triblock copolymers sequentially grown from a parent diblock copolymer. The objective of this study is to similarly elucidate the effects of N, f and n on the equilibrium network metrics and associated rheological properties of swollen multiblock copolymers.

Each experimental series listed in Table 1 was composed of low-polydispersity (Đ = 1.05-1.10) BCPs wherein the hard blocks were polystyrene (S) and the soft blocks were either poly(ethylene-*co*-butylene) (EB) or poly(ethylene-*alt*-propylene) (EP). The first series consisted of SEBS

triblock copolymers, obtained from Kraton Polymers, with comparable compositions (30-33 wt% S) but different number-average M ranging from 56 to 267 kDa. In another series, the block number (n) was varied in styrenic triblock (n=3), pentablock (n=5) and heptablock (n=7) copolymers (~20 wt% S and M ≈ 300 kDa) initially synthesized with polyisoprene midblocks by living anionic polymerization with *sec*-butyllithium and then hydrogenated (95-99%) to yield EP midblocks. In the cases of the pentablock and heptablock copolymers, $M_{S,endblock}$ is chosen to equal $½M_{S,midblock}$ to avoid morphological changes due to block size disparity. The molecular characteristics of all materials were measured by size-exclusion chromatography and ^{1}H NMR. Copolymers in both series, designated BCPM_n (with M expressed in kDa and n only included in the EP-based copolymer series), were combined with 1.0 wt% Irganox 1010 and a primarily aliphatic (*i.e.*, midblock-compatible) mineral oil (Hydrobrite 380, Sonneborn) so that the mass fraction of BCP in oil (φ) ranged from 0.02 to 0.10. These mixtures, dissolved in reagent-grade toluene at a concentration of 4% w/v, were then cast into Teflon molds and dried for 8-9 days at 25°C to constant weight. Resultant films measuring 1.2-1.5 mm thick were heated to 120°C for 6 h under vacuum (to remove residual solvent and promote equilibration) prior to dynamic rheological analysis conducted on an AR-2000 stress-controlled rheometer equipped with 25 mm serrated platens and operated at 25°C and 1 Pa in the linear viscoelastic regime.

Computer simulations performed to discern the dependence of υ on φ for selectively-solvated bicomponent BCPs differing in N (from 56 to 300 in the first series), f (from 0.3 to 0.7 in the second series) and n (from 3 to 7 in the third series) utilized both Monte Carlo (MC) and Dissipative Particle Dynamics (DPD) protocols. These simulations accurately describe nanostructure formation and associated chain packing, which would be entirely overlooked in a macroscopic analysis (*e.g.*, a simple mass balance). As detailed elsewhere,[37] the MC simulations

were conducted on an fcc lattice so that movement of one segment required cooperative motion of adjacent segments in the simulation box filled with chain segments, each equivalent to ~0.5 kDa to match M of the solvent (s). The size of each box was selected to accommodate fully extended copolymer chains. The pairwise interaction energy between species *I* and *j* (*I*,*j* = A, B or s) was designated as ε_{ij} with $\varepsilon_{AA} = \varepsilon_{BB} = \varepsilon_{ss} = \varepsilon_{Bs} = 1$ and $\varepsilon_{AB} = \varepsilon_{As} = \chi kT/(z - 2) = 2$, where k is the Boltzmann constant, T denotes absolute temperature, and z (= 12) is the lattice coordination number. Each simulation was run to equilibrium with parallel tempering to overcome local free energy traps.[38] The DPD simulations were likewise used to extract values of υ in systems containing 100-1000 chains, each composed of either ~0.5 or ~1.0 kDa coarse-grained beads. For this purpose, the system parameters previously detailed[34] for solvent-free ABA copolymers were incorporated in the Large-scale Atomic/Molecular Massively Parallel Simulator (LAMMPS) software suite. In similar fashion as the MC simulations and to ensure BCP self-assembly in the presence of a diluent, interaction energies were set to $\varepsilon_{AA} = \varepsilon_{BB} = \varepsilon_{SS} = \varepsilon_{BS} = 25kT$ and $\varepsilon_{AB} = \varepsilon_{AS} = 50kT$. After equilibration at $2kT/\varepsilon$, a density-based cluster-recognition algorithm[34] was used to identify BCP conformations (*i.e*. bridges, loops and dangles).

Representative ω spectra acquired from the selectively-solvated BCP95 copolymer are presented at different φ in Figure 1a and establish that G' is relatively independent of ω over the entire ω range examined, whereas G" exhibits a slight negative slope in the low-ω zone and then increases at high ω. (Although G" is not independent of ω, it does not vary substantially in the low-ω zone, suggesting that these swollen BCPs still behave as physical gels.) Even at the lowest φ explored (= 0.02), no ω spectra collected here display evidence signaling the onset of viscoelastic behavior (below the *cgc*). Complementary tests confirm that these solutions undergo gravity-induced flow at significantly lower φ that depends on N.[39] Within the experimental φ range tested, the copolymer

molecules are highly swollen, but entanglements, in addition to bridges, contribute to the mechanical response of these selectively-solvated BCPs.[40] Included in the inset of Figure 1a are values of G' evaluated in the low-ω zone and provided as a function of φ. These results reveal that $G' \sim \varphi^k$, where k ranges from 2.14 (BCP56) to 2.43 (BCP72) with an average of 2.30 ± 0.07 for the SEBS-type gels (k increases to 3.15 for the gel composed of BCP300_3 due likely to the different EP midblock chemistry). This scaling behavior, predicted[41] for entangled homopolymers in solvent, is consistent with the findings of prior studies[39,42,43] of midblock-swollen triblock copolymers. We thus conclude from our dynamic rheological analysis that the *cgc* at the sol-gel transition does not exist in the range of φ examined here and that, despite the low values of φ tested, the role of midblock entanglements remains non-negligible. The progression that G' decreases with increasing M at constant φ in Figure 1a moreover confirms that the presence of an elastic network formed by bridged molecules contributes to G'.

A molecular-level approach to pinpointing the equilibrium network fraction (φ_{eq}) involves assessment of υ(φ), which is displayed for BCPs at constant f (= 0.3) and variable N (where N ≈ M in kDa) from MC simulations in Figure 1b. Two important observations are apparent. The first is that the value of υ associated with network formation (υ_N) not only becomes independent of φ as φ is increased but also increases with increasing N. Secondly, although some of the υ(φ) data exhibit an initially sharp slope change attributed to φ_{eq}, φ_{eq} can alternatively be identified at the onset of υ_N (indicated for N = 28 in Figure 1b) in the case of more gradual variation in υ(φ). Values of φ_{eq} extracted from these simulations in this fashion are presented in the inset of Figure 1b and imply the existence of a scaling relationship between φ_{eq} and N. Regression analysis of these findings signify that $\varphi_{eq} \sim N^b$ with b = −1.39. In similar fashion as in Figure 1b, υ(φ) results generated from MC simulations are provided in Figure 2a for selectively-solvated BCPs wherein

N is fixed at 36 and f is varied from 0.3 to 0.7. While the precise reason responsible for the apparent difference in the shape of $\upsilon(\varphi)$ at f = 0.7 is not known at present, we presume that it reflects a change from hairy micelles with long midblocks (at low f) to crewcut micelles with relatively short midblocks (at high f). These outcomes confirm that υ_N decreases significantly, while φ_{eq} increases slightly, with increasing f (the explicit dependence of υ_N on f is seen in Figure 2b). Since φ_{eq} = (number of BCP molecules)/(total number of molecules) at the onset of network formation and υ_N = (number of bridged BCP molecules in a network)/(number of BCP molecules), their product provides a measure of bridged BCP molecules in gels at φ_{eq} irrespective of f at constant N: (8.8 ± 0.4)%. In these first two series of selectively-solvated BCPs, only triblock copolymers (with n = 3) have been considered. Next, we examine the effect of n on network characteristics in homologous BCP systems with constant f (= 0.2) and M (300 kDa).

Frequency spectra of G' measured at ambient temperature for BCP300_5 and BCP300_7 at several φ are presented in Figures 3a and 3b, respectively, and confirm rheological behavior that is consistent with physical gels. [Corresponding ω spectra for G" appear similar to those provided in Figure 1a.] At low φ, however, some of the spectra exhibit a slight reduction of G' in the low-ω zone, suggestive of a finite relaxation time. Mean values of G' in this plateau regime are displayed as a function of φ for the BCP300 series in Figure 3c and reveal that (*i*) G' increases as the blocks become shorter with increasing n (recall that M remains constant) and (*ii*) the scaling relationship $G' \sim \varphi^k$ previously observed in the inset of Figure 1a is retained for gels composed of BCPs with n = 5 and 7. Values of k extracted for these systems – 1.33 (n = 5) and 1.23 (n = 7) – are, however, much lower than those measured for the triblock copolymer gels, indicating that the multiblock copolymer gels (n > 3) can be formulated at lower polymer concentrations than their triblock analogs and cost less. In addition, the lines included in Figure 3c for n > 3 correspond to $G' \sim \varphi$

expected for crosslinked polymer networks. This marked difference in k indicates that swollen midblock entanglements for gels with n > 3 do not influence rheological behavior as strongly as for gels with n = 3, in which case we now consider the BCP chain conformations responsible for network formation. Unlike triblock copolymer molecules that are able to adopt 3 chain conformations – bridges, loops and dangles – upon microphase separation (at sufficiently high incompatibility to preclude unsegregated chains), the pentablock and heptablock copolymers can adopt a larger number of conformations, which increase the crosslink density by connecting more micelles and thus lessen the dependence of G' on φ (*cf*. Figure 3c).

To describe the variety of accessible conformations for linear multiblock copolymers that self-assemble into A-rich micelles in the presence of a B-selective solvent, we introduce a midblock conformation index (MCI) written in the form [mbLD], where m, b, L, and D represent the number of spanned micelles, bridges, loops, and dangles for a given conformation. While comprehensive details of this indexing scheme are forthcoming, an abbreviated set of chain conformations for the case of n = 7 is depicted in Figure 4a. In Figure 4b, υ(φ) from DPD simulations is presented for multiblock copolymer systems wherein extended chains incorporate the maximum number of micelles ($m = m_{max}$) so that L = D = 0 and b = m −1: labeled as [2100] for BCP300_3, [3200] for BCP300_5 and [4300] for BCP300_7. As n is increased, however, this conformation becomes less favorable. As the number of micelles spanned by a single chain is reduced along with the number of swollen midblock bridges (in which case either L or D becomes non-zero), υ(φ) increases substantially in the cases of [21LD] for BCP300_5 and [32LD] for BCP300_7. The most compact conformation of [21LD] for BCP300_7 included in Figure 4b illustrates the highest initial increase in υ(φ) for this system. In fact, multiblock copolymer molecules (with n > 3) that connect fewer than m_{max} micelles consistently appear to be primarily responsible for φ_{eq} to lie between φ = 0.02

and $\varphi = 0.04$. The compact (not fully extended) conformations considered here (excluding more highly compact conformations that do not contribute very much to υ) play a critical role in network formation and, hence, gelation of multiblock copolymers in selective solvent, and are directly manifested in the reduced dependence of G' on φ in Figure 3c.

Since the sol–gel transition has not been identified here by dynamic rheology over the range of φ examined but unambiguous values of φ_{eq} heralding the formation of equilibrium networks from simulations have, an apparent disconnect exists suggesting that the transition does not require $\upsilon = \upsilon_N$. If an equilibrium network is not achieved, then long-lived, swollen-midblock entanglements or large-scale morphological heterogeneities (*i.e.*, flocs[42]) might play a nontrivial role in the rheological identification of the transition. The experimental findings reported herein systematically reveal the effects of copolymer molecular weight, architecture, and concentration on mechanical properties (and associated scaling relationships) of selectively-solvated multiblock copolymer gels at relatively low φ. Complementary simulation results establish that the fraction of swollen midblocks responsible for forming bridges, $\upsilon(\varphi)$, and ultimately producing a network at υ_N depends on all these copolymer attributes and, in each case, attains a φ-independent plateau indicative of an equilibrium network. The molecular-level descriptions afforded by $\upsilon(\varphi)$ values at different MCI designations corresponding to various BCP gels, which are of increasing technological relevance and molecular complexity,[24,44] are expected to benefit the development of theoretical formalisms aimed at addressing, *e.g.*, the mechanism of gelation of BCPs in selective solvents.[45] Moreover, such detailed descriptions are necessary to elucidate and ultimately control network formation in, and the associated properties of, these scientifically interesting and commercially versatile soft materials.

7.2. Acknowledgments

This work was supported by the NC State Nonwovens Institute, MANN+HUMMEL GmbH and the Polish National Science Centre (Grant No. DEC-2012/07/B/ST5/00647). Simulations were conducted at the NC State High-Performance Computing Center and Poznan Computer and Networking Center. We thank Mr. J.C. Tilly for technical assistance.

7.3. References

1. Z. J. Guo, G. J. Zhang, F. Qiu, H. D. Zhang, Y. L. Yang and A. C. Shi, Phys. Rev. Lett. 101, 028301 (2008).
2. M. W. Matsen, Macromolecules 45, 2161 (2012).
3. C. M. Bates and F. S. Bates, Macromolecules 50, 3 (2017).
4. P. Müller-Buschbaum (ed.), ACS Appl. Mater. Interfaces *9* 31213 (2017).
5. D. A. Hajduk, P. E. Harper, S. M. Gruner, C. C. Honeker, G. Kim, E. L. Thomas and L. J. Fetters, Macromolecules 27, 4063 (1994).
6. H. Jinnai, Y. Nishikawa, R. J. Spontak, S. D. Smith, D. A. Agard and T. Hashimoto, Phys. Rev. Lett. 84, 518 (2000).
7. C. A. Tyler and D. C. Morse, Phys. Rev. Lett. 94, 208302 (2005).
8. H. Jinnai, T. Kaneko, K. Matsunaga, C. Abetz and V. Abetz, Soft Matter 5, 2042 (2009).
9. T. P. Lodge, B. Pudil, B. and K. J. Hanley, K. J., Macromolecules 35, 4707 (2002).
10. A. S. Krishnan, S. D. Smith and R. J. Spontak, Macromolecules 45, 6056 (2012).
11. H. Q. Hu, M. Gopinadhan and C. O. Osuji, Soft Matter 10, 3867 (2014).
12. D. J. Lunn, O. E. C. Gould, G. R. Whittell, D. P. Armstrong, K. P. Mineart, M. A. Winnik, R. J. Spontak, P. G. Pringle and I. Manners, Nat. Commun. 7, 12371 (2016).
13. R. Shankar, T. K. Ghosh and R. J. Spontak, Adv. Mater. 19, 2218 (2007).
14. B. Kim, Y. D. Park, K. Min, J. H. Lee, S. S. Hwang, S. M. Hong, B. H. Kim, S. O. Kim and C. M. Koo, Adv. Funct. Mater. 21, 3242 (2011).
15. A. P. Sudarsan, J. Wang and V. M. Ugaz, Anal. Chem. 77, 5167 (2005).
16. K. P. Mineart, Y. Lin, S. C. Desai, A. S. Krishnan, R. J. Spontak and M. D. Dickey, Soft Matter 9, 7695 (2013).

17. C. M. Flanigan, A. J. Crosby and K. R. Shull, Macromolecules 32, 7251 (1999).
18. Q. Zhang, S. Song, J. Feng and P. Wu, J. Mater. Chem. 22, 24776 (2012).
19. K. P. Mineart, S. S. Tallury, T. Li, B. Lee and R. J. Spontak, Ind. Eng. Chem. Res. 55, 12590 (2016).
20. S. Woloszczuk, M. O. Tuhin, S. R. Gade, M. A. Pasquinelli, M. Banaszak and R. J. Spontak, ACS Appl. Mater. Interfaces 9, 39940 (2017).
21. P. Alexandridis, U. Olsson and B. Lindman, Langmuir 14, 2627 (1998).
22. Y. Y. He, P. G. Boswell, P. Buhlmann and T. P. Lodge, J. Phys. Chem. B 111, 4645 (2007).
23. D. T. Hallinan and N. P. Balsara, Ann. Rev. Mater. Res. 43, 503 (2013).
24. W. Shen, K. C. Zhang, J. A. Kornfield and D. A. Tirrell, Nat. Mater. 5, 153 (2006).
25. J. Yoon, D. K. Kang, J. Won, J. Y. Park and Y. S. Kang, J. Power Sources 201, 395 (2012).
26. H. A. Al-Mohsin, K. P. Mineart and R. J. Spontak, Adv. Energy Mater. 5, 1401941 (2015).
27. G. M. Geise, B. D. Freeman and D. R. Paul, Polymer 51, 5815 (2010).
28. L. Ansaloni, Z. Dai, J. J. Ryan, K. P. Mineart, K. T. Saud, Q. Yu, M.-B. Hägg, R. J. Spontak and L. Deng, Adv. Mater. Interfaces 4, 1700854 (2017).
29. M. Zhong, R. Wang, K. Kawamoto, B. D. Olsen and J. A. Johnson, Science 353, 1264 (2016).
30. Y. Li, Z. Sun, T. Shi and L. An, J. Chem. Phys. 121, 1133 (2004).
31. M. E. Gindy, R. K. Prud'homme and A. Z. Panagiotopoulos, J. Chem. Phys. 128, 164906 (2008).
32. H. H. Winter and F. Chambon, J. Rheol. 30, 367 (1986).
33. M. W. Matsen and R. B. Thompson, J. Chem. Phys. 111, 7139 (1999).
34. S. S. Tallury, R. J. Spontak and M. A. Pasquinelli, J. Chem. Phys. 141, 244911 (2014).

35. M. W. Hamersky, S. D. Smith, A. O. Gozen and R. J. Spontak, Phys. Rev. Lett. 95, 168306 (2005).
36. S. S. Tallury, K. P. Mineart, S. Woloszczuk, D. N. Williams, R. B. Thompson, M. A. Pasquinelli, M. Banaszak and R. J. Spontak, J. Chem. Phys. 141, 121103 (2014).
37. S. Woloszczuk, M. Banaszak and R. J. Spontak, J. Polym. Sci. B: Polym. Phys. 51, 343 (2013).
38. T. M. Beardsley and M. W. Matsen, Eur. Phys. J. E 32, 255 (2010).
39. D. A. Vega, J. M. Sebastian, Y. L. Loo and R. A. Register, J. Polym. Sci. B: Polym. Phys. 39, 2183 (2001).
40. M. Rubinstein and S. Panyukov, Macromolecules 35, 6670 (2002).
41. P. G. de Gennes, *Scaling Concepts in Polymer Physics*, Cornell University Press, New York, 1979.
42. A. S. Krishnan, K. E. Roskov and R. J. Spontak, in *Advanced Nanomaterials* (K. E. Geckeler and H. Nishide, eds.), Wiley-VCH, Weinheim, 2010, pp. 791–834.
43. T. L. Chantawansri, T. W. Sirk and Y. R. Sliozberg, J. Chem. Phys. 138, 024908 (2013).
44. F. S. Bates, M. A. Hillmyer, T. P. Lodge, C. M. Bates, K. T. Delaney and G. H. Fredrickson, Science 336, 434 (2012).
45. R. E. Bras and K. R. Shull, Macromolecules 42, 8513 (2009).

7.4. Figures and Tables

Table 1. Molecular characteristics of the BCPs used here.

Specimen designation	n	M[a] (kDa)	S content (wt%)	Midblock[b]
BCP56	3	56	30	EB
BCP72	3	72	30	EB
BCP95	3	95	30	EB
BCP267	3	267	33	EB
BCP300_3	3	293	20	EP (97%)
BCP300_5	5	303	20	EP (99%)
BCP300_7	7	303	20	EP (95%)

[a] Expressed as the number-average molecular weight.

[b] Includes the degree of hydrogenation where applicable.

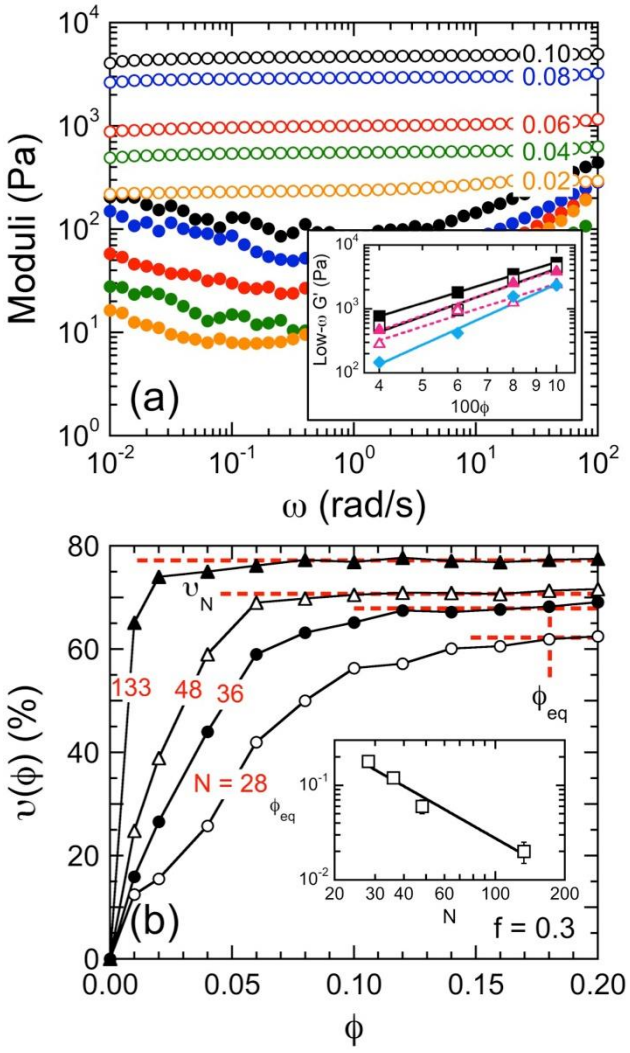

Figure 1. (a) ω spectra of the dynamic shear moduli (G', open circles; G", filled circles) from selectively-swollen BCP95 at different copolymer fractions (φ, color-coded/labeled). Included in the inset are low-ω values of G' for BCP56 (■), BCP72 (□), BCP95 (▲), BCP267 (△), and BCP300_3 (◆). The lines are power-law fits to the data. (b) υ(φ) from MC simulations of B-swollen ABA copolymers with f = 0.3 and different chain lengths (N, labeled). Dashed horizontal lines identify υ_N, whereas the dashed vertical line signifies φ_{eq} for gradually changing υ(φ). The solid lines in (b) connect the data. The inset displays φ_{eq} as a function of N, and the solid line is a power-law regression to the data.

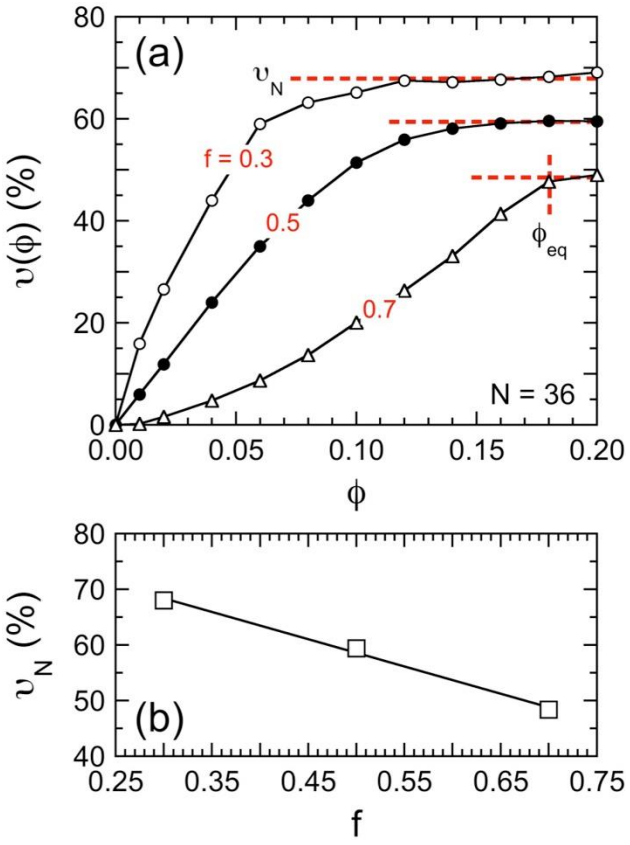

Figure 2. (a) υ(φ) from MC simulations of selectively-solvated ABA copolymers with N = 36 and different BCP compositions (f, labeled). Values of υ_N extracted from (a) are displayed as functions of f in (b). The solid lines in (a) connect the data, whereas the one in (b) is a linear regression to the data.

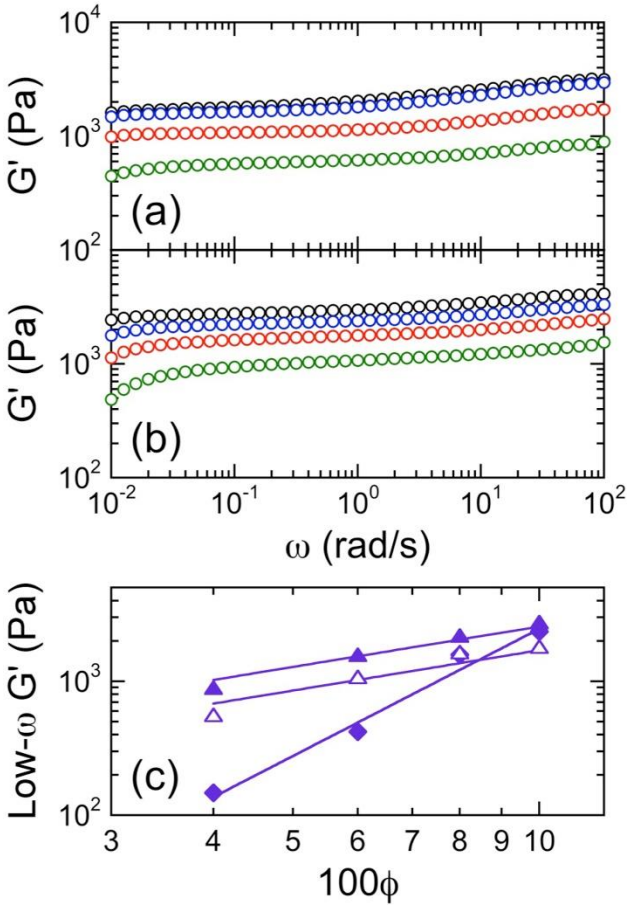

Figure 3. Frequency spectra of G' measured from selectively-solvated linear multiblock copolymers – (a) BCP300_5 and (b) BCP300_7 – at different φ (color-coded as in Figure 1a) and 25°C. In (c), low-ω values of G' displayed as a function of φ for systems consisting of BCP300_3 (◆), BCP300_5 (△) and BCP300_7 (▲). The solid lines are power-law fits of the data to $G' \sim \varphi^k$ (for BCP300_3) and $G' \sim \varphi$ (for BCP300_5 and BCP300_7).

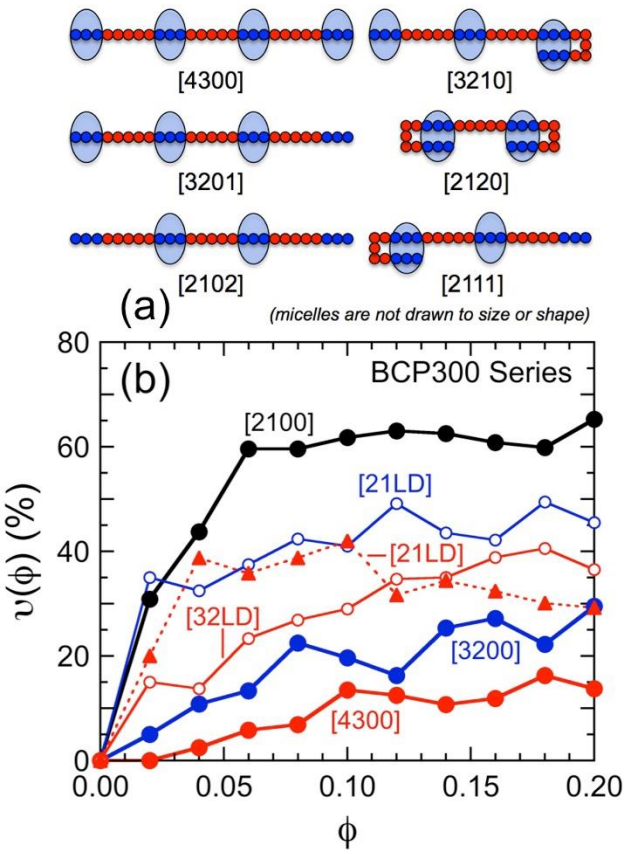

Figure 4. In (a), schematic illustration of several midblock conformation indices (MCIs) for a select subset of heptablock chain conformations. In (b), several υ(φ) from DPD simulations of selectively-solvated multiblock copolymers in the BCP300 series with f = 0.2 and N = 300 at different n: 3 (black), 5 (blue) and 7 (red). Extended chain conformations connecting the maximum number of micelles possible (m_{max}) are assigned filled circles and labeled with color-coded MCIs of the form [m_{max},m_{max}–1,0,0]. More compact conformations involving fewer micelles ($m < m_{max}$) include non-zero L and/or D values in the MCI labels, as indicated in (a). The lines serve to connect the data.

CHAPTER 8

CONCLUSIONS AND FUTURE WORKS

8.1. Conclusions

Having a simple narrative of the sequences and the significance of the individual studies comprised of the previous chapters can be a good starting point as a way of putting the pieces together to see a more solidified findings and paved paths of this whole study. This study, as sub-divided into eight chapters, aimed to expand the scientific understanding of linear multiblock copolymer systems from the perspective of piezoresistivity and physical organogels. Before stepping into new addition of knowledge, the existing branch of knowledge of block copolymer-based systems and research tools were illustrated in the first chapter as a showcase of both current advancement of the field and the potential frontiers of exploration that the subsequent chapters aimed to address with new findings. These fundamental understanding of how block copolymers are synthesized, self-assemble, form midblock fractions, get the microscopic properties define the mesoscopic characteristics along the challenges associated with the edges. The core concept of this study encompasses the formation, detection and application of the networks formed either by the midblock fractions of block copolymers and/or by the incorporated nanoparticles into block copolymer-based system developed as a piezoresistive material. Hence, the theory of percolation was also described in the second chapter of this dissertation. Having these pieces together was the building blocks that set the contents of subsequent chapters in motion.

Regarding the percolation of network, two extreme edges of the three-dimensional network formation was pin-pointed and was attempted to correlate those to the mesoscopic properties of the materials. In the study of piezoresistive properties of the triblock copolymer-based nanocomposites (Chapter 03), it was the carbon nanofibers (CNF) that was examined for the

percolation of network as the matrix made up of block copolymer and block copolymer/mineral oil gel already had molecular network throughout the materials. Hence, both electrical and electro-mechanical responses provided the node of changes due to the distribution, alignment, and mobility of the incorporated nanoparticles. In another study of detecting the critical gel fraction (Chapter 06) a series of triblock copolymers, along architecturally more complex pentablock and heptablock copolymers, were used to detect the endpoint of the molecular network when the material starts possessing very high quantity of the midblock selective solvent, mineral oil (MO). It's the point where the polymer/MO matrixes are no longer gel as the they lose the connectivity of the network throughout the matrix. Observing from the reverse point of view, it's synonymous to state that more than 'critical gel fraction' of the quantity of block copolymer is required to mark the percolation of molecular network in block copolymer/MO gels. Thus, this whole study encompasses from the start of network percolation by gradually adding the network forming ingredients (CNF) to the other end where gradually removing the network forming elements (block copolymer molecules) mark the point. In the latter case, as the sophisticated tools with the required resolution range for detecting and quantifying the intended material properties i.e. molecular conformations is not available-yet, dissipative particle dynamics (DPD) simulation was used to compensate for that gap along the mesoscopic property evaluation by rheological tools.

Before stepping into linear pentablock and heptablock copolymer associated studies, linear triblock copolymer/MO gels were examined for different molecular architectures having end block fractions ranging from 0.2 to 0.8 (Chapter 04). The compositions were studied for the changes of their morphological and molecular topological features and a detail phase diagram was constructed as an orderly method of presentation of the findings. Considering the dimensions of the tasks examined here, it would be laborious, highly expensive and time consuming to utilize the

experimental tools to study the whole matrix. Hence, computational tools of Monte Carlo (MC) simulation and DPD simulation were used for these entire series of studies as the viable methods. Having these results served multiple purposes that strengthened and paved the way for the studies in subsequent chapters. The comparative molecular conformations for triblock copolymers for different morphologies confirmed that spherical morphologies (end block fraction = 0.2) provided the maximum bridge fractions both in neat and gel composition of the triblock copolymers. This guidance helped to set the direction of the next sections and, hence, it's the spherical morphologies that were studied in those considering the topological importance. In addition to that, this series of probing enabled the discovery of unique 'Octahedral' morphology as a new addition to the family of block copolymer generated nanoscale morphologies, which is expected to deliver various potential applications.

The examinations of the self-assembled nanodomains and the corresponding molecular topologies were reported in the subsequent section (Chapter 05). The block copolymers used in this chapter had midblocks consisting of poly[ethylene-*b*-propylene] which was produced by hydrogenating the block copolymers having midblocks of polyisoprene. As the endblock fraction of all block copolymers of this section were chosen to be 0.2, the morphologies of the neat block copolymers were expected to be either sphere or semi-sphere e.g. ellipsoidal in shape. Addition of the midblock selective solvent yielded only spherical nanodomains. Such observation of the morphologies of the systems were corroborated by both experimental tools of small angle x-ray scattering (SAXS) and DPD simulation to confirm the consistency of the findings. As the molecular weight of all of these chains were fixed to 300 kDa, the size of the blocks was gradually decreased as the architectural segment increased from 3 to 5 or 7. In influence of this difference in the block length was also reflected from the radius of the spheres obtained from both analysis of the SAXS data

and the visual observation of the VMD images taken from molecular trajectories obtained from DPD simulation. Afterwards, pentablock and heptablock copolymers, along their analogous triblock ones, were detail studied for the molecular conformations. While architectural difference induced by the number of blocks were reported, there might be some impact induced by the difference in the size of blocks of these copolymers, which was not deconvoluted in these results.

8.2. Recommendations for Future works

In the introduction part, the figure 02 is an illustration of how the field of block copolymer is expanding in case of exploration, understanding, and application. However, the implications of the scientific outreach of the field is far bigger than what can be captured by taking the snapshot of the dynamics of this individual field. It's more realistic to approach the understanding and outcomes through the lens of self-assembled material properties which encompasses other fields like surfactants, self-folding proteins etc. Even a surprisingly bigger picture of cosmic events was also mentioned in Ref. 40 of the introduction part of this dissertation, although the similarity holds upto the qualitative picture because, till now, no specific known attempt was reported yet to compare these nanostructures and those cosmic length scale arrangements.

The understanding, and expansion of all those applications of block copolymer field are primarily focused on the shape and arrangement of the nanostructures having some intuitive insight on the molecular conformations. After the current study, it's found that there are disciplines among the molecules as well, at least up to linear heptablock copolymers, as was found from the previous sections. This discovery may have binary possibilities: first, these molecular topologies can be used along with the nanodomains for potential applications, and second, the molecular conformations can themselves be considered for applications. By putting an analogy, as setting up the space stations is analogous to establishing a basement of exploration into outer space, getting

hands on control on the smaller scale materials i.e. molecular level can be synonymous to having basement for exploring into further deeper down the road regarding the size scale. However, to hone a substantial prediction and outline of the possibilities, it's important to develop and implement experimental methods and required tools to examine the molecular topologies found here. Thereafter, exploring the additional networks and applications, like the piezoresistivity observed as a result of percolation of CNF networks within the existing nerworks of block copolymers using carbonaceous nanoparticle, will be more viable entrance to explore and examine. Several immediate outlook of the possible future steps are listed as following-

Determination of loop-loop interlocking and entanglements in Multiblock copolymers: So far there have been effort in exploring, understanding, and connecting the molecular bridges and loops of different conformations with the respective mesoscopic properties of the block copolymer-based systems. However, the lies another important conformational combination where two or more loops can entangle or can form knots. Intuitively, such kind of molecular arrangement is expected have countable impact on the mesoscopic properties of the corresponding materials.

Stress relaxation behavior of multiblock copolymers: Polymers relax over longer period, and because of self-assembled characteristics, the block copolymers are expected to have different degree of relaxation depending on the molecular conformations. Hence, it might be proved to be pertinent important to evaluate how the relaxation behavior can be tuned using different molecular arrangement.

Molecular alignment induced porosity to create the channeling of porous network:

Polymers have been used as a robust material for the day-to-day devices like laptops, cell phone, television etc.; especially because of the light weight nature of the polymers. One

challenge associated with all these electronic devices is to dissipate the heats and thus saving the devices from over-heating. Polymeric materials are so poor heat conductor that there have been dynamic fields associated with them using to produce insulating materials. Some researchers of MIT recently devised a method of using the plastics as heat conductor where the porosity induced channeling was used to vent out the heat through the material.[1] In case of block copolymers, the nanostructures have already been used to construct the nanoporosity induced channeling to help fluids pass through for the application of filtration media. Now that the molecular assembly of the multiblock copolymers were found to have some discipline, it can be further studied if these conformational arrangements can be tuned to obtain molecular level channeling for the applications like heat conduction.

8.3. A summary note of aspiration

Following the previous centuries, multi-facet and comprehensive practice of sector-wise scientific upbringings resulted the simultaneous, or at the closer proximity, evolution of step-stones of development, not necessarily as arranged according to the immediate need or incentive of some type of Bucket sort algorithm [2-3]. The quantitative prediction of growth and development in a specific sector i.e. the field of transistor, for a period of decades were even proved to be successful, as is evident from the extrapolation of Moor's law [4]. Hence, in near future, it's expected to add more game changing markers in the bucket if we continue the skyrocketing aspirations, understandings, and endeavors of scientific explorations. Such titanic optimism arises from the fact that human beings had long been capable of having an overall continuation of developments for such long time considering the time scale of human existence on the earth. Especially, dynamic change in material science i.e. polymeric field, is not a mere hope out of optimism, rather a necessity of the century as we are at the door of starting our

journeys of space travel, building underwater cities etc. to solve the fundamental problems of humanity like the issue of habitat, food etc. The findings of this research investigation are expected to be a tiny push towards that direction.

8.4. References

1. Xu, Y., Wang, X., Zhou, J., Song, B., Jiang, Z., Lee, E. M., ... & Chen, G. (2018). Molecular engineered conjugated polymer with high thermal conductivity. *Science advances*, *4*(3), eaar3031.
2. Cormen, T. H., Leiserson, C. E., Rivest, R. L., & Stein, C. (2009). *Introduction to algorithms*. MIT press.
3. Corwin, E., & Logar, A. (2004). Sorting in linear time-variations on the bucket sort. *Journal of computing sciences in colleges*, *20*(1), 197-202.
4. Schaller, R. R. (1997). Moore's law: past, present and future. *IEEE spectrum*, *34*(6), 52-59.